Synthetic, equilibrium, kinetic and mechanistic studies of the reactions between azo dye ligands and Ni^{2+}

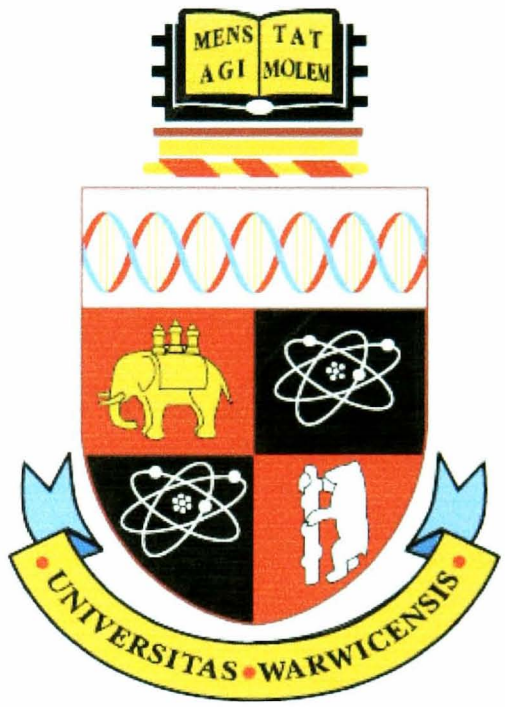

The University Of Warwick

By

Jay A. Blount

A thesis submitted as part requirement for the degree of Doctor of Philosophy

Department of Chemistry

University of Warwick

August 2008

Table of contents.

List of figures and tables.

Page

Chapter 1

Acknowledgements.

I wish to express my sincerest gratitude and thanks to my supervisor Prof. Peter Moore for his invaluable knowledge, help, guidance, advice, support and continued encouragement throughout this work.

I would also like to thank my deputy supervisors Prof. Michael Hannon and Dr. Peter Scott for their advice and help

I would like to express my gratitude and thanks to Dr. Rachel James of the company Avecia for her time and help during my time spent at Avecia and also for her help, suggestions and input throughout this work. I would also like to express thanks to Mr. Doug Spencer of Avecia for his help, suggestions and input throughout this work.

Sincerest thanks also to all the members of the Department of Chemistry and Molecular Sciences who keep the machines maintained, chemicals available, and specialist equipment accessible without which this project would not have been possible.

I wish to acknowledge and thank the EPSRC and Avecia for financial support.

Finally I wish to thank my family and friends for their continuous support

Declaration.

To the best of my knowledge the work described in this thesis is original if not otherwise indicated.

J. A. Blount (B.Sc(Hons), M.Sc)

Summary.

12 azo dye ligands L1-L12 that are used in the inkjet printer industry have been synthesised and characterised. The dyes L5B and L3765 were supplied as gifts by the chemical company Avecia. All dyes were fully examined by ^{1}H NMR, ^{13}C NMR, IR spectroscopy, electrospray mass spectroscopy, atomic absorption spectroscopy, UV-Visible spectroscopy and microanalyses. Melting points were also determined.

pK_a values have been determined by visible spectroscopy for the dyes PAN(Aldrich), L7, L3765, L1, L5 and L5B. Stability constant measurements have been attempted for the Ni(II) complexes of PAN, L1 and L5 using UV-Visible spectroscopy. Single wavelength stopped-flow kinetic studies of the reactions of Ni(II) with PAN(Aldrich), PADA(Aldrich), SUDAN I(Aldrich), L3765 and L7 were carried out.

Multi wavelength stopped-flow kinetic studies of the reactions of Ni(II) with L1, L7, L5 and L5B were examined and rate constants for complex formation (k_f) were determined. Rates of dissociation of $[Ni(PAN)_2]$ using ligand exchange with either EDTA or 2,2':6',2''-Terpyridine (Terpy) were investigated using UV-Visible spectroscopy. Relative stabilities of $[Ni(II)(PAN)]^+$, [Ni(II)(L7)] and $[Ni(II)(L3765)]^-$ have been determined. Dissociation of Ni(II) complexes of L1, L5, L5B, L6, PAN, L7 and L3765 using excess Terpy have been studied using UV-Visible spectroscopy and relative stabilities have been compared.

Abbreviations.

Bipy	Bipyridine
C	Centigrade
cm^{-1}	Wavenumber
o	Degrees
DMF	Di-methyl formamide
DMSO	Di-methyl sulfoxide
DPAP	Pyridine-2-azo-(4-di-methylaminobenzene)
EDTA	Ethylenediaminetetraaceticacid
FTIR	Fourier transform Infra red
H acid	4-Amino-5-hydroxy-napthalene-2,7-di-sulfonic acid
Hz	Hertz
Ir	Infra red
MeOH	Methanol
METRIAP	3-(3,4-Di-hydroxyphenylazo-1)-5-mercapto-1,2,4-triazole
min	Minutes
$\mu S/cm^{-1}$	Micro Siemens per cm^{-1}
m/z	Mass to charge ratio
nm	Nanometer
NMR	Nuclear magnetic resonance
PADA	Dimethyl-[4-(pyridine-2-ylazo-phenyl)]amine
PAN	1-(2-Pyridylazo)-2-napthol
PAR	4-(2-Pyridylazo)resorcinol

Phen	1,10-Phenathroline
r/t	Room temperature
TAN	1-(2-Thiazolylazo)-2-napthol
TRIAP	3-(3,4-Dihydroxyphenylazo-1)-1,2,4-triazole
Terpy	2,2':6',2"-Terpyridine
TPTZ	2,4,6-Tri(2-pyridyl)-1,3,5-triazine
UV-Visible	Ultra-Violet Visible

Chapter 1: Introduction.

1.1 Qualities of a perfect printer.

"In the 1960s many reprographic technologies were emerging to compete for the lucrative printing markets".[1] A perfect printer would have the qualities of being low cost, produce text and graphics in monochrome and colour to high quality, be fast and be able to print on a number of substrate materials such as paper. "Ink jet printers satisfy these requirements best and it is not surprising that ink jet printing is becoming the dominant non impact printing technology"[2].

1.2 History and development of ink-jet technology.

The first use of ink jets in printing devices dates back as far as 1930 and the first successful product using ink jets was developed by Elmquist in Sweden in 1951.[3] It was not until the 1960s, 70s and 80s that the inventions were made upon which today's ink jet technology is based. In 1964 Sweet invented the continuous ink jet method, and this was modified by Hertz in 1967.[3] The second major ink jet technology of drop on demand was invented by Zoltan in 1972.[3] This used a piezoelectric element to eject the ink. The use of heat to eject the ink by bubble formation was discovered accidentally by Canon.

"It is hard to imagine that the simple natural phenomenon involved in making a cup of tea, namely bubble formation when water is heated would have a revolutionary impact on modern printing technology."[2] This lay behind the discovery of bubble jet technology by Canon in 1979.[4,5]

An unsuspecting Canon researcher had no idea that he was on the brink of translating this wonder of nature into a technological application that would completely transform the printing industry. By accident he reportedly brought a soldering iron into contact with an ink filled syringe. A bubble formed and to his amazement, forced a spurt of ink from the nozzle. He was so intrigued that he decided that this "accident" was worth reporting and did so. At around the same time researchers at Hewlett Packard (HP) also discovered the technology which they named thermal ink jet.[6,7] "These discoveries launched thermal, drop on demand ink jet printing, the major technology behind many of today's ink jet printers".[2] More recently, the hot-melt ink-jet system (also known as solid ink jet and thermoplastic ink-jet) was discovered by Data products (formerly Exxon)[8] and Howtek.[9] Tektronix are also involved in this technology.[10]

1.3 Ink-jet technology.

Ink jet is divided in to two basic types, namely continuous ink-jet and drop on demand ink-jet.

1.31 Continuous ink-jet.

In continuous ink-jet systems a continuous stream of ink droplets are ejected from a nozzle.[3,11] Some of the droplets are targeted at the substrate to form the image while the remainder are collected in a gutter and either recycled or rejected. This selective deflection is achieved by first electrostatically charging some of the ink droplets, and then deflecting those that are charged using high voltage electrodes.[12] Obviously, two designs are possible.

In the first design, the charged ink droplets are deflected on to the paper to form the image and the uncharged droplets are collected in a gutter. This is the raster scan continuous ink-jet method (Figure 1).[13]

Figure 1: Components for a single-nozzle, Raster-scan, continuous ink-jet print head.[13]

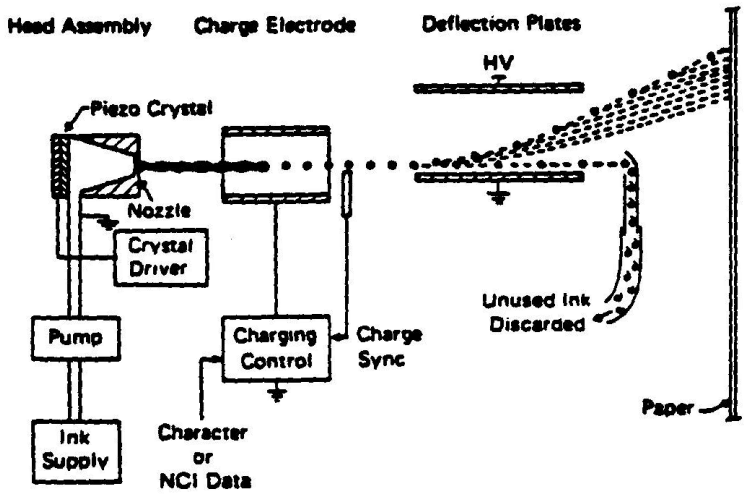

In the second design, the uncharged ink droplets form the image and the charged ink droplets are deflected into the gutter. This is called the binary continuous ink-jet system (Figure 2).[13]

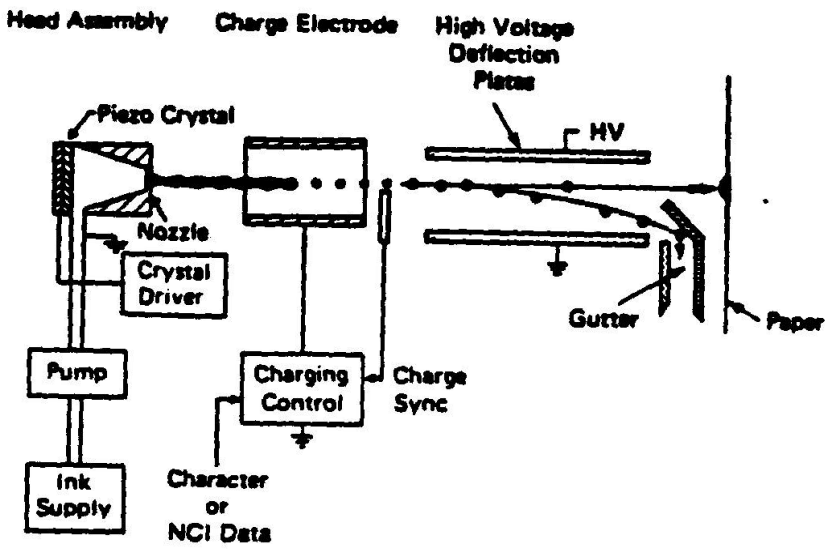

Figure 2: Components for a single-nozzle, binary, continuous ink-jet print head.[13]

"Both the raster scan and binary continuous ink-jet systems are based on the original Sweet technology and are especially suited for monochrome printing".[12]

The Hertz technology, whereby a fine mist of irregular sized ink droplets is formed, uses the binary design of the uncharged droplets forming the image (Figure 3).[13] It is more suited to colour printing than the previous two methods.[12]

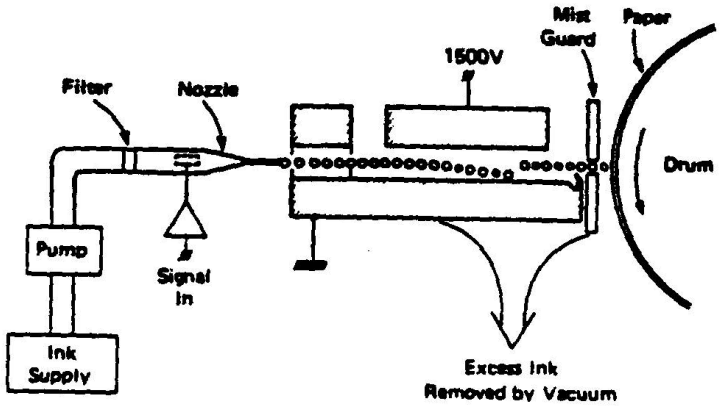

Figure 3: Components for a single nozzle, Hertz, continuous ink-jet print head.[13]

1.32 Drop on demand Ink-Jet.

Drop on demand or impulse ink jet systems differ in two major ways from continuous ink-jet systems. Firstly all the ink droplets are used to form the image, hence none are wasted. Ink droplets are only ejected where a dot is required on the substrate i.e. they are produced on demand.

Secondly, the droplets are not charged. Hence, there is no deflection involved. Instead the droplets are fired in a straight line to the desired position on the paper. This feature highlights an important point , namely that the print head in drop on demand ink jet printing should be as close as possible to the substrate surface so that the ink droplets travel as short a distance as possible to produce accurate images.[12]

In continuous ink-jet systems the droplets can travel greater distances. Consequently, continuous ink-jet systems are more suited to industrial applications such as the printing of rough, irregular surfaces, such as cardboard boxes. In contrast drop on demand ink-jet systems are suited to printing on plain, smooth substrates were higher quality is required.[12]

In thermal or bubble jet printers, a pulsed signal (electric current) in the heater at the tip of the nozzle produces many thousands of sudden temperature rises (to around 300-400 ^{o}C) per second; each of these leads to the formation of a tiny bubble which exerts pressure, causing a single ultra fine droplet, followed by collapse of the bubble, creates a vacuum, drawing new ink to replace the ejected ink and the process starts again (Figure 4).[2]

Droplet ejection may also be effected by a piezoelectric crystal (Figure 5)[2], whereby an electric signal produces a deformation of the crystal which produces a pressure wave in the ink (Figure 2).[13] Seiko Epson (SEC) is the company that developed piezoelectric ink jet into a technology that could compete with thermal ink jet, and all their ink jet printers are based on piezoelectric technology. "HP (about 45% of the world market). SEC (about 20%), (Canon about 18%) and Lexmark (about 14%) currently dominate DOD ink jet printing".[2]

Figure 4: Drop on demand thermal ink jet printing process.[2]

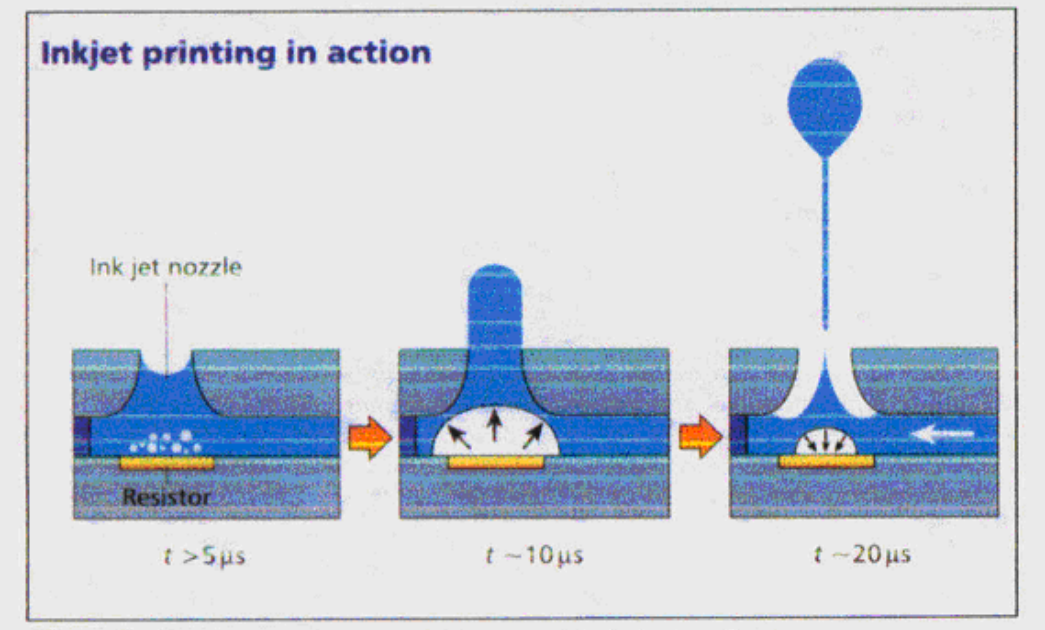

Figure 5: Drop on demand piezoelectric ink jet printing process.[2]

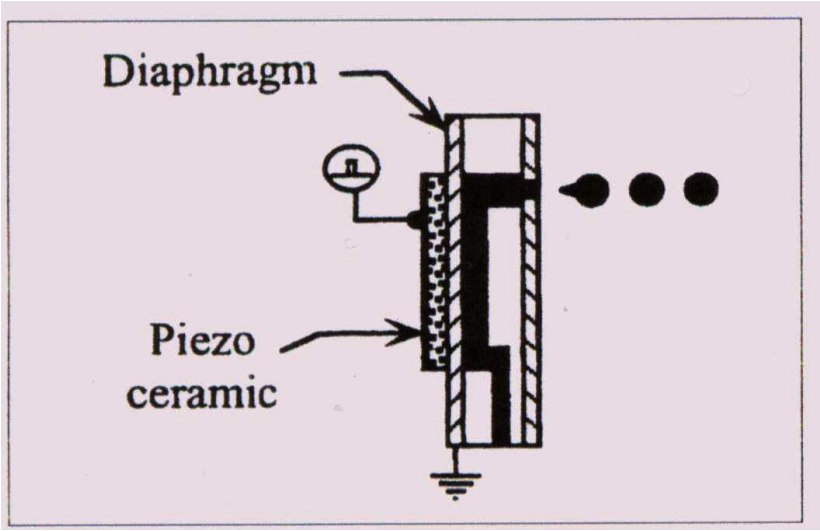

Ink jet printing has achieved its position as the dominant non impact printing technology from a platform of low cost, full colour, very good (and ever improving) quality and reasonable speed. "For example good quality ink jet printers retail for under £50 whereas the cheapest colour laser printer costs about £1000".[2]

1.4 Ink jet inks.

There are three main types of inks, aqueous, solvent, and hot melt. The most common inks for drop on demand ink-jet printers for office quality output are aqueous based inks.[12]

Ink jet inks are made up mainly of water soluble dyes in an aqueous vehicle. Water is chosen as the major solvent for several reasons the three most important being.

- It is an excellent solvent for the dyes used in ink jet printers, namely anionic water soluble dyes.
- It is better than any solvent at bubble formation, indeed thermal ink jet inks must contain a minimum of 30% water for the process to work.[2]
- It is safe (and low cost)

Table 1: Typical ink jet (colour) rough % constituents[2].

Dye(water soluble)	3-6%
Water	70-80%
Humectant	5-10%
Surfactant	1%
Penetrant	2-10%

The functions of the dye and water are fairly apparent. Humectant is needed to prevent evaporation of water from the print head nozzles when the printer is not in use. If evaporation occurs to any extent, dyes crystallize from the ink and form a crust on the nozzle, effectively blocking the nozzle and preventing ink from being ejected. Typical humectants are high boiling point water-miscible compounds such as Diethylene glycol and 2-Pyrrolidone.[14]

Surfactants and penetrants are used to lower surface tension and effect rapid penetration of the ink into the medium being used. Low surface tension (penetrating) inks are used for the ink jet colour inks so that they diffuse very rapidly into the

substrate without lateral spread (Figure 6).[2] This minimizes colour to colour and colour to black bleed. Care has to be taken to ensure that the optical density of the print is acceptable and that "strikethrough", i.e. penetration of the ink to the underside of the medium is avoided. "Pentane-1,5-diol is a typical penetrant, whilst Surfynol 465 is a common surfactant".[2]

Figure 6: Penetrating and non penetrating inks on paper.[2]

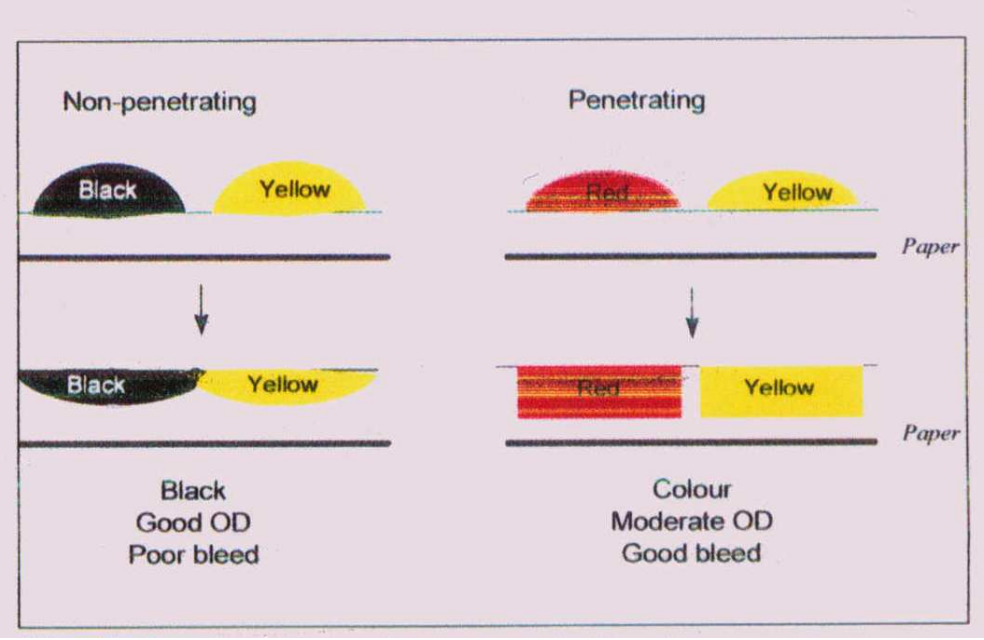

A non penetrating black ink is normally used to produce intense black text. (Bleed is not an issue with printed text since no adjacent colours are present.) Consequently surfactants and penetrants are not normally needed in black inks (Figure 3). The undesirable effects of colour to colour bleed are shown in Figure 7.[2]

Figure 7: Colour inks which (left) bleed and (right) do not bleed.[2]

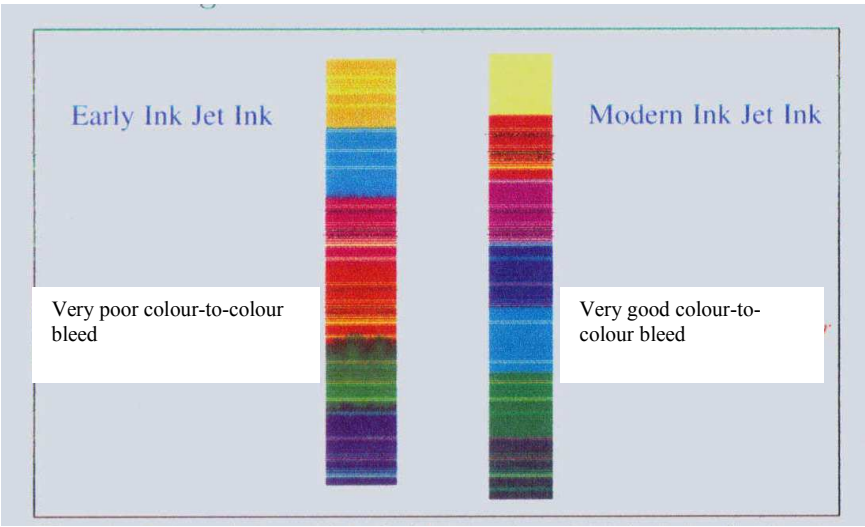

1.5 Ink jet colorants.

"Japanese (Canon and SEC) and American (HP and Lexmark) companies developed ink jet printers. However the colorant expertise needed for the ink resided largely in Europe, with companies such as BASF, Bayer and Hoechst from Germany, Sandoz and Ciba-Geigy from Switzerland and now Avecia(formerly ICI) from the UK"[2].

This mismatch of the electronics set with the chemistry set caused some initial problems. Companies such as HP, Canon and SEC had to develop their own inks using standard, commercially available dyes that were not designed for ink jet use. These first generation "off the shelf" dyes were chosen from existing dyes used for various applications, such as the colouration of paper, textiles and even food.[12,13] However, they had to be purified to much higher standards to meet the more

demanding criteria for ink jet printers. The high levels of purity are necessary to minimize nozzle clogging and print head corrosion.[15]

Anionic water soluble dyes i.e. Dye-SO_3^- are the dyes of choice for ink jet printers. The first generation anionic water soluble ink jet dyes had to fulfil several requirements. Most importantly hue (colour), chroma (vividness), operability (reliability) and safety.[16,17] High thermal stability is an additional requirement of dyes for thermal ink jets, since as mentioned earlier the localized ink temperatures can reach 350^{o}C.[18,19]

Imaging systems use black plus the three subtractive primary colours yellow, magenta and cyan. These three colours are chosen because they are the highest chroma colours available. This can be seen from the colour map (Figure 8).The yellow magenta and cyan colours are the points furthest away from the centre of the colour map and chroma is the distance from the centre to a point in colour space.

Figure 8: Colour map showing yellow, magenta and cyan chroma.[2]

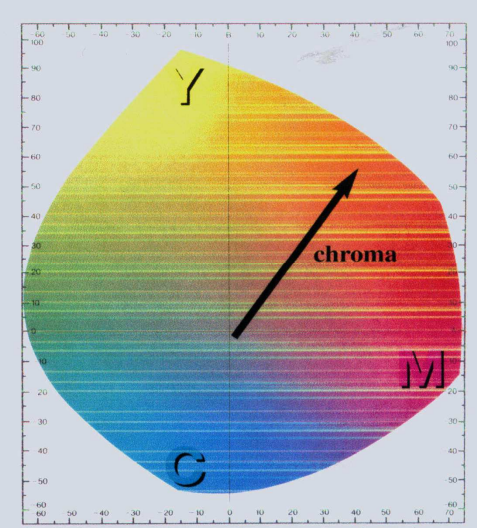

Prints made from vivid, bright colours look much more attractive than prints made from dull colours. Hence the first generation of dyes selected (See Figure 9, p.15) had very vivid colours, such as **1.** [CI Acid yellow 23 (Tartrazine)] used to colour orange juice; the xanthene dye **2.** [CI Acid Red 52] and the Tri-phenylmethane dye **3.** [CI Acid Blue 9]. Both 2 and 3 are paper dyes renowned for their brilliant colours.

Unfortunately, the penalty for this brilliant colour is poor light fastness[17,20], i.e. the dyes fade quickly in light. Chemists at Avecia selected dyes having superior light fastness such as the azo dye **4.** [CI Direct yellow 132], and the Copper phthalocyanine dye **6.** [CI Direct blue 199], whilst Mitsubishi developed the Hydrazone magenta dye **5**.[13] Dyes of this type are used extensively in special media applications such as photorealistic ink jet printing.[2]

Because of the amount of printed text, black is the most important colour. A dye used for colouring liquorice and wine gums, **7.** [CI Food Black 2] was selected as the first generation black dye. It was chosen for several reasons, including its high solubility in water to give a reliable ink[21] and for safety because it is edible.

1.6 Ink jet media.

The substrates are many and varied but are conveniently divided into two basic types (i) (Plain) paper and (ii) special media. For plain paper, print quality (edge activity), water fastness and optical density, especially for black, are the key requirements.[22,23] Special media include photographic type media for photorealistic ink jet printing, vinyl type media for wide format and overhead transparencies.[24]

All of these have in-built mechanisms to give high water fastness.[25] Hence the main dye requirements are high chroma (vividness) and light fastness. For

both special media and plain paper applications, excellent ink operability (reliability) is required. Azo dyes will now be discussed in greater detail as they are the subject of this thesis.

1.7 History of azo dyes.

The discoveries of Azo benzene (Mitscherlich, 1834)[26] and Azoxybenzene (Zinin, 1841)[27] took place in the early days of organic chemistry. Immediately after the beginning of the classic period of this subject, characterised by the work of Kekule[28] and Couper[29], Griess started his attack on the aromatic diazo compounds (1858).[30] His research formed the foundation from which the chemistry of the azo dyestuffs grew to reach its zenith at about the end of the nineteenth century. The problems of azo chemistry were tackled in the most intensive manner, both scientifically and technologically, not only in industrial laboratories, but also in the universities.[29]

On the other hand, the development of aliphatic diazo compounds after Curtius's discovery of Diazoacetic ester (1883)[31] set in only slowly and hesitantly. Two reasons are responsible for this marked contrast to the aromatic analogues. Azo coupling permits introduction of the aromatic azo group into organic molecules, and the aryldiazo compounds are therefore the most important starting materials for the preparation of aromatic azo derivatives, but since in most reactions of the diazoalkanes nitrogen is liberated, alkyldiazo residues can only be rarely introduced in this way. However, for alkylation several reagents other than diazoalkanes can be used, and the splitting off of nitrogen does lead in part to highly unstable intermediates, which frequently give rise to complex products which are difficult to interpret.[29]

Although it was anticipated to a good extent by chemists such as Staudinger,[32] it is no great shock that the systematic and fruitful exploration of the potentialities of the diazoalkanes did not begin before the 1930s. Only then had the necessary development taken place in physical organic chemistry to enable the behaviour of diazoalkanes to be understood.[29]

Figure 9: Dyes discussed.

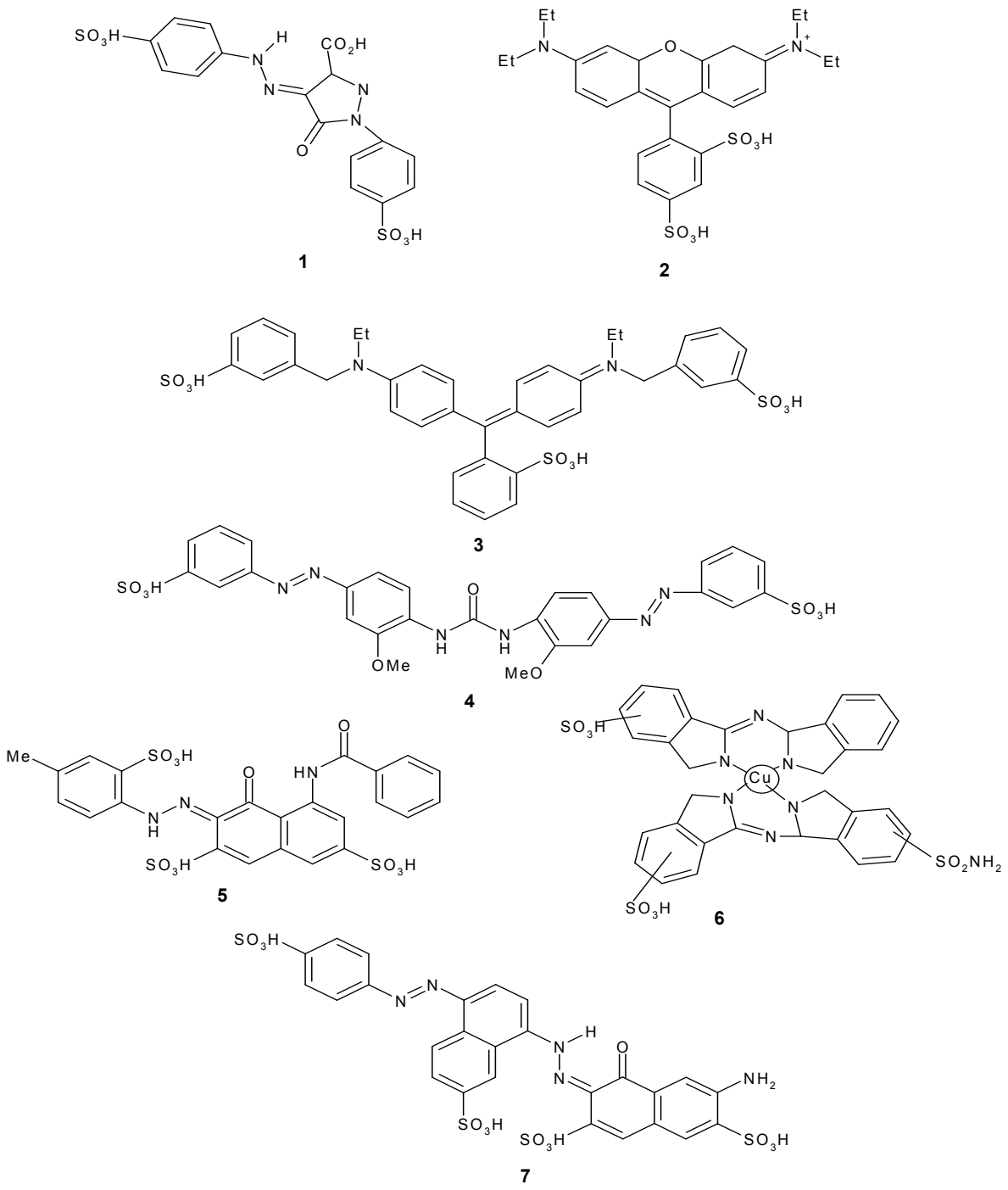

1.8 Useful properties of metallised azo dyes.

Avecia, the sponsors of this project, are interested in the research and development of metallised azo dyes to be used in their ink-jet printer inks. The interest in metallised dyes arises from their useful properties. They often give bright, high intensity colours,[33,34] and the components involved can be varied greatly to give a wide variety of dyes. They also have the advantage of being cost effective due to the materials and conditions used for their manufacture.[35]

As was mentioned in section 1.5 another important quality required for dyes used by the ink-jet printing companies is that the dye/ink has a good light fastness (i.e. does not fade). Azo dyes do have a relatively good light fastness but they do fade over time.[36,37] The main reason for the fading is due to the oxidation and reduction of the compounds.[38-40] Metallised azo dyes have an improved light fastness compared with the unmetallised dyes.[40-42] The main reasons suggested for this are the ability of the metal to protect, by both steric and electronic effects, the azo-hydrazo nitrogen atoms from attack by reactive species, for example, singlet oxygen and radicals.[42-47] Metals can promote aggregation of the dye, and this leads to an improvement in light fastness.[47-49]

1.9 Issues with azo dyes and metallised azo dyes.

1.9.1 Variety of possible complexation modes.

Some azo dyes have more than one metal co-ordination site, and this can lead to a variety of possible complexation modes and the formation of complexes with, for example, 1:2, 1:1, 2:1, 2:2 or more complex metal to ligand stoichiometries.

1.9.2 Azo/hydrazone tautomerism.

Another complication arises because some azo dyes can undergo azo/hydrazone tautomerism.[50-54] This is common when there is an hydroxyl group in an ortho or para position to the azo group[54-57], viz:

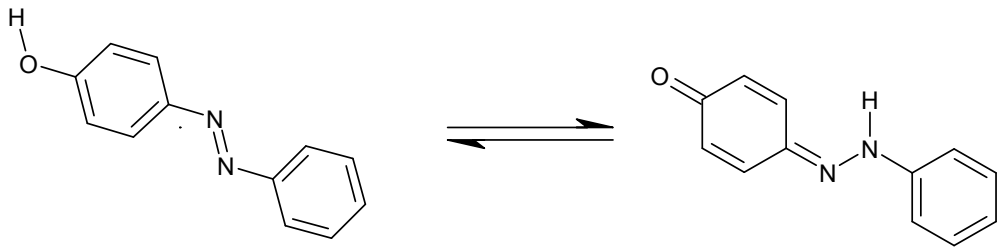

Azo form **Hydrazone form**

Attempts have been made to characterize azo tautomers by UV-Visible[58.59], infra-red[60-62], Raman[63,64], ^{1}H NMR[65-68], ^{13}C NMR[67-69], ^{15}N NMR[67-70], ^{19}F NMR spectroscopy[71], X-ray crystallography[72,73] and mass spectroscopy[74]. The main points to be noted are that some tautomeric forms are more stable than others, and the position of the tautomeric equilibrium can be affected greatly by pH[75], solvent used[76-78] and temperature.[79] Some azo dyes can exist as a mixture of the two species in sometimes varying ratios depending on conditions and state.[76-83] The equilibrium of the two tautomeric species can also be effected by the substituent R groups attached to the dye. It has been found that electron donating R groups tend to favor the azo form,[84] whereas electron withdrawing groups stabilize the hydrazone structure[85].

Figure 10: Some azo dyes previously studied.

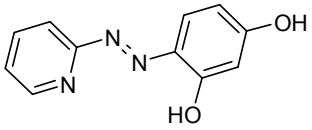

PAR

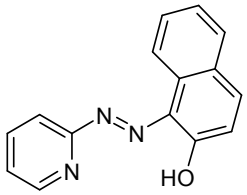

PAN

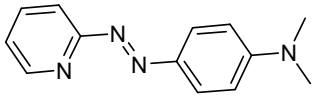

PADA

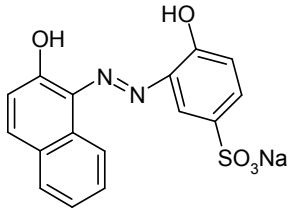

SOLOCHROME VIOLET

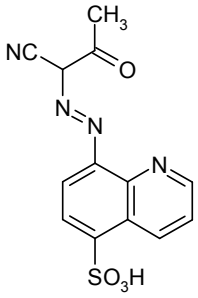

8-(1-Cyano-2-oxo-propylazo)-quinoline-5-sulfonic acid

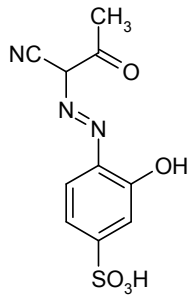

4-(1-Cyano-2-oxo-propylazo)-3-hydroxy-benzenesulfonic acid

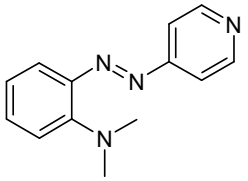

DPAP

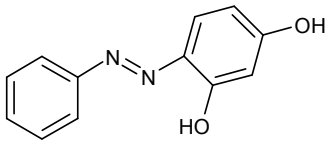

SUDAN ORANGE

Many tautomeric forms are also difficult to characterize as often they can have the same characteristic UV-Visible, infra-red and NMR spectra.[86-93] Keto hydrazones have bonds that undergo a bathochromic shift compared to their counterpart hydroxyazo forms.[94] In UV-Visible spectra ketohydrazones also have higher molar extinction coefficients.[95]

Molecular mechanics calculations, and gas phase energy predictions have been carried out on some azo tautomers,[96-99] in order to obtain a better understanding of which forms are the most stable from a theoretical viewpoint. Research in the field is still being carried out to gain a fuller understanding of azo dye tautomers and tautomeric effects.

1.9.3 Aggregation of azo dyes.

It has been established that aggregation of azo dyes can occur stepwise to give dimers and higher oligomers.[100-105] Aggregation usually occurs by π–stacking of the flat molecules, and the growth is unidirectional. It is reported that aggregates larger than dimers form at concentrations in excess of 1 mmol dm^{-3}.[104-107]

The monomer–dimer equilibrium of SOLOCHROME VIOLET has been studied by spectrophotometry.[108] Previously it has been studied by potentiometry,[109] conductivity,[110] and calorimetry.[110-111] The concentration range over which the dimerization equilibrium can be studied is severely limited by the formation of higher aggregates.[112-115] The dimer formation constant K_D was found to be in the region of 10^3 dm^3 mol^{-1}, and at dye concentrations of 10^{-5} mol dm^3 dimerization is found to be less than 1%.[100-105]

1.9.4 Ageing of azo dyes.

It has been found that the visible absorption curves of many of the dye solutions change due to ageing effects. Measurements were made as a function of solution age, and showed very small changes of the absorption curves with concomitant changes in the computed dimerization constants and dimer spectra.[116]

It was established that the ageing of solutions was due to physical changes as opposed to chemical decomposition.[117-118] They illustrated this by taking aged dyes and analysing them with high resolution chromatography using Sephadex G–25 columns. No new bands were found when compared with fresh solutions of the dyes. These physical effects have been put down to the fact that supersaturated solutions of the dyes can be produced with ease, and at the concentrations used the dyes slowly nucleate.[117-119]

The factor of dye ageing is important in that if the absorbances are changing due to the physical changes it may mean that dyes will have to be made fresh every time a study is carried out. Another solution could be to prevent the nucleation and super saturation by working in non aqueous media.

1.9.5 Metal complex stabilities.

In solution the reaction between a metal ion (M) and a ligand (L) involves substitution of co-coordinated solvent molecules (S) by the incoming ligand. Leaving out charges for convenience:

$$MS_m + nL \rightleftharpoons MS_{m-x}L_n + xS \quad (1)$$

Equation (1) may be abbreviated as equation (2)

$$M + nL \rightleftharpoons ML_n \quad (2)$$

The overall formation constant associated with reaction (2) is given by equation (3)

$$\beta_n = \frac{[ML_n]}{[M][L]^n} \qquad (3)$$

The stepwise formation constants (K_n) are related to the overall formation constants (β_n) by equation (4).

$$\beta_n = K_1 K_2 K_3 \ldots\ldots\ldots K_n \qquad (4)$$

Stepwise formation constants relate to the process of consecutive substitution as shown:

$$M + L \rightleftharpoons ML \; ; \quad K_1 = \frac{[ML]}{[M][L]}$$

$$ML + L \rightleftharpoons ML_2 \; ; \quad K_2 = \frac{[ML_2]}{[ML][L]}$$

$$ML_{n-1} + L \rightleftharpoons ML_n \; ; \quad K_n = \frac{[ML_n]}{[ML_{n-1}][L]}$$

Stepwise and overall formation constants are often measured either potentiometrically, by UV-Visible spectroscopy, or by other spectroscopic methods e.g. NMR. Visible spectrophotometry is a convenient method for studying azo–dye metal reactions.

Complex stability can also be investigated through the kinetics of metal complex formation (k_f) and dissociation (k_d) to obtain equilibrium constants (K) using equation (5)

$$K = k_f/k_d \qquad (5)$$

For labile metal ions rate constants for metal complex formation (k_f) are often determined by direct stopped-flow measurement. Kinetics of dissociation (k_d) can also be determined either by metal exchange (equation 6) or by ligand exchange studies (equation 7):

$$ML + M' \rightleftharpoons M'L + M \qquad (6)$$

$$ML + L' \rightleftharpoons ML' + L \qquad (7)$$

To study reactions of type (6), either an excess of M', or an M' that forms a more stable complex with Ligand L is used. Reaction (7) requires L' to form a more stable complex than ligand L with the metal ion M.

1.9.6 Previous kinetic studies of reactions of azo-dye ligands with metal ions.

The kinetics of the complexation of lanthanide ions[120] and d–block first row transition metal ions with PAR and PAN has been reported.[121-132] The bonding between PAR and Eu^{3+} was investigated by kinetic studies using the stopped–flow method.[133]

Comparison of the visible spectra associated with the ligands SUDAN ORANGE bonded to Eu^{3+}, and 2-(2-Hydroxyphenyliminomethyl)-pyridine and 2-(Saliclideneamino)pyridine to Cu^{2+} with the visible spectra of PAR bonded to Eu^{3+} and Cu^{2+} were carried out to establish the mode of coordination of the complexes.[134]

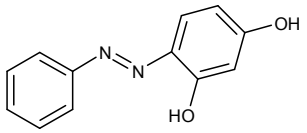

SUDAN ORANGE

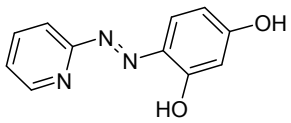

PAR

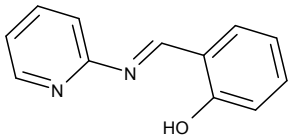

2-(Saliclideneamino)pyridine

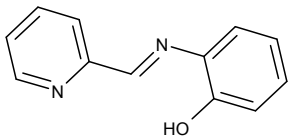

2-(2-Hydroxyphenyliminomethyl)-pyridine

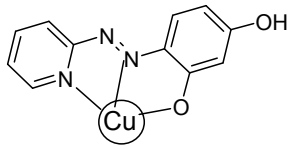

Mode of coordination of Cu(II) with PAR

It was found that coordination occurs through the pyridine N-atom, the N-atom of the azo group furthest from the pyridine, and the deprotonated OH-group of the ligand PAR.

The kinetics of chelation of pyridylazo ligands with Ni(II) has been studied. The ligands investigated were predominantly the bidentate ligand Dimethyl-[4-(pyridine-2-ylazo-phenyl)]amine (PADA),[135-138] and the terdentate ligands 4-(2-Pyridylazo)resorcinol (PAR), and 1-(2-Pyridylazo)-2-napthol (β-PAN).[121-132] The stoichiometries of the reactions vary between dyes. When excess Ni(II) is reacted with PADA it forms a 1:1 Ni(II)-dye complex, and the rate determining step is loss of the first water molecule from the inner co-ordination sphere of the $[Ni(H_2O)_6]^{2+}$ ion.[135] Chelation of Ni(II) by β-PAN is reported to give a 1:1 complex with a large excess of Ni(II), but a 1:2 complex is formed when a moderate excess of metal is used.[121] Chelation of Ni(II) and cobalt(II) by PAR is reported to give the 1:2 metal:ligand complexes with an excess of metal ion.[123]

The large difference between the reactivity of PAR and β-PAN with Ni(II) and Co(II) has been examined.[125,139,140] The value for the formation rate constant k_f for the chelation of Ni(II) by PAR is close to that expected if the loss of the first water from the co-ordination shell of the metal is the rate determining step.[123] The 1:2 metal:ligand complex is the product formed, and the rate constant for adding a second PAR molecule is larger than adding the first.[123] This raises the possibility that stacking interactions between the dyes may be important in forming the bis complex. Azo dyes do have a tendency to stack.[134]

The value of k_f for forming the 1:1 $[Ni(\beta\text{-PAN})]^+$ complex using a large excess of Ni(II) is significantly less than that expected if first bond formation were the rate determining step.[125]

Using β-PAN in excess over Ni(II), it was found that the rapid chelation gave firstly the mono(dye) Ni(II) complex, and then the 1:2 complex, $Ni(dye)_2$.

At pH 8 and Ni(II) concentrations < 0.4 mmol dm^{-3}, it was established that the rate determining step is the initial substitution to form a unidentate intermediate. At high Ni(II) concentrations ≥ 0.1 mol dm^{-3} the rate–determining step changes to that of ring closure. At Ni(II) concentrations near 0.01 mol dm^{-3}, initial ligation and ring closure proceed at comparable rates, and rate constants for both steps were estimated.[125]

The kinetics of complexation of Ni(II) in water with other azo dye ligands has been studied. The mechanism generally accepted for the reactions involves rapid formation of an outer–sphere complex between the two reacting species, followed by the rate limiting replacement of a water molecule in the inner co-ordination sphere by the ligand as shown. [129]

$$[Ni(H_2O)_6]^{2+} + L \underset{}{\overset{K_0}{\rightleftharpoons}} [Ni(H_2O)_6]^{2+}....L$$

$$[Ni(H_2O)_6]^{2+}....L \xrightarrow{k_{ex}} [Ni(H_2O)_5L]^{2+} + H_2O$$

This mechanism has been written for the case of a neutral monodentate ligand; when the incoming ligand is multidentate additional steps leading to ring closure must be considered. Usually the release of the water molecule often remains the rate limiting

step of the complexation reaction. If the concentration of the outer-sphere complex is small the rate constant for the complex formation k_f is given by the expression:

$$k_f = K_o \; k_{ex}$$

k_{ex} is equal to the rate constant for total solvent exchange, and K_0 is the outer–sphere pre–association constant. K_0 can be estimated through the following theoretical equation derived independently by Fuoss and Eigen.[129]

$$K_o = \frac{4\pi N a^3}{3000} \; e^{-U(a)/kT}$$

$$where \; U(a) = \frac{z_1 z_2 e^2}{Da}$$

a represents the minimum distance of approach between the metal solvate and the ligand, $U(a)$ represents the electrostatic potential at that distance, e is the charge of the electron, z_1 and z_2 are the charges of the metal solvate and ligand, D is the dielectric constant of the solvent and all the other symbols have their usual meaning. Although values of observed rate constants k_f for substitution reactions in water are usually in good agreement with those evaluated by the product $K_0 k_{ex}$, it is sometimes inadequate to predict the values of rate constants in non aqueous solvents.[141–144] This observation is relevant to reactions with multidentate ligands which sometimes produce steric retardation in one of the steps of ring closure,[143–145] and in other cases enhance their reactivity through an extra electronic interaction during the formation of the outer–sphere complex (such as π–stacking).[146–147] If kinetic studies of Ni(II) chelation are performed in non–aqueous solvents to reduce ageing effects, such predictions will need to taken into account.

Studies of the reactions of metal ions with the dye DPAP have been made in a variety of non–aqueous solvents, methanol, Dimethylformamide and Dimethylsulphoxide. Dimethylsulphoxide was the solvent used for studies of the reactions of PAR and PAN.[129] At 25 ^{o}C, the rate constants k_f for Ni(II)–DPAP in methanol, Dimethylformamide and Dimethylsuphoxide were found to be 3.6×10^3, 4.4×10^3 and 7.9×10^2 dm^3 mol^{-1} s^{-1} respectively, and the rate constants for [Ni (PAN)]$^+$ and [Ni(PAR)]$^+$ were 8.0 x 10^2 and 0.6 x 10^2 dm^3 mol^{-1}s^{-1}.[129]
The cause of the variation in formation rates with changes in the solvent can usually be traced to variations in either k_{ex} or K_0.[148]

These studies are useful for the research being undertaken here, in that it gives a method of determining the position of metal binding by the reaction of metal with compounds similar to the ligand being studied, and it helps to clarify which atoms of the ligand play the biggest role in the colourimetric reaction.

1.9.7 pK_a measurements.

Acid dissociation constants of 8-(1-Cyano-2-oxo-propylazo)-quinoline-5-sulfonic acid and 4-(1-Cyano-2-oxo-propylazo)-3-hydroxy-benzene sulfonic acid were determined potentiometrically over the pH range 5-12. The pK_a values were found to be pK_{a1} = 3.13 and pK_{a1} = 12.12 for each dye respectively.[149]

pK_a values of PAN and PAR were determined spectrophotometrically and electrochemically in 50% dioxane–water mixtures at dye concentrations of 10^{-6} mol dm^{-3}. The pK_a values for PAN were determined to be pK_{a1} = 2.90 and pK_{a2} = 12.20, and for PAR, pK_{a1} = 2.69, pK_{a2} = 12.41 and pK_{a3} = 12.60.[150,151]

pK_a values of SUDAN ORANGE were determined potentiometrically over the pH range 9-14 in both water and ethanol and were found to be pK_{a1} = 12.42 and pK_{a2} = 12.81 and pK_{a1} = 12.65 and pK_{a2} = 12.91 respectively.[152]

pK_a values of C.I pigment red and SOLOCHROME VIOLET were determined spectrophotometrically in water over the pH range of 2-13 and were found to be pK_{a1} = 3.42 and pK_{a2} = 12.39 and pK_{a1} = 12.45 and pK_{a2} = 12.60 respectively.[153]

pK_a values of AMIDONAPTHOL were determined potentiometrically in acetonitrile over the pH range of 5-13 and were found to be pK_{a1} = 7.61 and pK_{a2} = 12.61.[154] For dyes and values see Figure 11(p.29).

1.9.8 Stability constant measurements.

Stability constants for the metal complexes of PAN[155,156], PAR[157,158], SUDAN RED B[159], p-Cl-Phenylazo-R-acid[160], TRIAP[161] and METRIAP[162] with a range of metal ions have been determined either spectrophotometrically or potentiometrically. A summary of the results can be seen in Table 2. For dyes see Figure 12(p.30).

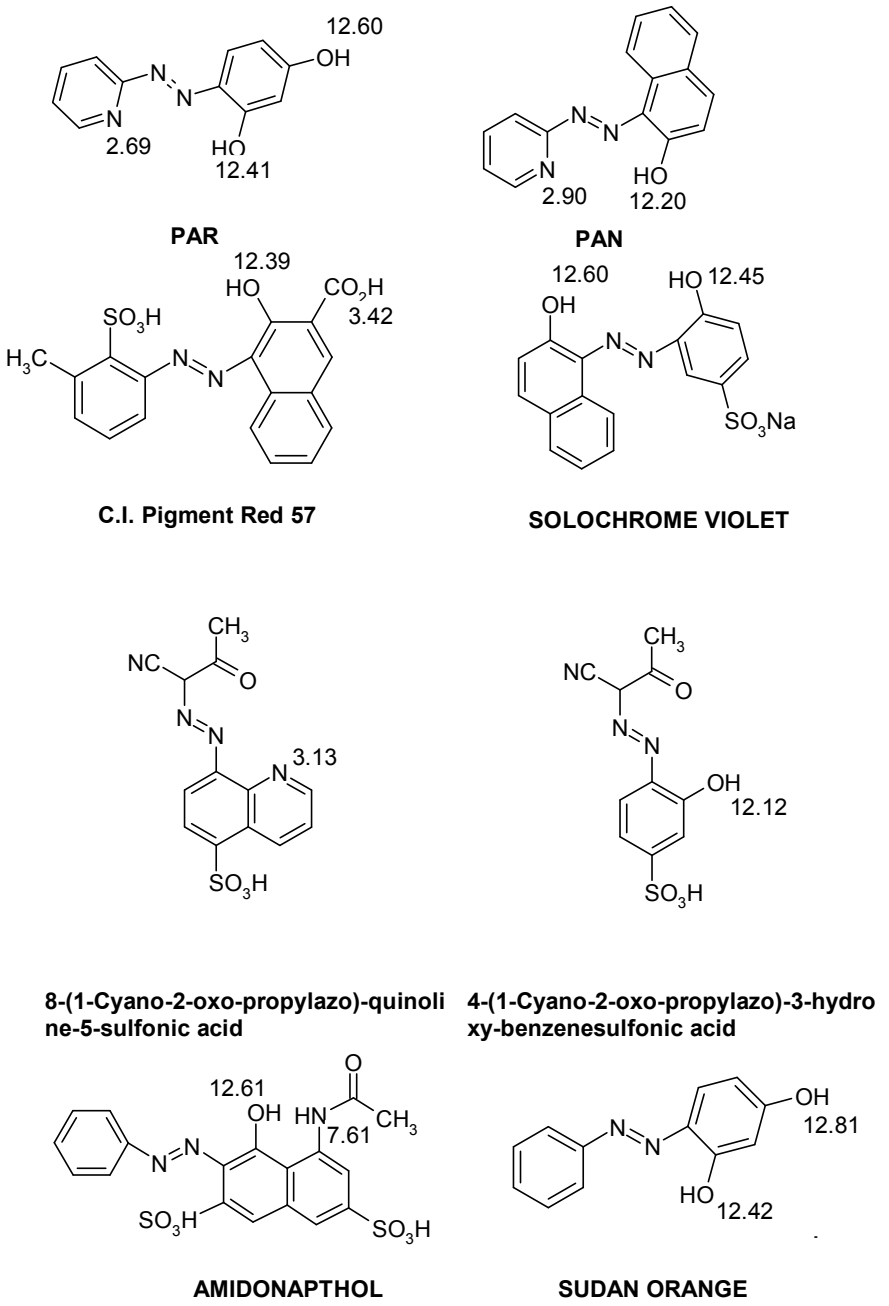

Figure 11: pK_a values of previously studied azo dyes. (For refs see p.27-28)

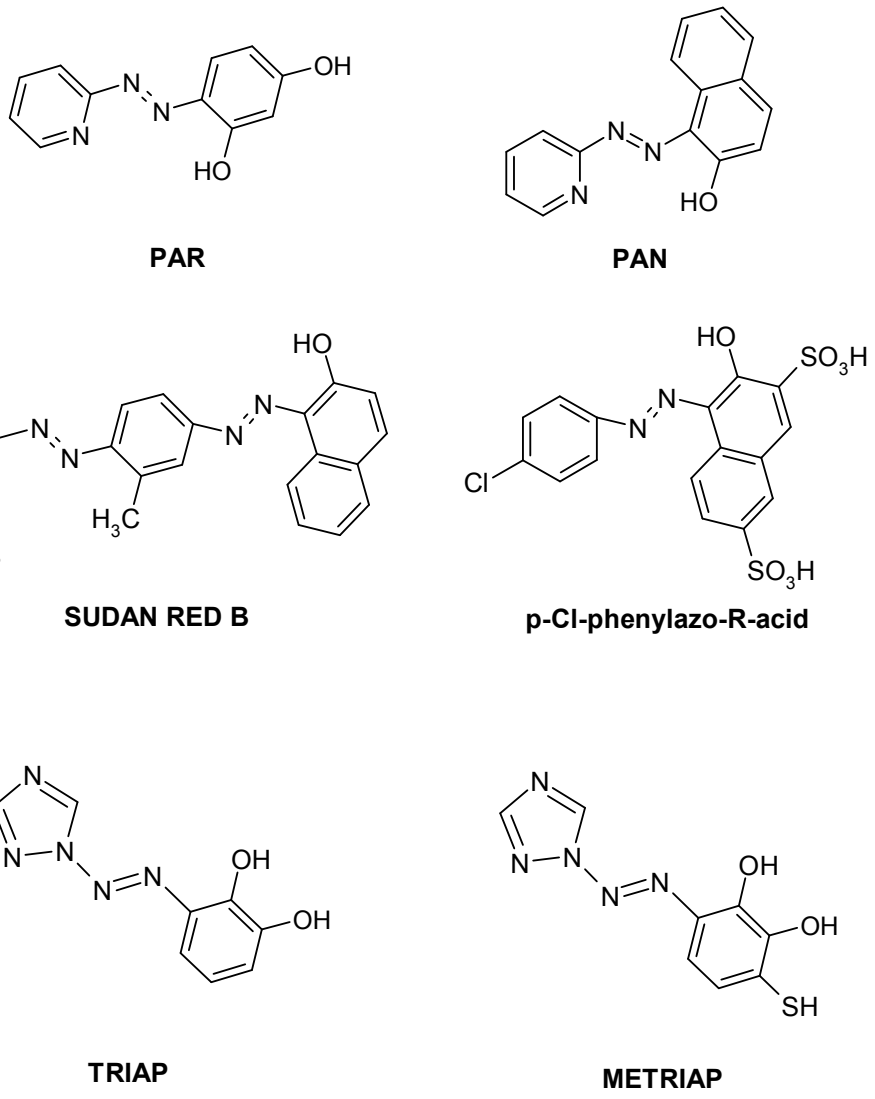

Figure 12: Dyes involved in stability constant measurements. (For refs see p.28)

Ligand	Medium	Metal ion	log K_1	log K_2
PAN	50% dioxane-water	Mn^{2+}	8.5	7.9
		Co^{2+}	12.15	12.01
		Ni^{2+}	12.7	12.6
		Zn^{2+}	11.2	10.5
PAR	Aqueous	Mn^{2+}	9.7	9.2
		Co^{2+}	14.8	8.2
		Ni^{2+}	13.2	12.8
		Zn^{2+}	12.4	11.1
p-Cl-phenylazo-R-acid	Aqueous	Pd^{2+}	8.6	3.8
SUDAN RED B	Aqueous	Mn^{2+}	7.5	N/a
		Fe^{2+}	8.3	N/a
TRIAP	50% aqueous methanol	Al^{3+}	8.4	N/a
METRIAP	50% aqueous methanol	Al^{3+}	12.6	N/a

Table 2: Stability constants of some metal azo dye complexes. (For refs see p.28)

1.9.9 Crystal structures of azo dyes and azo dye metal complexes.

Crystal structures have been found for a variety of mono azo dyes by X-ray crystallography. Some dyes crystallise in the azo form, namely Disperse red 167,[163] TAN,[164] 2,2-Azobipyridine,[165] 2,6-Dimethyl-4-(phenyldiazenyl)phenol,[166] 3,4-Dichlorodimethylamino-azobenzene,[167] PAN,[168] o-Amino-azotoluene,[169] 3-Methoxy-5-(4-methylphenyldiazenyl)salicylaldehyde,[170]5-Allyl-3-methoxy-2-(*p*-tolylsulfonyloxy)azobenzene[171] and 4-[(2-Chloro-4-nitrophenyl)-diazenyl]phenol[172] (Figure 13, p.33).

Other dyes, namely 1-[(4-Formylphenyl)hydrazono]naphthalen-2(1H)-one,[173-174] 2-Chloro-3,4-dimethoxybenzaldehyde(4-nitrophenyl)hydrazone,[175] SUDAN RED G,[176] 3-Hydroxy-4-methoxybenzaldehyde(pyridine-2-carbonyl)hydrazone,[177] 3,4-(Methylenedioxy)benzaldehyde-benzoylhydrazone,[178] 2-Nitrobenzaldehyde picoloylhydrazone,[179] Pyridine-2-carboxaldehyde picoloylhydrazone,[180] SUDAN I[176] and 5-Bromo-2-hydroxybenzaldehyde-(4-phenyl-1,3-thiazol-2-yl)hydrazone[181] crystallise in the hydrazone form (Figure 14, p.34).

Crystal structures of mono azo dye metal complexes have also been found for bis-(SUDAN I)Cu(II),[182] bis(2-Anthranilic acid-azo-5-butyl-2-phenol)Al(III),[183] bis(2-Anthranilic-acidazo-2-napthol)Al(III),[183] and bis(2-Anthranilic acidazo-3-methyl-1-phenylpyrazol-5-one)Al(III) (Figure 15, p.35).[184]

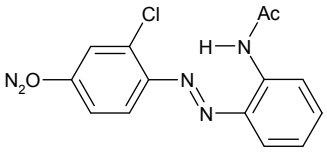

Disperse Red 167

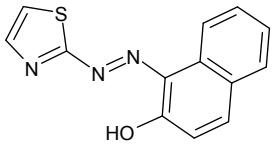

TAN

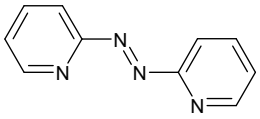

2,2-Azobipyridine

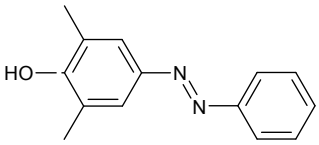

2,6 Dimethyl-4-(phenyldiazenyl)phenol

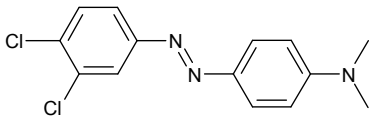

3,4-Dichloro-4-dimethylaminoazobenzene

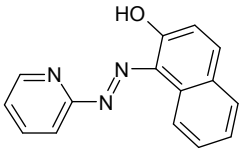

PAN

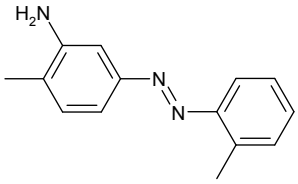

o-Aminoazotoluene

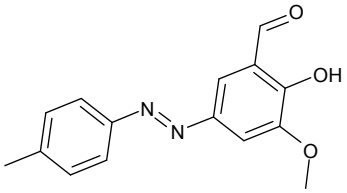

3-Methoxy-5-(4-methylphenyldiazenyl)salicylaldehyde

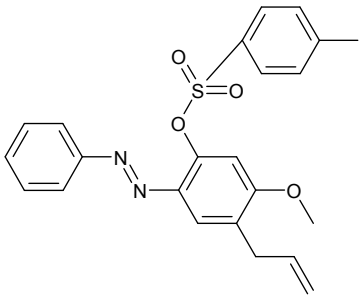

5-Allyl-3-methoxy-2-(p-tolysulfonyloxy)azobenzene

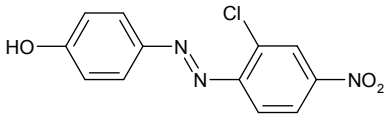

4-[(2-Chloro-4-nitrophenyl)diazenyl]phenol

Figure 13: Dyes found in the azo form by X-ray crystallography.

(For refs see p.32).

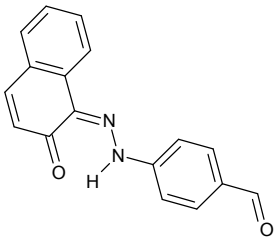

1-[(4-Formylphenyl)hydrazono]napthalen-2(1H)-one

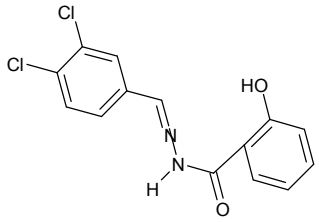

3,4-Dichlorobenzaldehyde(2-hydroxybenzoyl)hydrazone

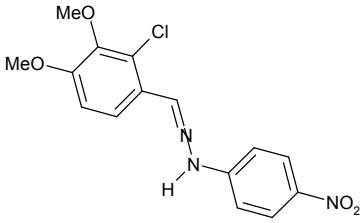

2-Chloro-3,4-dimethoxybenzaldehyde(4-nitrophenyl)hydrazone

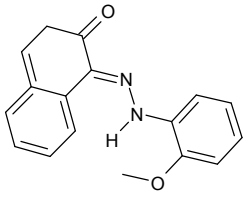

SUDAN RED G

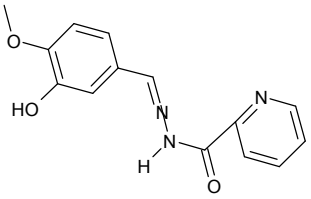

3-Hydroxy-4-methoxybenzaldehyde(pyridine-2-carbonyl)hydrazone

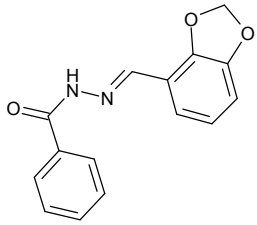

3,4-(Methylenedioxy)benzaldehyde benzoylhydrazone

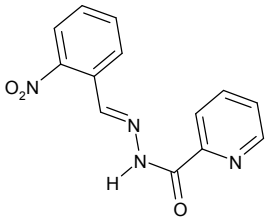

2-Nitrobenzaldehyde picoloylhydrazone

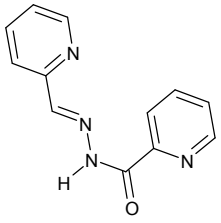

Pyridine-2-carboxaldehyde picolylhydrazone

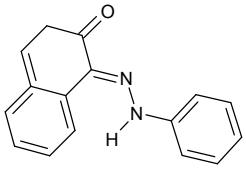

SUDAN I

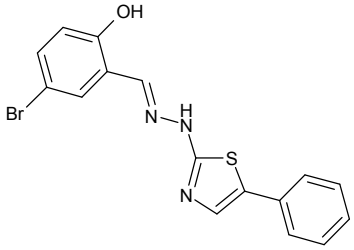

5-Bromo-2-hydroxybenzaldehyde(4-phenyl-1,3-thiazol-2-yl)hydrazone

Figure 14: Dyes found in the hydrazone form by X-ray crystallography.

(For refs see p.32)

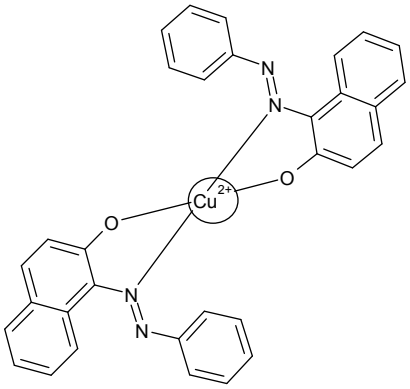

bis(Sudan I)Cu(II)

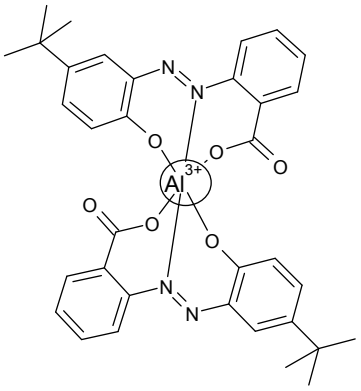

bis(2-Anthranilic acid-azo-5-butyl-2-phenolato)Al(III)

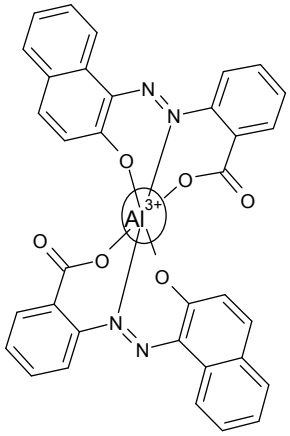

bis(2-Anthranilic acid-azo-2-naptholato)Al(III)

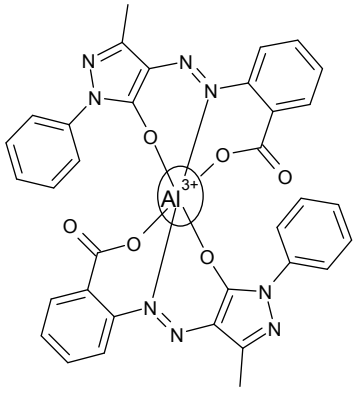

bis(2-Anthranilic acid-azo-3-methyl-1-phenylpyrazol-5-one)Al(III)

Figure 15: Azo dye metal structures found by X-ray crystallography.

(For refs see p.32)

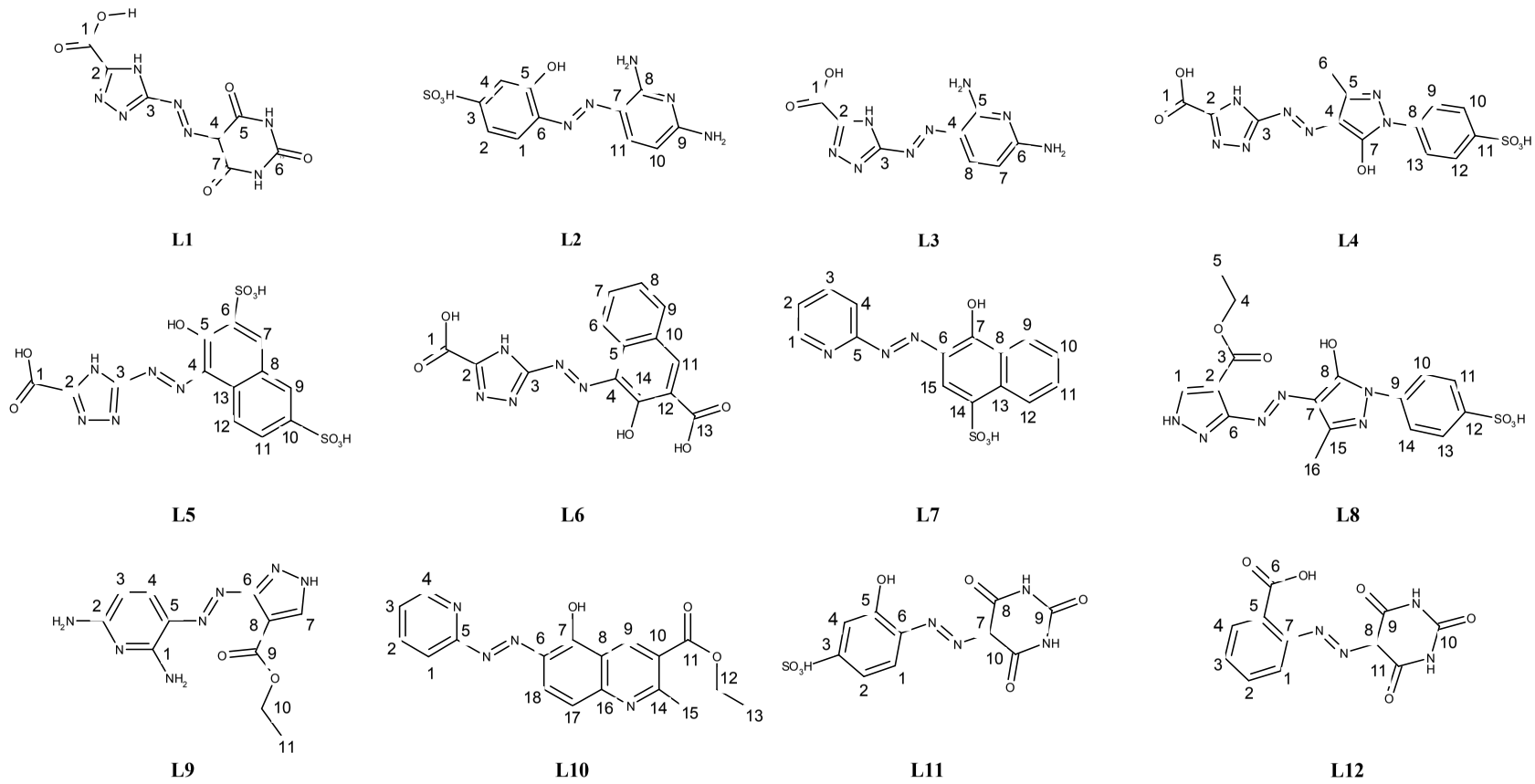

Figure 16: Azo dyes L1-L12 showing atom assignments.

36

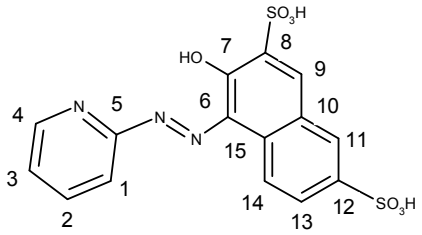

L3765

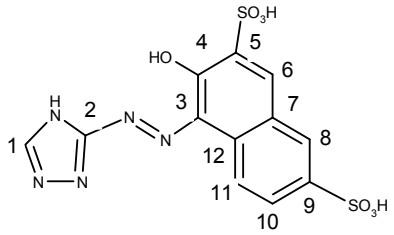

L5B

Chapter 2: Azo dye syntheses and characterisation.

Introduction.

The azo dye ligands L1-L12 have been synthesised(See p.36, Chapter 1), and two others (L5B and L3765) were obtained as gifts from the chemical company Avecia. The dyes were characterised using ^{1}H NMR, ^{13}C NMR, IR spectroscopy, electrospray mass spectroscopy, atomic absorption spectroscopy, UV-Visible spectroscopy and microanalysis. Melting points were also determined.

2.1 Synthesis of Azo dyes L1-L12.

Materials and equipment. All chemicals were supplied by the Aldrich chemical company, were of the highest available purity and were not purified further. NMR spectra were recorded with a Bruker Avance 500 MHz spectrometer, mass spectra with an Hewlett Packard 5989B (Electro spray) MS Engine spectrometer, UV–Visible spectra with a Perkin Elmer lambda 25 spectrometer, infra-red spectra with a Perkin Elmer spectrum 1 FTIR Spectrometer, and melting points with a Gallencamp melting pointing apparatus. Microanalyses were obtained commercially from AVECIA and Warwick Analytical Services.

2.1.1 Formation of 5-(2,4,6-Tri-oxo-hexahydropyrimidin-5-ylazo)-4H[1,2,4]triazole-3-carboxylic acid (L1).

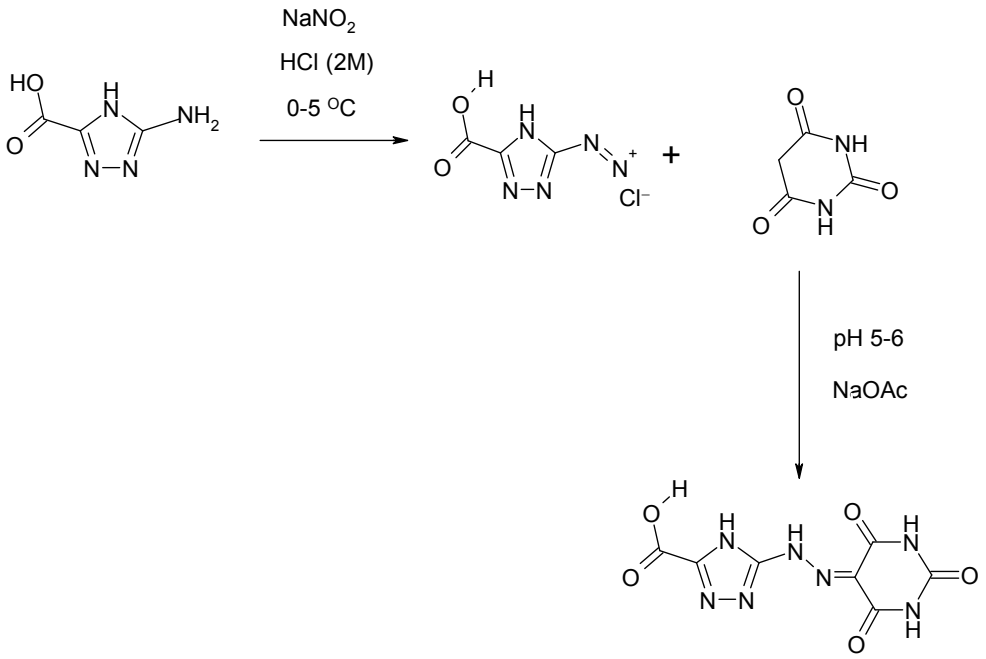

To an aqueous solution of 5-Amino-4H-[1,2,4]triazole-3-carboxylic acid (5.08 g, 0.04 mol) in distilled water (150 cm^3) was added sodium nitrite (2.76 g, 0.04 mol) and the mixture stirred for 10 minutes until the sodium nitrite had dissolved. HCl (2 mol dm^{-3}; 10 cm^3) and distilled water (50 cm^3) were mixed in a separate beaker (1000 cm^3) which was placed in an ice bath to keep the temperature between zero and 5 ^OC. The triazole/nitrite solution was then added to the cold diluted HCl. The reaction mixture was left to stir for 30 minutes and the temperature was maintained between 0 and 5 ^OC by adding more ice when required. To establish that an active diazonium solution has formed a compound known as H ACID (shown overleaf) was used.

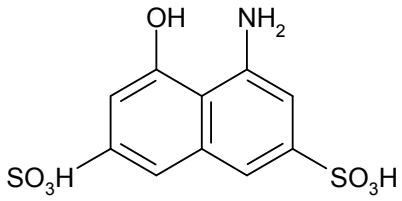

4-Amino-5-hydroxy-napthalene-2,7-disulfonic acid (H ACID)

This compound was used because it reacts rapidly with the diazonium salt. An aqueous solution of H ACID (0.5 mol dm^3) was spotted onto a filter paper and a few drops of the diazonium solution were added by Pasteur pipette. The colour changed from brown to crimson and hence this showed that the diazonium salt was present.

Any unreacted excess sodium nitrite was quenched by the use of an excess of sulfamic acid. A few spatulas full were added to the solution until no more nitrogen gas was evolved and hence the solution stopped effervescing. This was carried out so that there is no sodium nitrite around to cause any unwanted diazotisation of the coupling components.

The coupler Pyrimidine-2,4,6(1H,3H,5H)-trione (5.12 g, 0.04 mol) was dissolved in distilled water (100 cm^3). The diazonium solution was slowly added over 25 minutes to the coupler whilst maintaining a pH between 5-6 with the addition of sodium acetate and using a pH meter. The reaction mixture was left to stir for 2 hours once the addition of the diazonium salt was complete. The solution was tested with H ACID to show that the diazonium salt had all been converted to the azo product i.e. the brown colour no longer faded to crimson.

To establish the best method of product separation from the solution three 5 cm^3 aliquots of the solution were treated respectively with HCl (2 mol dm^3; 5 cm^3), four spatulas of solid NaCl and acetone (5 cm^3). Acetone helped separation the best and

to the remainder of the mixture was added acetone (500 cm^3) and stirred for 1 hour. The product was collected by filtration and dried in an oven for 16 hours at 60 ^oC. 11.0 g of a yellow powder was obtained.

To remove excess sodium and inorganic ions from the product it was partially dissolved in distilled water (2 dm^3) and the dye solid/solution mixture was added and suspended in dialysis tubing. A bucket was filled with 3 dm^3 of water and its conductivity reading taken and found to be 3 $\mu S/cm^{-1}$. The tubing and sample were placed into the bucket. The conductivity reading of the water increased to a value of 180 mS cm^{-1} after 30 minutes. The water was then changed every 30 minutes for 1.5 hours and tested each time until a constant conductivity reading of 20 $\mu S/cm^{-1}$ was achieved.

The sample was collected then dried in an oven at 60 ^oC overnight for 16 hours.

Yield: 10.12 g, 0.038 mol.

Ligands L2-L6, L11 and L12 were synthesised in the same way as L1. Amounts and conditions that varied are shown below. The molar amounts of sodium nitrite used were the same as the respective molar amounts of the diazonium components.

2.1.2 Formation of 4-(2,6-Di-aminopyridin-3-ylazo)-3-hydroxy benzene sulfonic acid (L2).

From 4-Amino-3–hydroxybenzenesulfonic acid (7.60 g, 0.04 mol) 2,6-Di-aminopyridine (4.37 g, 0.04 mol) coupled at pH 4–5. Yield: 9.20 g, 0.032 mol,

2.1.3 Formation of 5-(2,6-Di-amino-pyridin-3-ylazo)-4H-[1,2,4]triazole-3-carboxylic acid (L3).

5-Amino-4H-[1,2,4]triazole-3-carboxylic acid (6.40 g, 0.05 mol) and 2,6-Di-amino-pyridine (5.46 g, 0.05 mol) coupled at pH 4–5. Yield: 9.74 g, 0.039 mol.

2.1.4 Formation of 5-[5-Hydroxy-3-methyl-1-(4-sulfo-phenyl)-1H-pyrazol-4-ylazo]-4H-[1,2,4]triazole-3-carboxylic acid (L4).

From 5-Amino-4H-[1,2,4]triazole-3-carboxylic acid (6.40 g, 0.05 mol) and 4-(5-Hydroxy-3-methyl-pyrazol-1-yl)-benzenesulfonic acid (13.25 g, 0.05 mol) coupled at pH 5. Yield 15.00 g, 0.038 mol.

2.1.5 Formation of 5-(2-Hydroxy-3,6-di-sulfo-napthalen-1-ylazo)-4H-[1,2,4]triazole-3-carboxylic acid (L5).

From 5-Amino-4H-[1,2,4]triazole-3-carboxylic acid (3.84 g, 0.03 mol) and 3-Hydroxynapthalene-2.7-di-sulfonic acid (10.44 g, 0.03 mol) coupled at pH 8-9. Yield: 3.30 g, 0.0074 mol.

2.1.6 Formation of 5-(3-Carboxy-2-hydroxy-napthalen-1-ylazo)-4H-[1,2,4]triazole -3-carboxylic acid (L6).

From 5-Amino-4H-[1,2,4]triazole-3-carboxylic acid (5.08 g, 0.04 mol) and Carboxy-2-hydroxynapthalene(7.52g, 0.04 mol) coupled at pH 6. Yield: 6.24 g, 0.019 mol.

2.1.7 Formation of 3-Hydroxy-4-(2,4,6-tri-oxo-hexahydro-pyrimidin-5-ylazo)-benzene sulfonic acid (L11).

From 4-Amino-3-hydroxy-benzenesulfonic acid (6.96 g, 0.037 mol) and Pyrimidine-2,4,6(1H,3H,5H)-trione (4,74 g, 0.037 mol) coupled at pH 4-6. Yield: 9.26 g , 0.028 mol.

2.1.8 Formation of 2-(2,4,6-Tri-oxo-hexahydro-pyrimidin-5-ylazo)-benzoic acid (L12).

From 2-Amino-benzoic acid (5.49 g, 0.044 mol) and Pyrimidine-2,4,6(1H,3H,5H)-trione (5.60 g, 0.044 mol) coupled at pH 4–6. Yield: 9.60 g, 0.035 mol.

2.1.9 Formation of 4-Hydroxy-3-(pyridin-2-ylazo)-napthalene-1-sulfonic acid (L7).

A solution of Pyridin-2-yl-hydrazine (2.20 g, 0.02 mol) in distilled water (140 cm^3), was added drop wise to a solution of 3,4-Dioxo-3,4-di-hydro-napthalene-1-sulfonic acid. (5.40g, 0.02 mol) in a mixture of distilled water (185 cm^3) and HCl (2 mol dm^{-3}; 185 cm^3). The solution was stirred for 1 hour at 40 ^oC, then left to stir for a further hour at room temperature. The product was then filtered off and washed with distilled water (300 cm^3), acetone (100 cm^3) and diethyl ether (100 cm^3). The product was then dried for 16 hours at 60 ^oC. A red powder was obtained.

Yield: 4.3 g, 0.013 mol.

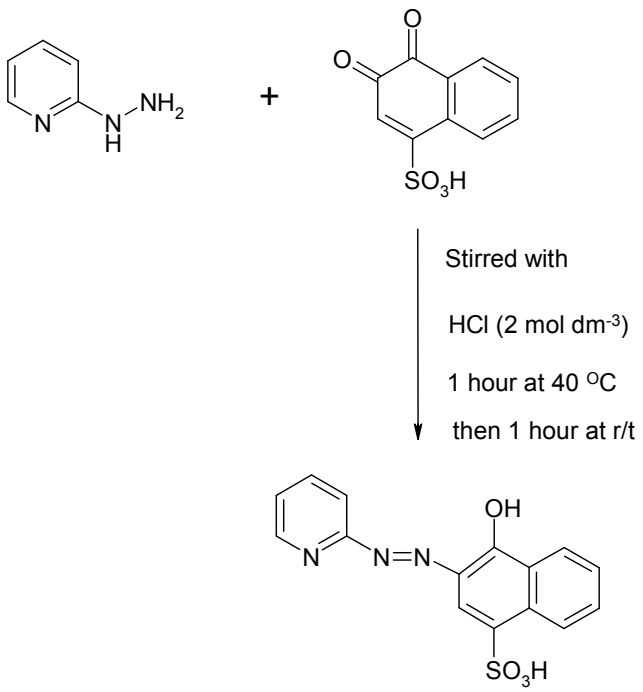

L7

2.1.10 Formation of 3-[5-Hydroxy-3-methyl-1-(4-sulfo-phenyl)-1H-pyrazol-4-ylazo]-1H-pyrazole-4-carboxylic acid ethyl ester (L8).

A mixture of acetic acid (15 cm^3) and propionic acid (10 cm^3) was cooled in an ice bath to 0-5 ^oC. Nitrosyl sulphuric acid (6 cm^3, 0.035 mol) was then added drop wise over 10 minutes. A solution of 3-Amino-4-carbethoxypyrazole (4.65 g, 0.03 mol) in a mixture of acetic acid (15 cm^3) and propionic acid (10 cm^3) was then added slowly over the course of 15 minutes to the nitrosyl sulfuric solution. The diazonium salt was allowed to form for a further 20 minutes at 0-5 ^oC and was tested for its formation by the use of H acid. Any excess nitrosyl sulfuric acid was quenched with

the use of a few spatulas full of sulfamic acid until no more nitrogen gas was evolved.

The diazonium solution was added gradually over 20 minutes to a cooled (0-5 ^{o}C) solution of 4-(5-Hydroxy-3-methyl-pyrazol-1-yl)benzene sulfonic acid (8.39 g, 0.03 mol) in distilled water (200 cm^3). Using a pH meter, the pH of the reaction was kept between 4.5 and 6 by addition of sodium acetate. The extent of the reaction was monitored with H acid. The reaction mixture was left to stir overnight at room temperature. The product was collected by filtration and then dried for 16 hours at 60 ^{o}C. Yield: 11.63 g, 0.028 mol.

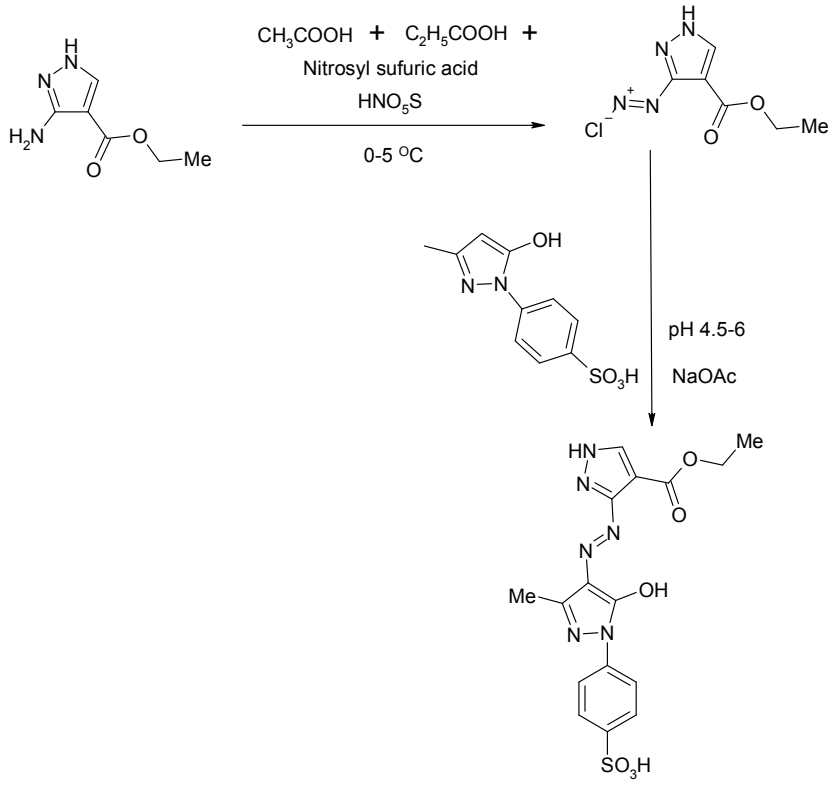

L8

2.1.11 Formation of 5-Hydroxy-2-methyl-6(pyridin-2-ylazo)-quinoline-3-carboxylic acid ethyl ester (L10).

A solution of ceric ammonium nitrate (34.8 g, 0.06 mol) in distilled water (150 cm^3) was added to a solution of 5,8-Di-methoxy-2-methylquinoline-3-carboxylic acid ethyl ester (6.88 g 0.025 mol) in a mixture of THF (100 cm^3) and ethyl acetate (200 cm^3). The reaction mixture was stirred at room temperature for 90 minutes. The separated organic phase was washed with distilled water (2 x 100 cm^3), dried with anhydrous $MgSO_4$, and evaporated at 40 ^oC. Methanol (200 cm^3) and 2 mol dm^{-3} HCl (1.25 cm^3) were added to the solution at room temperature. A solution of Pyridin-2-yl-hydrazine (2.73 g, 0.025 mol) in methanol (50 cm^3) and HCl (2 mol dm^{-3}; 1.25 cm^3) was added to the quinoline solution. The reaction mixture was stirred at room temperature for 9 hours. It was then stood in an ice bath for 1 hour. The product was filtered off, washed with methanol (50 cm^3) and dried using a vacuum pump. The product was stirred in ethanol (75 cm^3) at reflux for 5 minutes, cooled in ice and left in a refrigerator overnight. The product was collected by filtration and dried in an oven at 60 ^oC for 16 hours. A brown powder was obtained. Yield: 0.9 g, 0.0027 mol.

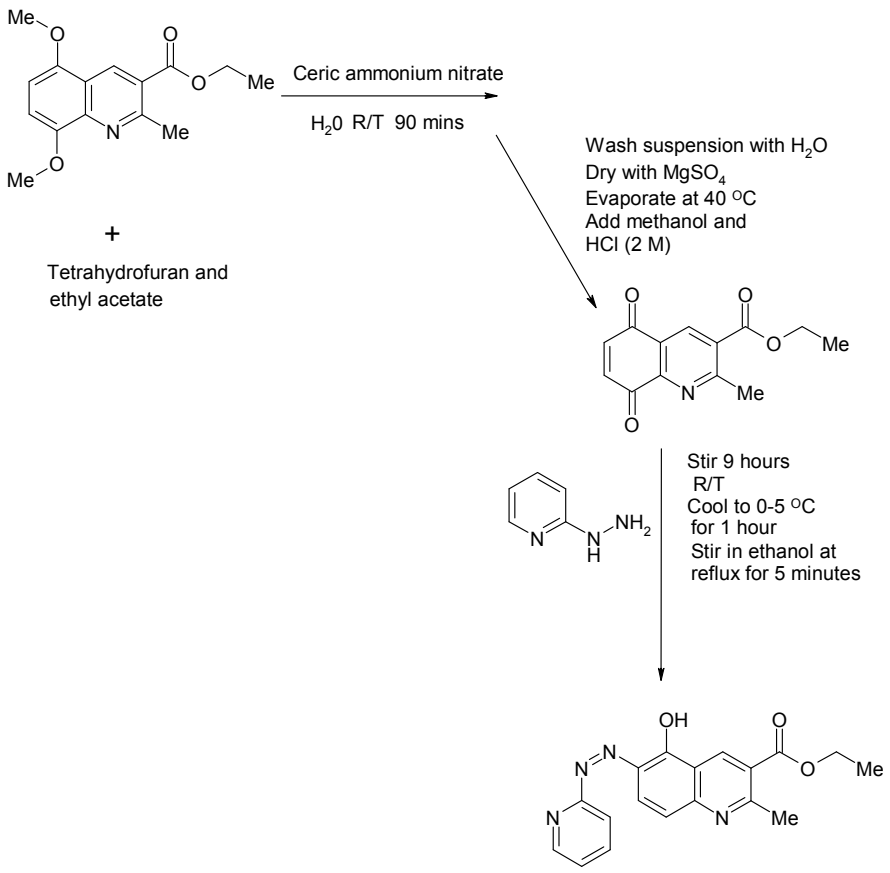

L10

2.2 Characterisation of azo dyes L1-L12, L5B and L3765.

Specimen spectra are shown for L5, and data for the other ligands are shown in tables. All numbers that are shown represent C atoms to identify the relevant ^1H and ^{13}C NMR resonances.

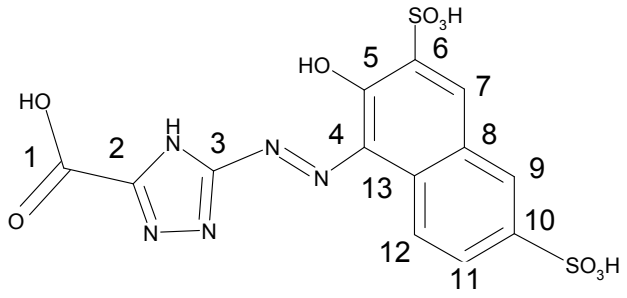

L5

Figure 17: ^{1}H NMR spectrum of L5 (OH and NH protons H-D exchanged).

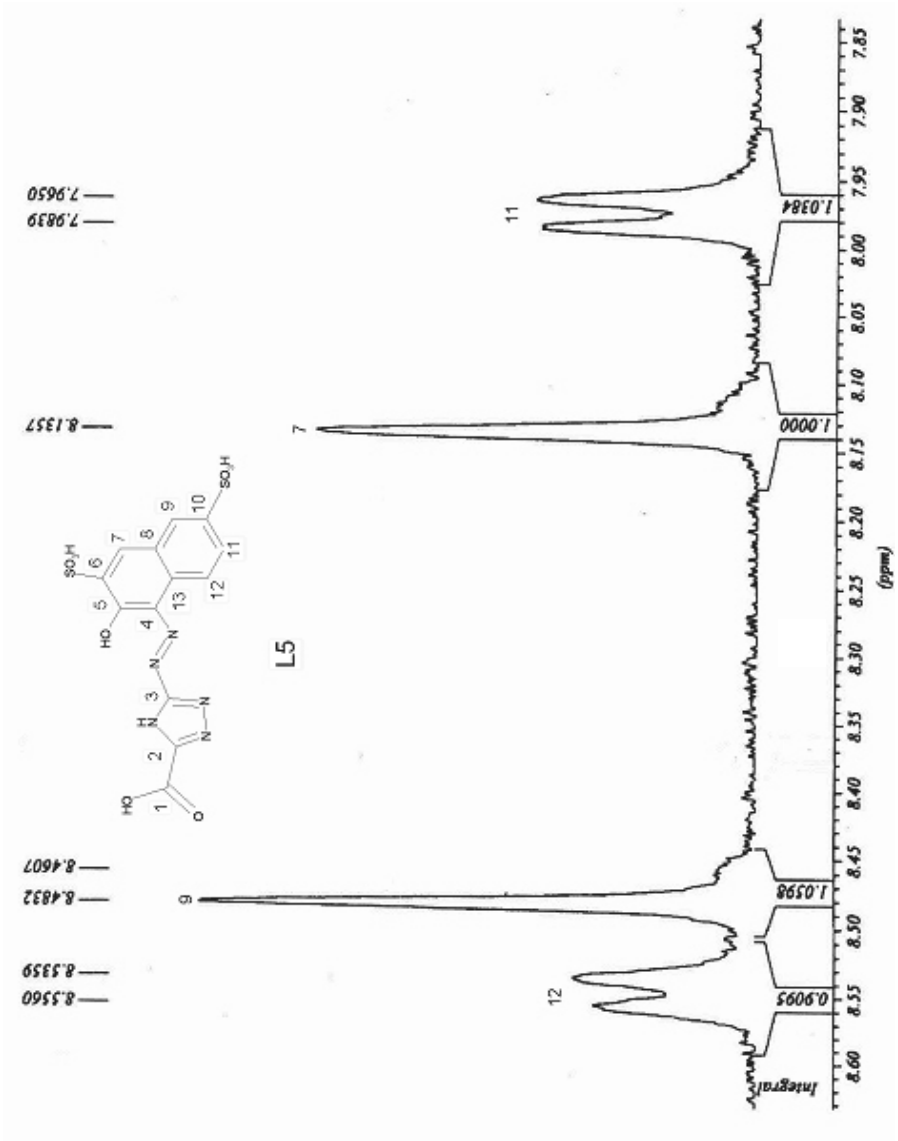

Figure 18: ^{13}C NMR spectrum of L5.

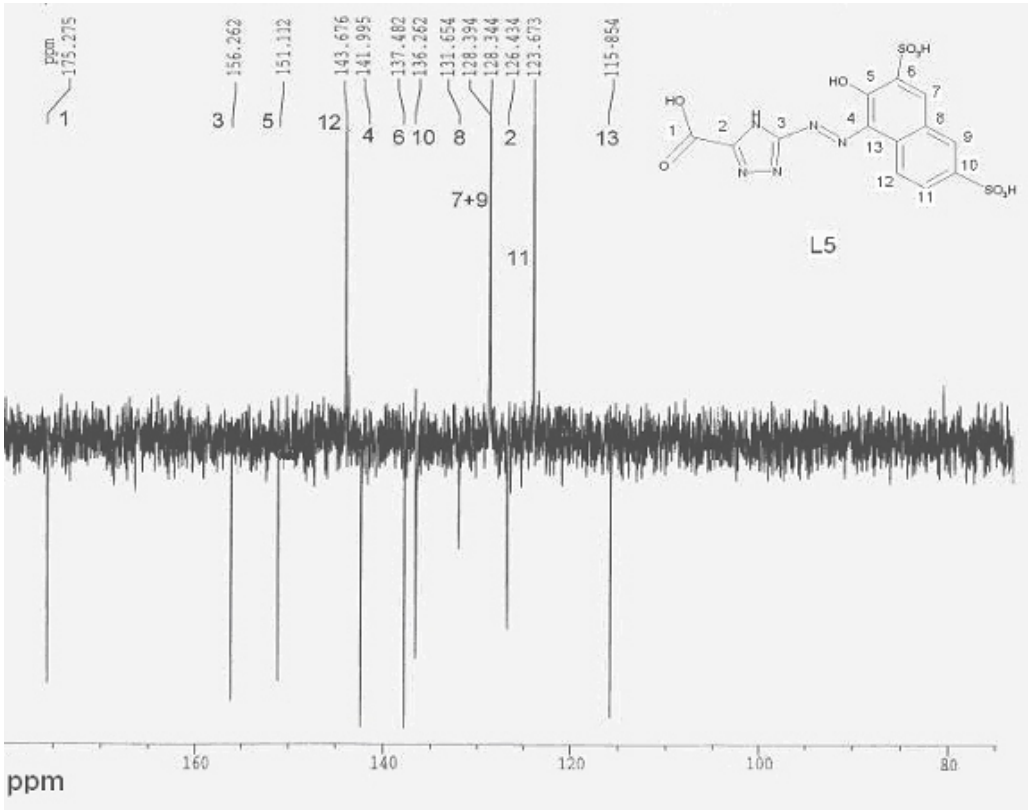

48

Figure 19: Ir spectrum of L5.

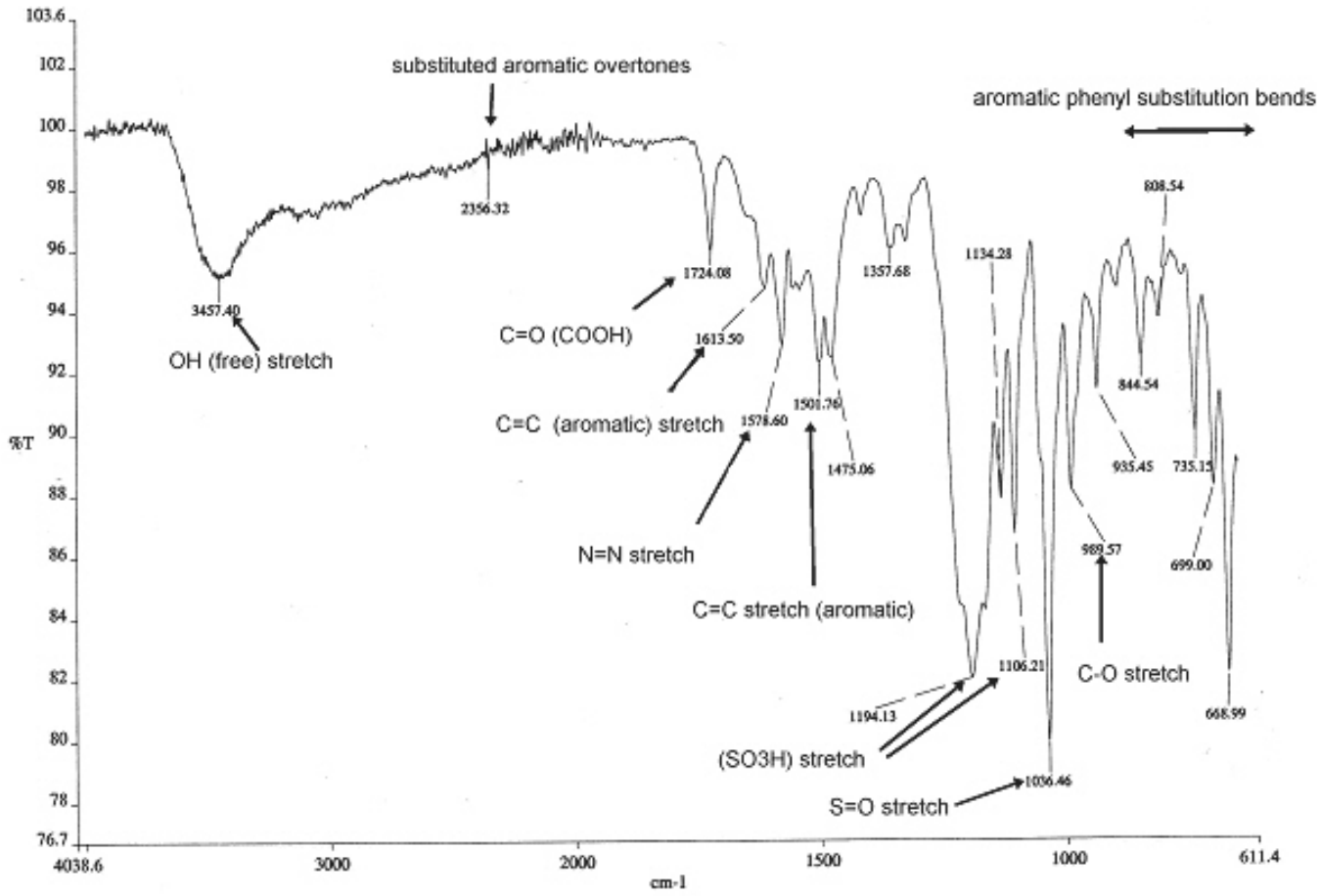

49

Figure 20: Atomic absorption sodium analysis calibration curve showing estimated L5 sodium content.

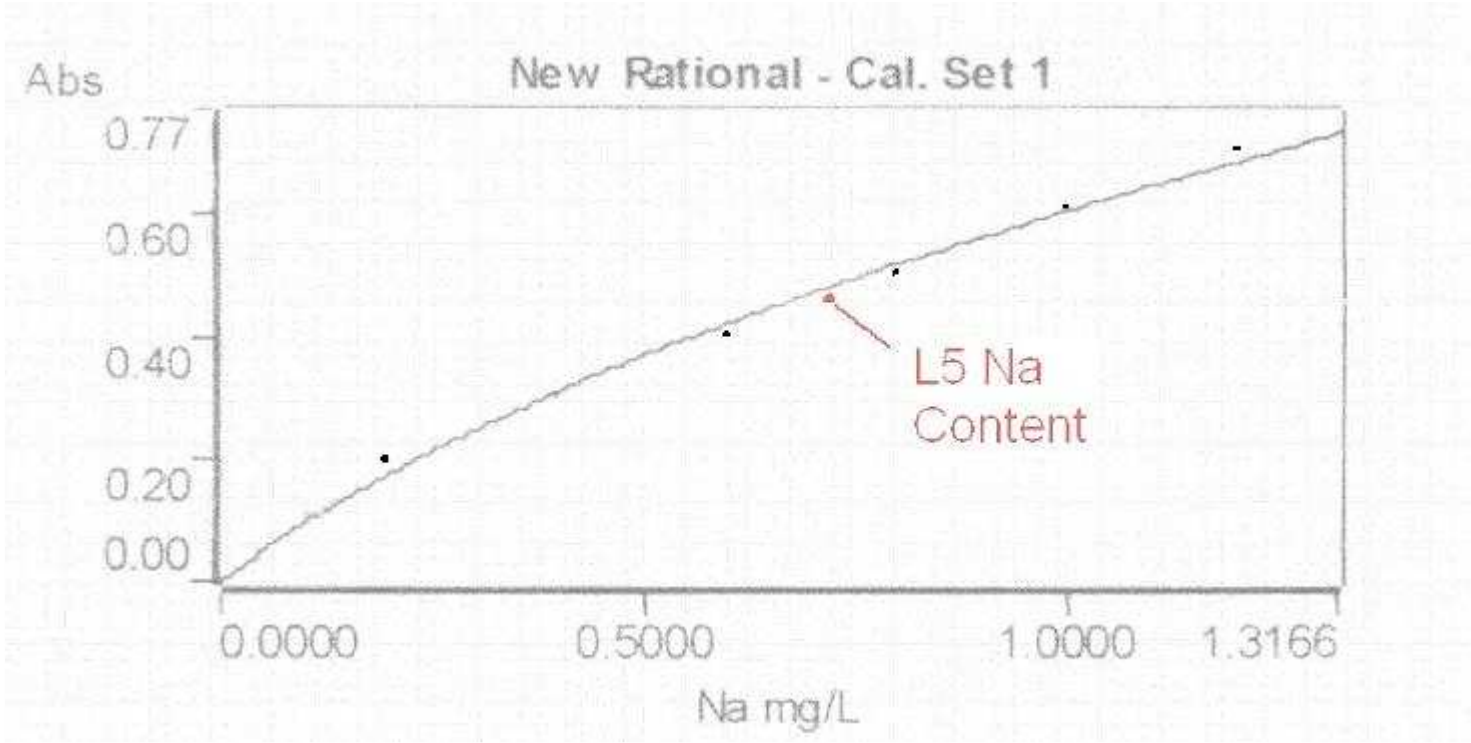

2.246 mg of dye in 250 cm^3 gave:
[Na] = 0.713 and 0.711 (av 0.712 mg dm^{-3})
% Na = 0.712 x 100/((4 x 2.246) = 7.93%

50

Azo dyes L1-L12 were synthesised and characterised, L5B and L3765 were obtained as gifts from Avecia.

2.2.1 5-(2,4,6-Tri-oxo-hexahydropyrimidin-5-ylazo)-4H[1,2,4]triazole-3-carboxylic acid (L1).

^{1}H NMR (DMSO–d_6): proton silent (OH and NH protons undergo H–D exchange).

^{13}C NMR (DMSO–d_6): δ/ppm 162.97 (1), 145.98 (2), 156.81 (3), 91.28 (4), 159.16 (5), 150.63 (6), 159.16 (7)

Ir data: 3524, 3414, 3138, 2976, (w) NH stretch, 2814 (w) OH (COOH) stretch, 1692 (s) C=O (COOH) stretch, 1613 (s) C=O (Amide) stretch 1460, (m) C=N stretch, 1408 (m) NH bend, 1361, 1316, 1286, (s) C–N stretch, 1266,1042 C–O stretch 908 (w) NH wagging, 824, 777 C-C stretch cm^{-1}.

2.2.2 4-(2,6-Di-aminopyridin-3-ylazo)-3-hydroxy benzene sulfonic acid (L2).

^{1}H NMR (DMSO–d_6): δ/ppm 6.1 (d, 2NH (9)), 6.8 (d, 2NH (8)) 7.4 (dd, 2H, (10),(11)), 7.64 (d, 2H, (1), (2)), 7.8 (s, (4)).

^{13}C NMR (DMSO–d_6): δ/ppm 123.18 (1), 117.13 (2), 141.06 (3), 116.54 (4), 150.78.(5), 137.66 (6), 139.54 (7), 153.26 (8), 158.68 (9), 99.74 (10), 126.98, (11).

2.2.3 5-(2,6-Di-amino-pyridin-3-ylazo)-4H-[1,2,4]triazole-3-carboxylic acid (L3).

^{1}H NMR (DMSO–d_6): δ/ppm 7.65 (d, (7+8)) 7.98 (OH, NH,NH_2).

^{13}C NMR (DMSO–d_6): δ/ppm 163.59 (1), 144.83 (2), 155.51 (3), 124.34 (4), 149.36 (5), 152.12 (6), 94.95 (7), 102.68 (8).

Ir data: 3674 (m) NH_2, stretch, 2987, 2901 (s) C–H (aromatic) stretch, 2010, 1933 (w) (substituted aromatic ring overtones), 1668 (w) C=O (COOH), 1560, N=N stretch, 1452, 1405 (m) NH bend, 1393, 1382, (m) C–N stretch, 1249, 1241, 1229 (m) (SO_3H) stretch, 1066, 1056, (s) S=O stretch, 892, C–O stretch, 807, 800 (m) phenyl substitution bend 694 cm^{-1}.

2.2.4 5-[5-Hydroxy-3-methyl-1-(4-sulfo-phenyl)-1H-pyrazol-4-ylazo]-4H-[1,2,4]triazole-3-carboxylic acid (L4).

^1H NMR (DMSO-d_6): δ/ppm 2.35 (s, 3H, (6)) 7.65 (d, 2H, (9), (13)) 7.95 (d, 2H, (10), (12)).

^{13}C NMR (DMSO–d_6): δ/ppm 162.97 (1), 145.98 (2), 157.01 (3), 118.46 (4), 142.50 (5), 12.02 (6), 156.12 (7) 139.65 (8), 119.51 (9+13), 128.08 (10+13), 141.51 (11)

Ir data: 3670 (w), NH stretch, 2987, 2901 (s) C–H (aromatic) stretch, 2000, 1930 (w) (substituted aromatic ring overtones), 1683 (w) C=O (COOH) stretch, 1570 (s) N=N stretch 1503 (m) C=C (aromatic) bend, 1373 C–CH3 stretch, 1212, 1168,1126 (m) (SO_3H) stretch 1040, 1008, (s) S=O stretch, 912, C-O stretch, 838, 822, 768 phenyl substitution bend cm^{-1}.

2.2.5 5-(2-Hydroxy-3,6-di-sulfo-napthalen-1-ylazo)-4H-[1,2,4]triazole (L5B).

^1H NMR (D_2O): δ/ppm 7.85 (s (1)), (8.02(d, (10)), 8.14 (s, (6)) 8.51 (s, (8)), 8.56 (d, (11))

^{13}C NMR (DMSO–d_6): δ/ppm 143.87 (1), 157.87 (2), 129.91 (3), 150.82 (4), 129.36 (5), 119.32 (6), 126.87 (7), 121.21 (8), 143.71 (9), 125.12 (10), 117.87 (11), 133.41 (12).

Ir data: 3501, (b) OH (free) stretch, 2018, 2186, (w) substituted aromatic overtones, 1579 (s) C=C (aromatic) stretch, 1535 (s) N=N stretch, 1497 (w) C=C stretch (aromatic), 1186,1105 (s) (SO_3H) stretch, 1035, (s) S=O stretch, 988, (m) C–O stretch 849, 804 (s) aromatic phenyl substitution bends cm^{-1}.

2.2.6 5-(3-Carboxy-2-hydroxy-naphthalen-1-ylazo)-4H-[1,2,4]triazole-3-carboxylic acid (L6).

^{1}H NMR (DMSO-d_6): δ/ppm 7.25 (q, (7)), 7.55 (q, (8)), 7.80 (q, (6)), 8.25 (q, (9)), 8.49 (q, (11)), 9.2 (s, NH).

^{13}C NMR (DMSO–d_6): 162.97 (1), 145.98 (2), 159.77 (3), 132.62 (4), 134.94 (5), 129.52 (6), 127.79 (7), 133.00 (8), 127.58 (9), 129.14 (10), 130.91 (11), 111.20 (12), 169.26 (13), 142.92 (14).

Ir data : 3354 (b) OH (free) stretch, 2015, 1970 (w) substituted aromatic overtones, 1690 (s) C=O (COOH) stretch, 1569 (m) N=N stretch, 1500 (w) C=C (aromatic) stretch, 1207, 1158 , 1001 (m) C-O stretch , 910, (w) C–N stretch, 804, 735 (s) aromatic phenyl substitution bends cm^{-1}.

2.2.7 4-Hydroxy-3-(pyridin-2-ylazo)-napthalene-1-sulfonic acid (L7).

^{1}H NMR (DMSO-d_6): δ/ppm 7.30 (t, (2)), 7.5 (d, (10)), 7.58 (s, (15)) 7.75 (t, (3)), 7.85 (d, (1)), 8.05 (t, (11)), 8.30 (d, (12)), 8.45 (d, (4)), 8.55 (d, (9)).

^{13}C NMR (DMSO–d_6): δ/ppm 147.25 (1), 130.48 (2), 140.59 (3), 110.53 (4), 179.03 (5), 133.65 (6), 153.63 (7), 127.09 (8), 132.53 (9), 127.04 (10), 128.69 (11), 125.13 (12), 133.65 (13), 139.57 (14) 121.14 (15).

Ir data: 3500, (b) OH stretch, 3065 (w) C–H (aromatic stretch), 2153, (w) substituted aromatic overtones. 1609 (m), N-H, 1537, N=N stretch, 1509, 1472 C-H (aromatic) bend. 1245, 1186, 1156 (s) SO_3H stretch, 1049, (s) S=O stretch, 996, (s) C–O stretch, 932, 903, 878 (w) C–N stretch, 809, 712, 695 (s) aromatic phenyl substitution bends cm^{-1}.

2.2.8 3-[5-Hydroxy-3-methyl-1-(4-sulfo-phenyl)-1H-pyrazol-4-ylazo]-

1H-pyrazole-4-carboxylic acid ethyl ester (L8).

^{1}H NMR (DMSO-d_6): δ/ppm 1.33 (t, 3H (5)), 2.49 (s, 3H (16)), 4.30 (q, 2H (4)), 7.63 (d, 2H, (10), (14)), 7.97 (d, 2H, (11), (13)), 8.36 (s, (1)), 14.2 (b, (8).

^{13}C NMR (DMSO–d_6): δ/ppm 145.52 (1), 112.91 (2), 162.04 (3), 60.52 (4), 14.17 (5), 146.42 (6), 116.49 (7), 156.19 (8), 139.65 (9), 119.51 (10), 128.08 (11), 141.51 (12), 128.08 (13), 119.51 (14), 142.50 (15), 13.02 (16).

Ir data: 3724, (w) NH stretch, 3511, (b) OH (free) stretch, 1970, (w) substituted aromatic overtones, 1678, C=O (COOH) stretch, 1662, C=O (ester) stretch, 1570, 1555, N=N stretch, 1497, 1433 (m) C-CH_3 stretch, 1387, 1324, (m) CH_2CH_3 stretch, 1244, 1194 (SO_3H) Stretch, 1194, 1183, 1151, (s) C–O (ester) stretch, 1050, S=O stretch, 1007, (s) C–N bend, 954, (m) C-C stretch, 837, 768, 734 (s) aromatic phenyl substitution bends cm^{-1}.

2.2.9 3-(2,6-Di-amino-pyridin-3-ylazo)-1H-pyrazole-4-carboxylic acid ethyl ester (L9).

^{1}H NMR (DMSO-d_6): δ/ppm 1.31 (t, 3H (11)), 4.23, (q, 2H (10)), 6.14 (d, (3)), 7.50 (NH, NH_2), 7.72 (d, (4)) 7.95 (s, (7)).

^{13}C NMR (DMSO–d_6): δ/ppm 152.41 (1), 156.73 (2), 106.67 (3), 130.76 (4), 135.27 (5), 149.68 (6), 145.52 (7), 112.54 (8), 162.04 (9), 60.52 (10), 14,17 (11).

Ir data: 3689, (w) NH, NH_2 stretch, 3088, (m) C-H (aromatic), 2016, substituted aromatic overtones, 1667 (s) C=O (ester) stretch, 1626, C=C (w) (aromatic) stretch, 1582, (m) N=N stretch, 1498, (w) N-H bend, 1383, (m) CH_2-CH_3, 1342, (m) C-O(ester) stretch, 1253, (m) SO_3H stretch, 1191, (m) C-N stretch, 1100, 1019, S=O stretch, 984, 954 (m) C-C stretch, 824, 776 ,749, aromatic phenyl substitution bend cm^{-1}.

2.2.10 5-Hydroxy-2-methyl-6(pyridin-2-ylazo)-quinoline-3-carboxylic acid ethyl ester (L10).

^{1}H NMR (DMSO-d_6): δ/ppm 1.39 (t, 3H, (13)), 2.50 (s, 3H, (15)), 4.45 (q, 2H, (12)), 6.60 (d, (1)), 7.20 (t, (2)), 7.71 (t, 2H, (17), (18)), 7.91 (t, (3)), 8.45 (d, (4)) 8.92 (s, (9)).

^{13}C NMR (DMSO–d_6): δ/ppm 147.11 (1), 124.62 (2), 138.96 (3), 117.29 (4), 163.13 (5), 136.16 (6), 155.08 (7), 121.43 (8), 131.51 (9), 112.90 (10), 164.89 (11), 61.17 (12), 14.20 (13), 151.25 (14), 23.86 (15), 146.05 (16), 120.17 (17), 127.91 (18).

Ir data: 3724, (w) NH, 2990, (w) C-H (aromatic), 2112 (w) aromatic substitution overtones, 1716, (s) C=O (ester), 1639, (s) C=O (ketone), 1582, (s) C=N stretch, 1511, (s) NH bend, 1458, 1432, (s) C-CH_3 stretch, 1378, 1369, (m) CH_2CH_3, 1331,1304 (m) C-O (ester) stretch, 1262, (m) C-N stretch, 1165, (s) C-C stretch, 834, 772, 736 (s) aromatic phenyl substitution bend cm^{-1}.

2.2.11 3-Hydroxy-4-(2,4,6-tri-oxo-hexahydro-pyrimidin-5-ylazo)-benzene sulfonic acid (L11).

^1H NMR (DMSO-d_6): δ/ppm 2.50 (s, (7)), 6.85 (d, (4)), 7.35 (d, (2)), 7.93 (s, (1)) 10.80 (2 NH).

^{13}C NMR (DMSO–d_6): δ/ppm 118.78 (1), 127.21 (2), 131.30 (3), 113.40 (4), 146.94 (5), 134.54 (6), 90.32 (7), 160.29 (8), 150.63 (9), 160.29 (10).

Ir data: 3781, 3724 (w) NH stretch, 3179, 3063 (m) C–H (aromatic) stretch 2343, 1969 (w) substituted aromatic overtones, 1726, 1700, 1668 C=O (amide), 1530 (s) N=N stretch, 1432, 1400, (s) NH bend , 1308 (m) C–H (aromatic) bend, 1275, 1260,1189 (s) SO_3OH stretch, 1082, 1041 (s) S=O stretch, 867 (s) C-O stretch 846, (s) C-N stretch, 781,720 (s) aromatic phenyl substitution bends cm^{-1}.

2.2.12 2-(2,4,6-Tri-oxo-hexahydro-pyrimidin-5-ylazo)-benzoic acid (L12).

^1H NMR (DMSO-d_6): δ/ppm 7.25 (t, (3)), 7.69 (t, (2)), 7.98 (t, 2H, (1), (4)), 11.10 (d, 2 NH), 15.25 (s, OH)

^{13}C NMR (DMSO–d_6): δ/ppm 107.92 (1), 133.49 (2), 122.33 (3), 132.55 (4), 117.57 (5), 167.18 (6), 148.26 (7), 90.32 (8), 160.29 (9), 150.63 (10) 160.29 (11).

Ir data: 3675, 3564, (m) NH stretch , 3452 (m) OH (free) stretch, 2972, 2989, 2901, C–H, (aromatic), 2111, 1970 (w) substituted aromatic overtones, 1719, (s) C=O (COOH) stretch, 1694, 1664, 1626, (s) C=O (amide) stretch, 1597, (s) C=C (aromatic) stretch, 1510 (s) C=N stretch, 1498, (s) C=C (aromatic) stretch, 1423, (s) NH bend, 1394, 1341, 1301, C-H (aromatic) bend, 1202, 1146,1057, (s) C–N stretch , 940 (w) C–O stretch, 804, 766 ,695 (s) aromatic phenyl substitution bends cm^{-1}.

2.2.13 Hydroxy-2-(pyridin-2-ylazo)-napthalene-6-10-di-sulfonic acid (L3765).

^{1}H NMR (DMSO-d_6): δ/ppm 7.34 (t, (3)), 7.75 (t, (2)), 7.83 (d, (4)), 8.32 (d, (1)), 8.46 (d, (14)), 8.59 (s, (15)) 9.15 (s, 2H, (10), (12))

^{13}C NMR (DMSO–d_6): δ/ppm 148.25 (1), 132.42 (2), 143.69 (3), 113.52 (4), 180.03 (5), 130.90 (6), 149.52 (7), 125.48 (8), 119.42 (9), 118.69 (10), 121.12 (11), 142.31 (12), 125.72 (13), 119.57 (14), 132.18 (15).

Ir data: 3400, (b) OH stretch, 3055 (w) C–H (aromatic stretch), 2163, (w) substituted aromatic overtones. 1608 (m), N-H, 1536, N=N stretch, 1519, 1474 C-H (aromatic) bend. 1242, 1185, 1153 (s) SO_3H stretch, 1047, (s) S=O stretch, 994, (s) C–O stretch, 932, 901, 877 (w) C–N stretch, 806, 713, 695 (s) aromatic phenyl substitution bends cm^{-1}.

Table 3: Micro analytical data (calculated values in parentheses) and synthetic yields for ligands L1-L12. *L5B and L3765 were gifts from Avecia.

Ligand	Yield (%)	Formula	C	H	N	Na
L1	95	$C_7H_3N_7O_5Na_2.3H_2O$	23.43 (23.01)	2.30 (2.48)	27.01 (26.90)	12.53 (12.59)
L2	93	$C_{11}H_9N_5O_4SNa_2.2.5H_2O$	31.41 (33.20)	3.37 (3.54)	17.51 (17.59)	11.12 (11.55)
L3	78	$C_8H_8N_8O_2Na.2.5H_2O$	28.91 (29.52)	3.92 (4.34)	33.43 (34,46)	6.91 (7.07)
L4	76	$C_{13}H_8N_7O_6SNa_32.5H_2O$	31.22 (30.95)	2.51 (2.60)	19.35 (19.44)	12.96 (13.68)
L5	25	$C_{13}H_5N_5O_9S_2Na_2.4H_2O$	27.50 (28.00)	2.23 (2.35)	11.81 (12.57)	7.93 (8.26)
L5B*	N/A	$C_{12}H_5N_5O_7S_2Na_23H_2O$	29.97 (30.19)	1.89 (1.90)	14.24 (14.68)	9.52 (9.64)
L6	46	$C_{14}H_5N_5O_5Na_3.3H_2O$	35.70 (37.67)	2.35 (2.48)	15.12 (15.69)	14.93 (15.46)
L7	65	$C_{15}H_{11}O_4N_3S.5H_2O$	41.14 (42.94)	5.13 (5.05)	9.76 (10.02)	0 (0)
L8	92	$C_{16}H_{14}N_6O_6SNa_2.6H_2O$	31.42 (33.55)	4.56 (4.58)	14.58 (14.67)	7.61 (8.03)
L9	71	$C_{11}H_{10}N_7O_2Na.4H_2O$	35.12 (35.96)	4.76 (4.94)	24.92 (26.70)	5.72 (6.26)
L10	11	$C_{18}H_{15}N_4O_3Na.3H_2O$	50.31 (52.41)	4.97 (5.14)	12.91 (13.59)	5.32 (5.58)
L11	76	$C_{10}H_4N_4O_7SNa_2.4H_2O$	28.21 (29.55)	1.82 (1.98)	12.97 (13.79)	10.73 (11.33)
L12	80	$C_{11}H_7N_4O_5Na.3H_2O$	36.87 (37.49)	3.63 (3.72)	15.43 (15.91)	6.21 (6.53)
L3765*	N/A	$C_{15}H_{11}O_7N_3S_2Na_22H_2O$	36.42 (36.66)	3.02 (3.08)	8.42 (8.56)	9.26 (9.36)

Table 4: Melting points and λ_{max} values in aqueous solution.

Ligand	Melting Point/(^{o}C)	λ_{max}/nm
L1	380.6 decomposes	380
L2	263.0--267.0	458
L3	239.5--240	445
L4	390.5 decomposes	355
L5	380.2 decomposes	480
*L5B	376.1 decomposes	478
L6	393.0 decomposes	412
L7	327.0	455
L8	376.6 decomposes	380
L9	219.0—221.0	458
L10	203.2--203.5	470
L11	384.3 decomposes	387
L12	343.2--344.0	394
*L3765	335.0	455

Table 5: Electrospray mass spectroscopy data.

Ligand	Molecular Weight (g/mol)	Molecular Ions detected (m/z)
L1	267	266 (m-1) 222 (m-1) decarboxylated
L2	309	308 (m-1)
L3	248	199 (m-1) decarboxylated
L4	392	391 (m-1)
L5	443	398 (m-1) decarboxylated
*L5B	399	398(m-1)
L6	327	326 (m-1)
L7	329	328 (m-1)
L8	354	353 (m-1)
L9	275	274 (m-1)
L10	336	335 (m-1)
L11	328	327 (m-1)
L12	276	275 (m-1)
*L3765	409	408(m-1)

Chapter 3: Determination of the pK_a values of PAN, L7 and L3765, L1, L5, and L5B by visible spectroscopy using the program SPECFIT/32.

Introduction.

Ionisation constants show the proportions of the different ionic species into which a substance is divided at any chosen pH. "It can be seen that since the ionization constant of benzoic acid is 7.6 x 10^{-5}, it can be calculated that at pH 5 it is 89% in the form of the anion (I) and 11% in the form of the neutral molecule (II)".[184]

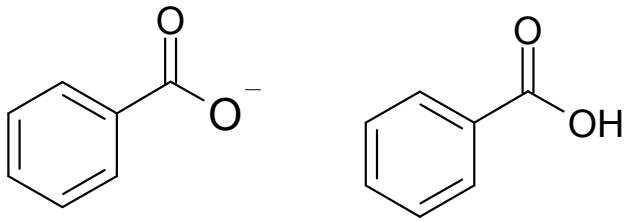

(I) (II)

This type of information is useful since "the ionic species of a given substance can differ in physical, chemical and biological properties."[184] Since different ionic species have different UV-Visible spectra, useful pH dependent spectrophotometry can be carried out.

Ionisation constants of a substance define the pH range in which it is least ionised, and indicate the conditions under which it can be isolated in maximal yield; this has great value in preparative chemistry. Ionisation constants are often used to help diagnose the structure of a newly isolated substance, and they can help to confirm the identity of two substances which have no melting point. They are also very useful in confirming which functional groups are present in a molecule, and can sometimes help identify which tautomeric form a molecule is in.

Ionisation constants are small and inconvenient figures, and it has become customary to use their negative logarithms to base 10 known as pK_a values.

pK_a values can be determined by potentiometry, spectrophotometry and conductimetry.[184] pK_a values of azo dyes have been determined by potentiometry,[149,150,151,152,154] and spectrophotometry[150,151,153] as illustrated in section 1.9.7 and Figure 11.

3. Results.

In this work pK_a values have been determined for PAN, L7, L3765, L1, L5 and L5B spectrophotometrically. The pK_a values were analysed and calculated by the computer software SPECFIT/32. Data obtained from the experiments can be seen in (Figure 21, p.63). The computer calculated spectra from SPECFIT/32 showing the stages of deprotonation and species distribution of the dye studied as a function of pH can be seen in (Figure 22, p.64) also all of the pK_a values determined are listed in Table 6 (p.74).

3.11 Determination of the pK_a values of PAN, L3765 and L7.

Figure 21: Complete UV-Visible data for PAN as a function of pH.

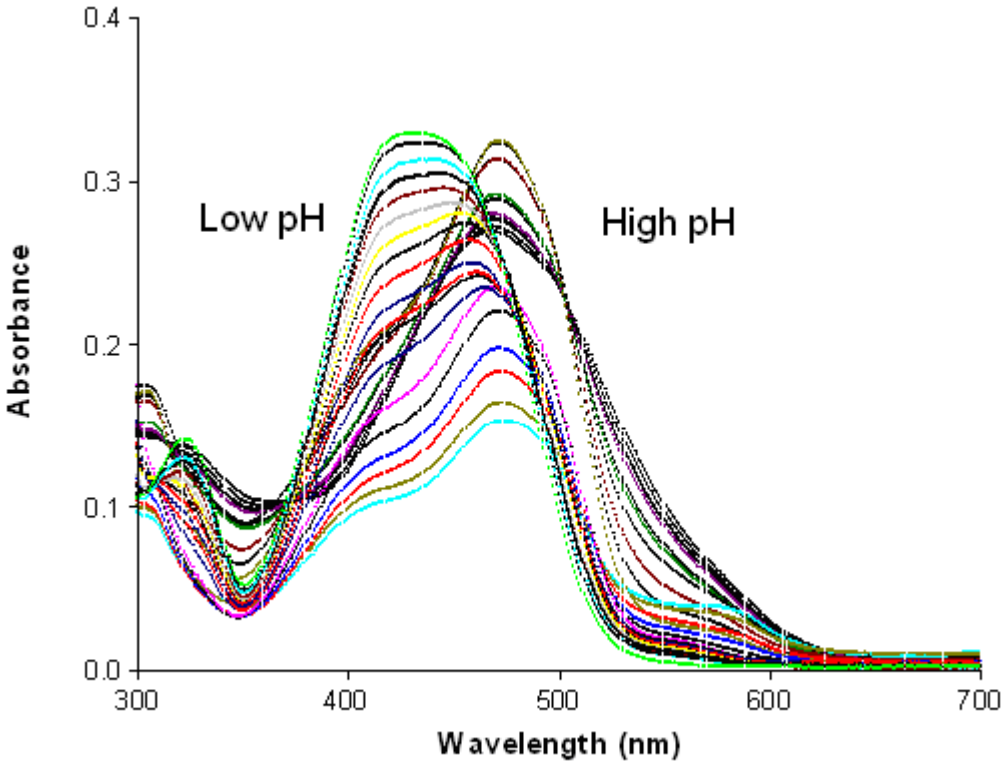

Figure 22: Computer fitted spectra of PAN at various stages of deprotonation.

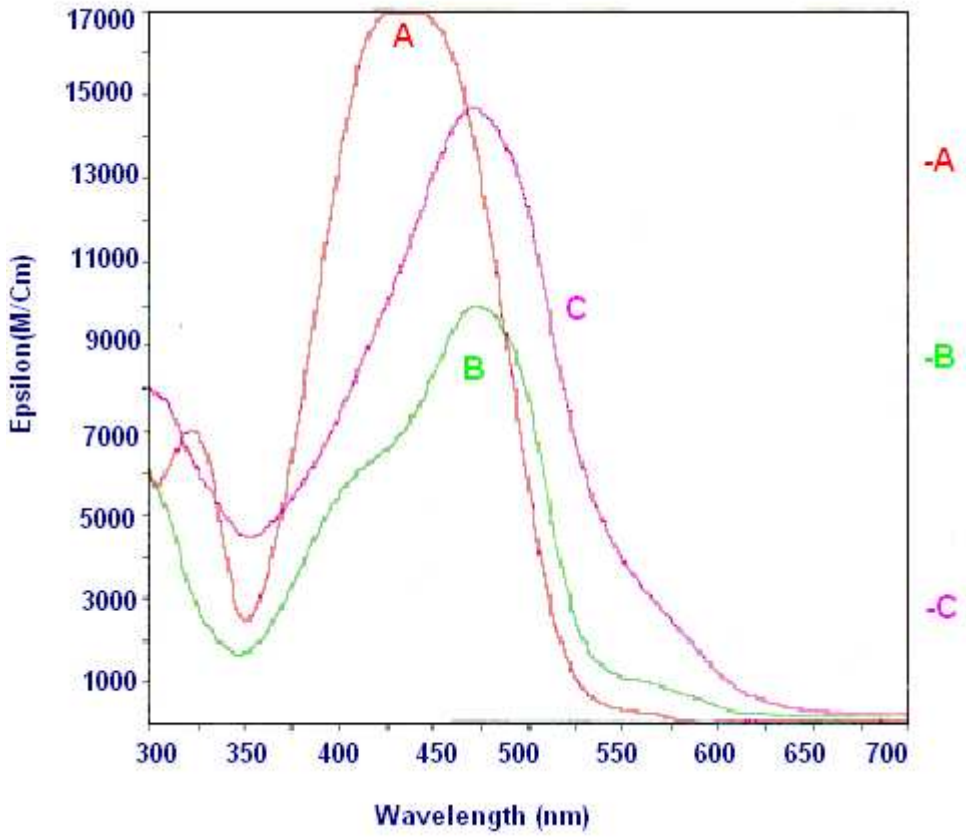

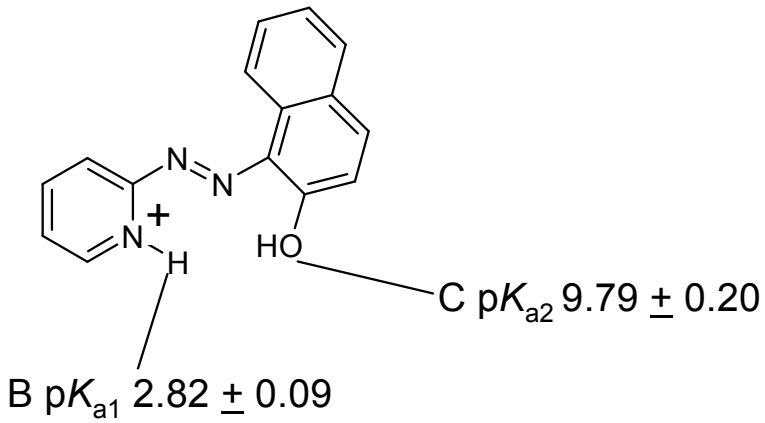

A = fully protonated species

Figure 23: PAN species distribution curves as a function of pH.

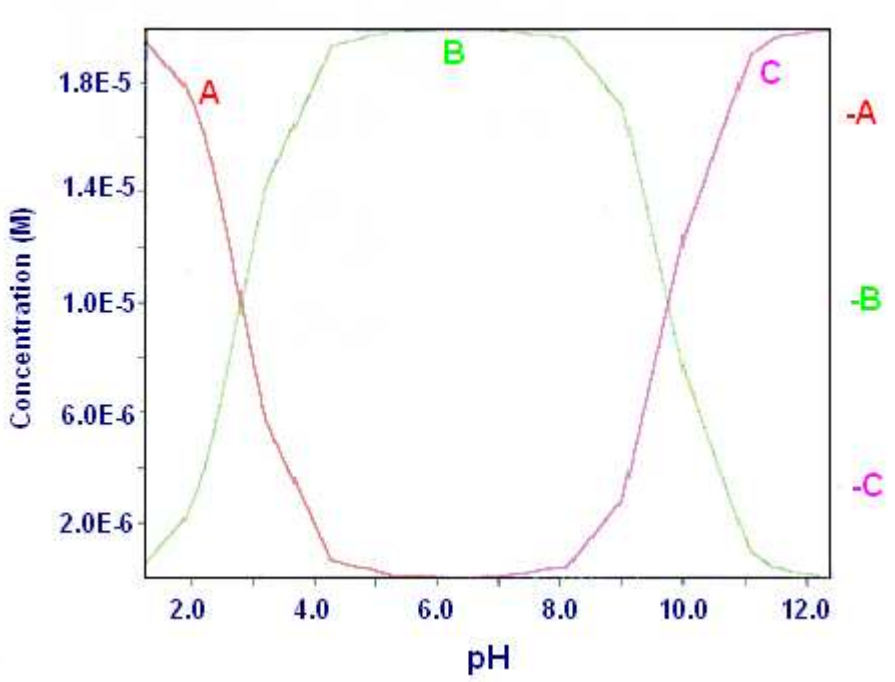

L7 and L3765 showed virtually identical spectra to PAN, as expected since these molecules are sulphonated and disulphonated PAN respectively. Their pK_a values are recorded in Table 6 (p.74). No pK_a values have been recorded for the sulphonate groups as these were completely deprotonated at the lowest pH used.

3.12 Determination of the pK_a values of L1.

Figure 24: Complete UV-Visible data for L1 as a function pH.

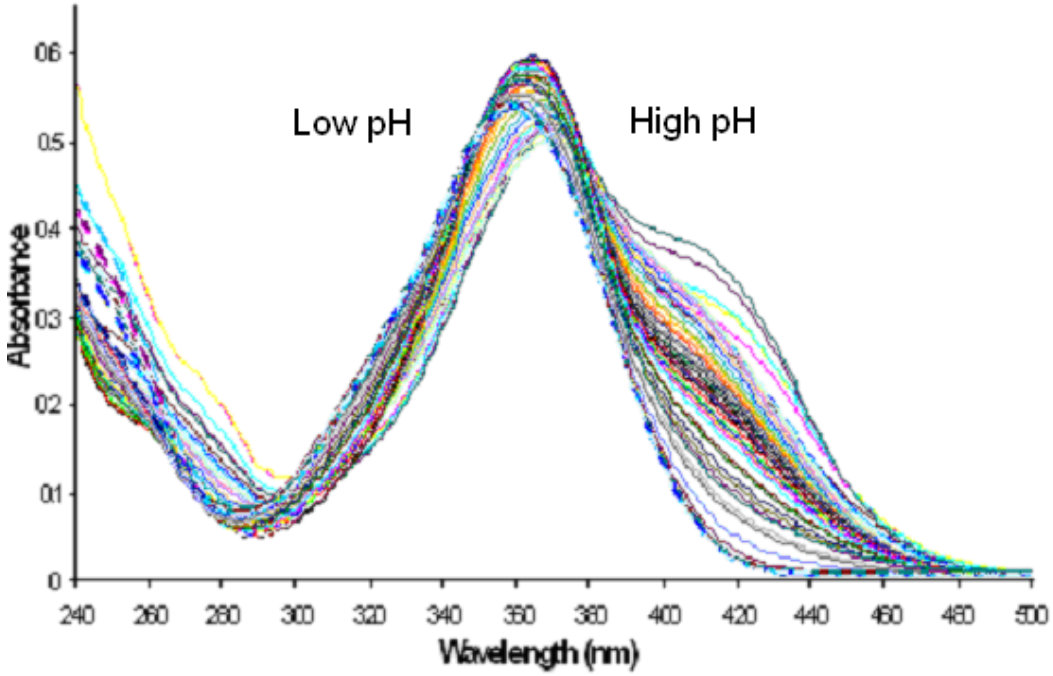

Figure 25: Computer fitted spectra of L1 at various stages of deprotonation.

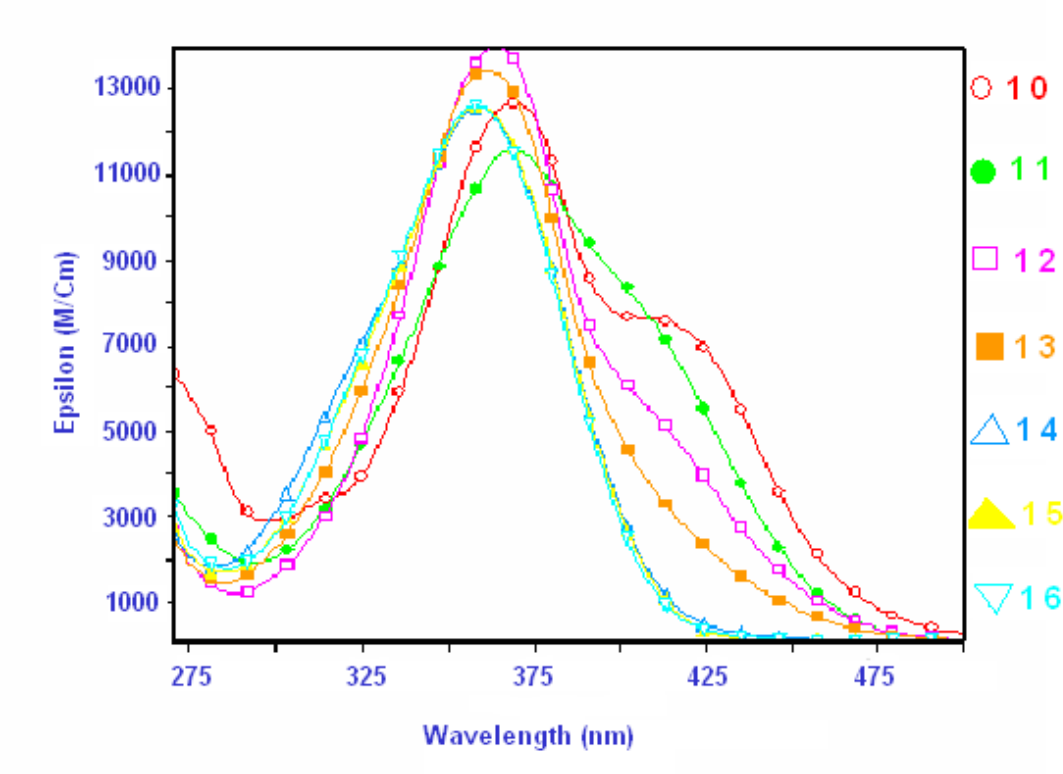

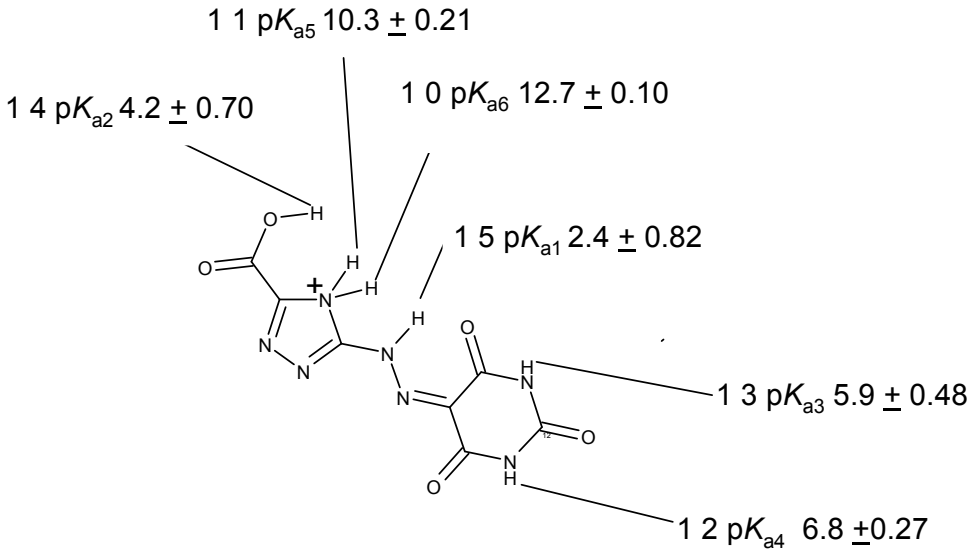

1 6 is the fully protonated species

Figure 26: L1 species distribution curves as a function of pH.

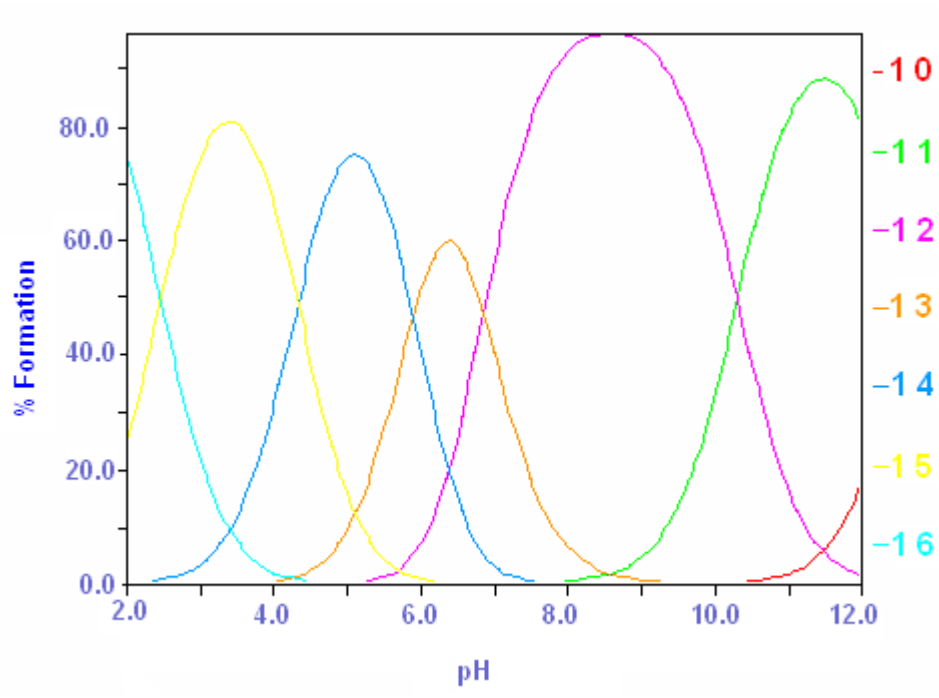

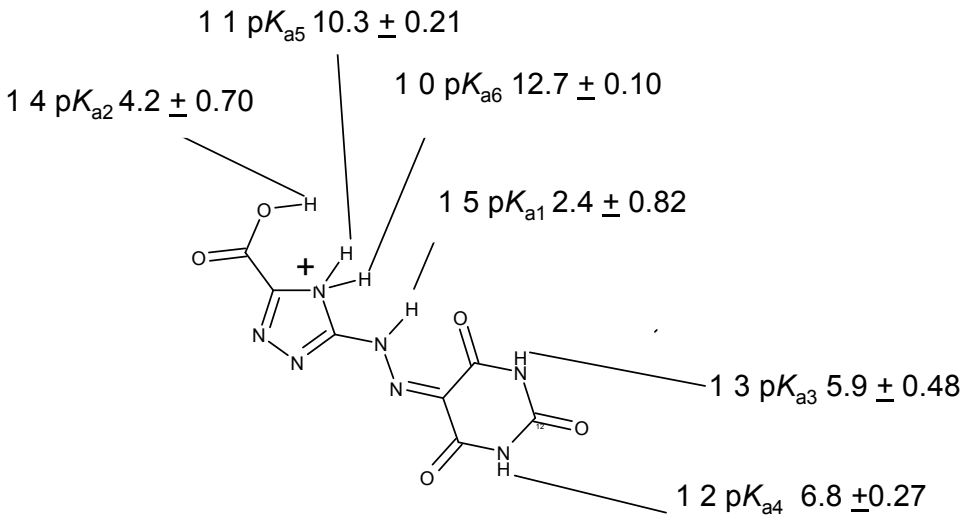

1 6 is the fully protonated species

3.13 Determination of the pK_a values of L5.

Figure 27: Complete UV-Visible data for L5 as a function of pH.

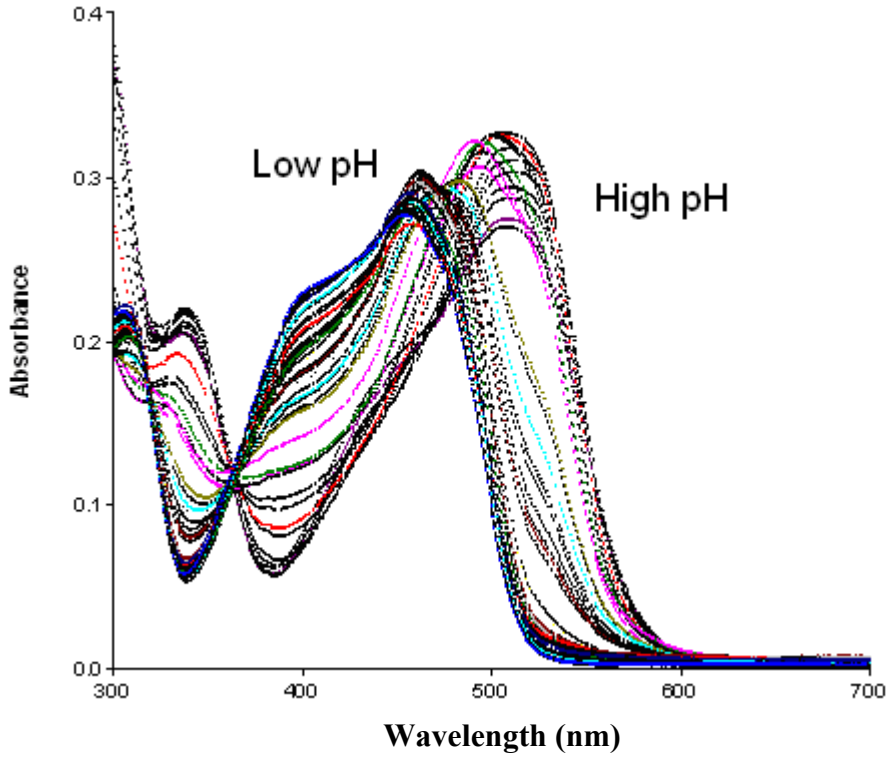

Figure 28: Computer fitted spectra of L5 at various stages of deprotonation.

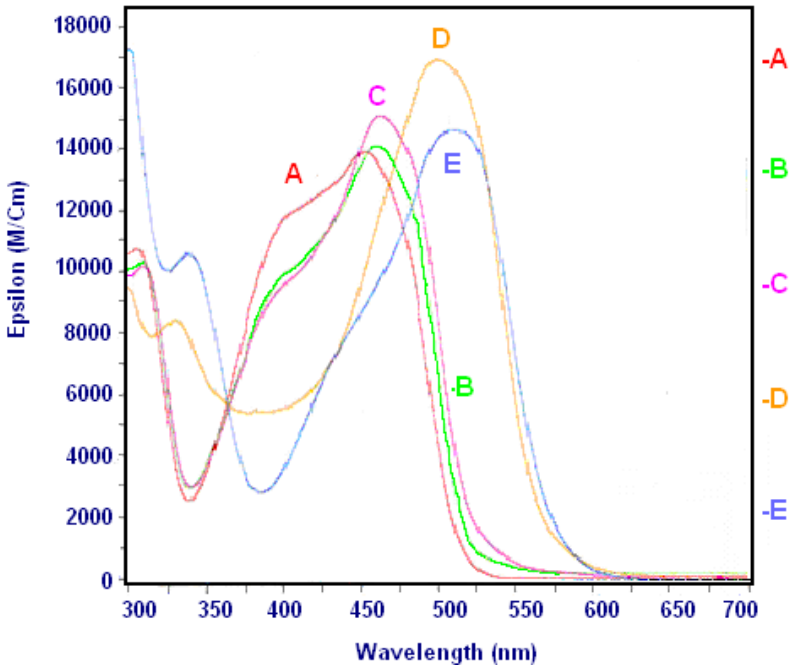

E pK_{a4} 10.68 + 0.09

B pK_{a1} 1.50 ± 0.17

D pK_{a3} 8.19 + 0.03

C pK_{a2} 2.98 ± 0.28

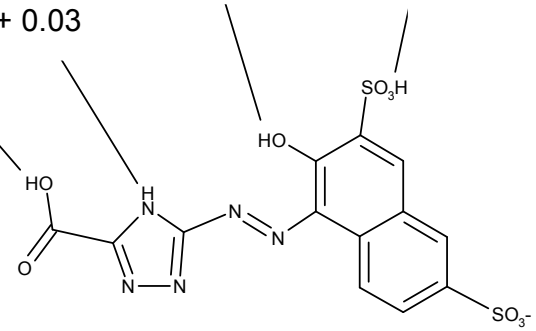

A Already deprotonated at starting pH

Figure 29: L5 species distribution curves as a function of pH.

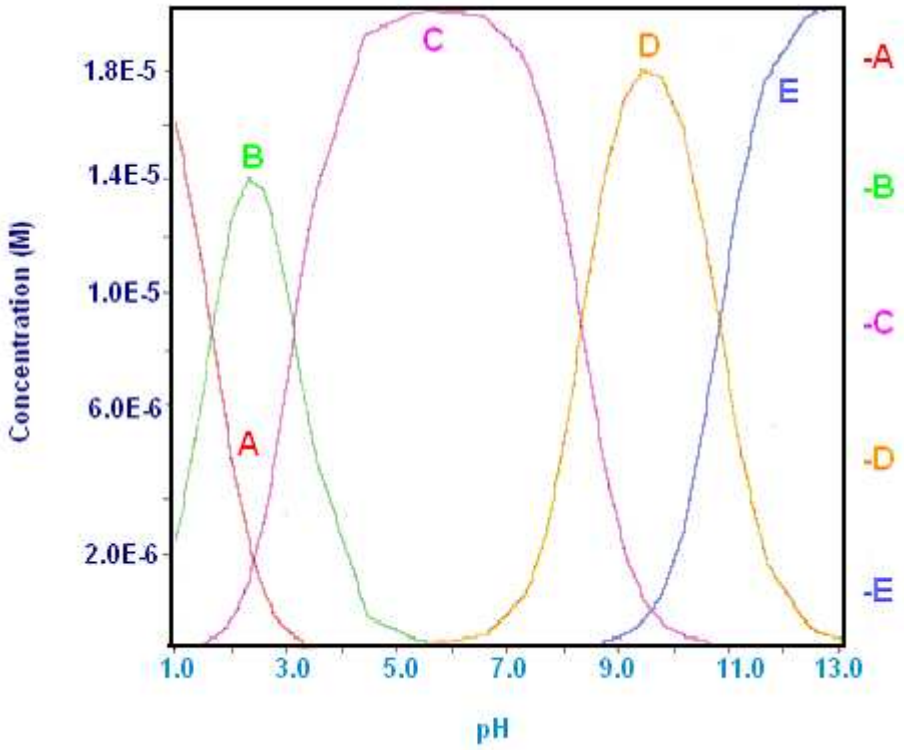

3.14 Determination of the pK_a values of L5B.

Figure 30: Complete UV-Visible data of L5B as a function of pH.

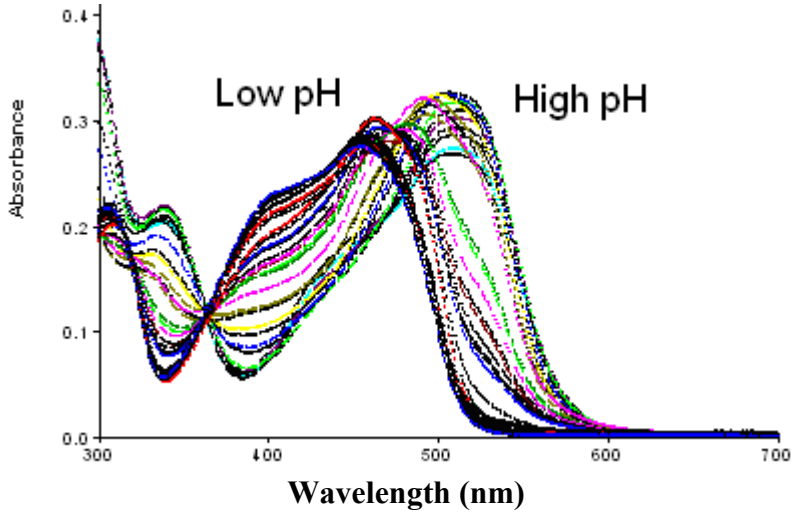

Figure 31: L5B Computer fitted spectra at various stages of deprotonation.

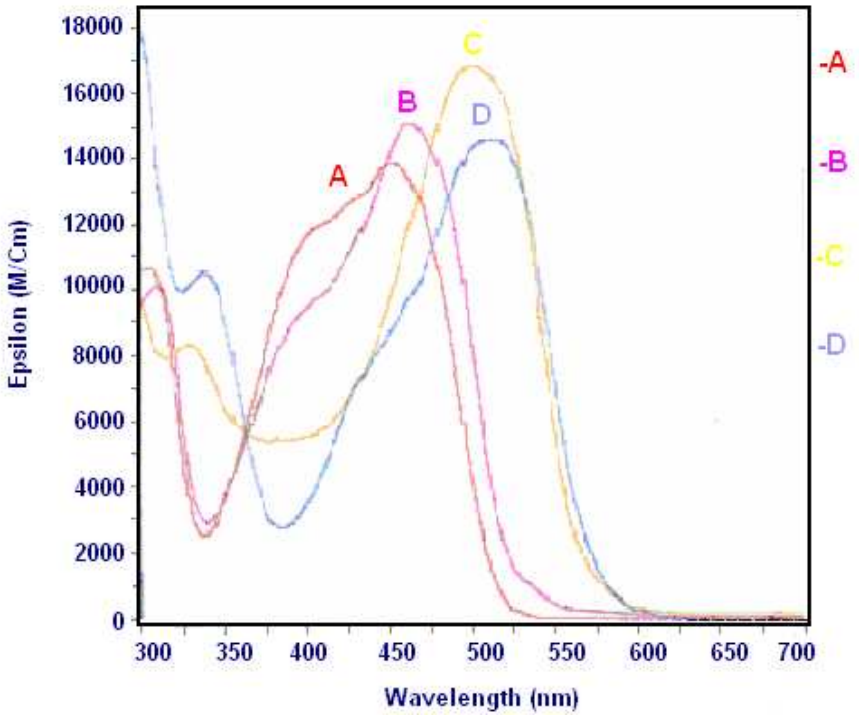

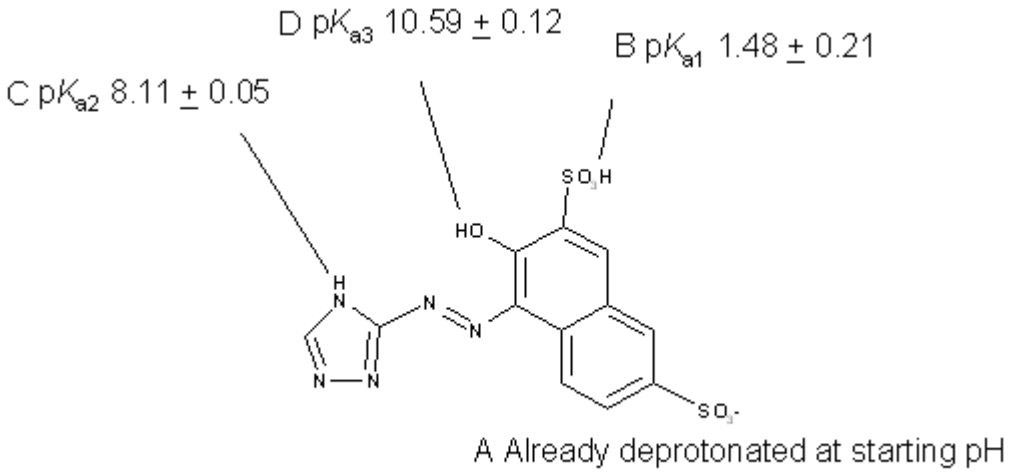

Figure 32: L5B species distribution curves as a function of pH.

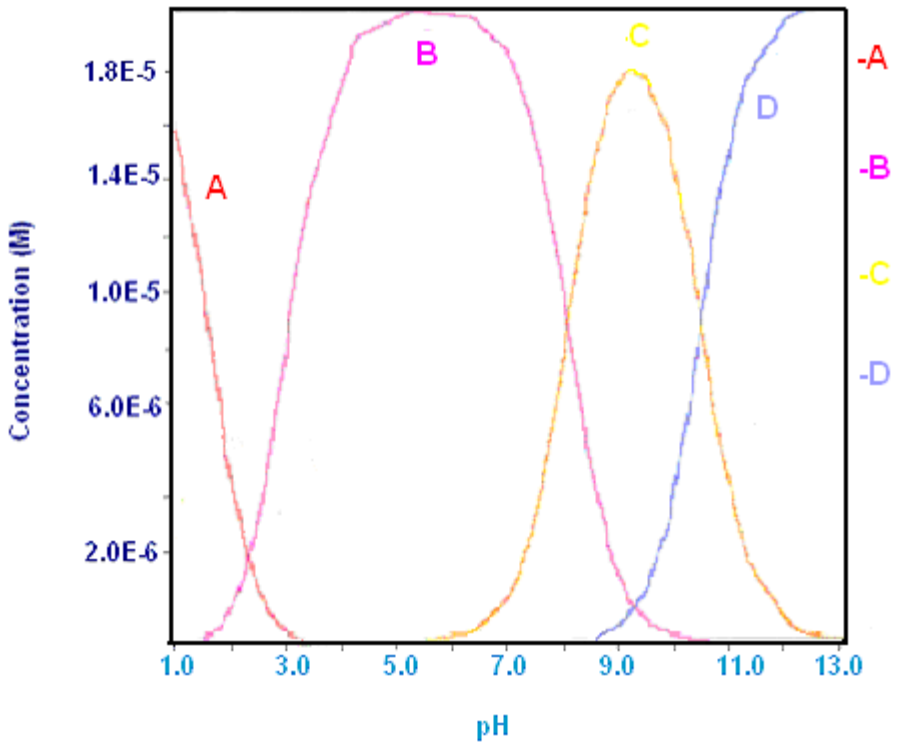

Table 6: Measured pK_a values of all dyes investigated.

Dye	pK_{a1}	pK_{a2}	pK_{a3}	pK_{a4}	pK_{a5}	pK_{a6}
L1	2.40 ± 0.82	4.20 ± 0.70	5.90 ± 0.48	6.80 ± 0.27	10.30±0.21	12.70±0.10
L5	1.50 ± 0.17	2.98 ± 0.28	8.19 ± 0.03	10.68± 0.09	N/A	N/A
L5B	1.48 ± 0.21	8.11 ± 0.05	10.59± 0.12	N/A	N/A	N/A
PAN	2.82 ± 0.09	9.79 ± 0.20	N/A	N/A	N/A	N/A
L7	2.87 ± 0.23	9.02 ± 0.08	N/A	N/A	N/A	N/A
L3765	2.85 ± 0.15	9.65 ± 0.25	N/A	N/A	N/A	N/A

3.2 Discussion of pK_a values.

3.21 PAN, L7, L3765.

The pK_a values determined for these three ligands are all very similar since the molecules are the same except for L7 and L3765 which contain mono- and di-sulphonate groups respectively.

The values obtained for the first pK_a are in good agreement with the previously reported pK_a value of PAN(around 3); this corresponds to the loss of the pyridinium proton. pK_a values for the loss of the napthol protons obtained in this study are around 9-10 whereas for PAN the reported value is around 12.[150]

The difference is attributed to the fact that this study was carried out in water whereas the previous study was carried out in 50% dioxane-water. The latter was also studied potentiometrically whereas this experiment was performed spectrophotometrically.

3.22 L1.

The values obtained for L1 are as expected for the various functional groups found in the molecule.[183] The data are consistent with the molecule having the hydrazo form as opposed to the azo tautomeric form. This was confirmed further by a theoretical study performed by Avecia using ACD Labs pK_a prediction software.

A comparison of calculated and predicted values can be seen in Table 7.

Table 7: Observed and ACD LABS calculated pK_a values for L1 in the hydrazo form.

	pK_{a1}	pK_{a2}	pK_{a3}	pK_{a4}	pK_{a5}	pK_{a6}
Observed	2.4 ± 0.82	4.2 ± 0.70	5.9 ± 0.48	6.8 ± 0.27	10.3±0.21	12.7 ± 0.10
Calculated	1.7 ± 0.2	2.5 ± 0.1	6.3 ± 0.5	8.4 ± 0.2	11.7 ± 0.2	13.8 ± 0.4

3.23 L5 and L5B.

The values obtained for L5 and L5B are in good agreement with pK_a values previously found for the various functional groups found in the molecule.[183] Avecia expressed a specific interest in the comparison of the two molecules L5 and L5B. As can be seen they are identical apart from the absence of the carboxylic acid group in L5B.

The pK_a determinations helped to illustrate the fact that the carboxylic acid is missing in L5B due to the absence of the pK_a of the carboxylic acid around pH 3. All the other pK_a values for L5B are apparent and are almost identical for those found for L5.

3.3 Experimental.

3.31 pK_a measurements of L1, L5, L5B, PAN, L7 and L3765

3.32 PAN, L7, L3765.

Two aqueous solutions of PAN (both 2 x 10^{-5} mol dm^{-3}) were made:

(a) To pH 2 using HCl and (b) to pH 13 using KOH

A series of samples were prepared by mixing (a) and (b) to give solutions over the range between pH 2 and pH 12.6. The visible spectra were recorded with a thermostatted Perkin Elmer UV-Visible lambda 25 spectrometer at 25^{o}C. The complete spectral data were then analysed using the computer program SPECFIT/32.

The experiment was repeated using the same conditions apart from the PAN was in 50% dioxane-water; this was carried out to compare with results obtained by Kortuglu et al[150].

The experiment was also repeated for L7 and L3765 in aqueous media and keeping all the other conditions the same.

3.33 L1.

The experimental conditions were kept exactly the same as in 3.32 apart from the pH range used was from 1.5-10.

3.34 L5 and L5B.

The experimental conditions were kept exactly the same as in 3.32 apart from the pH range used was from 0.6-13.6.

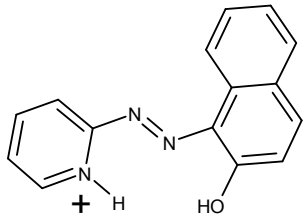

PAN

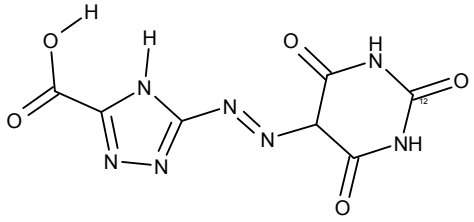

L1

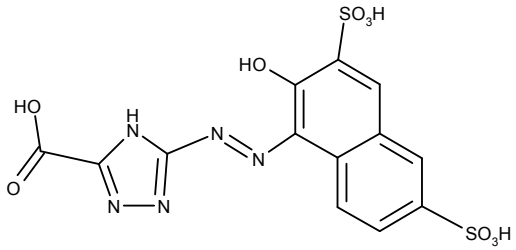

L5

Chapter 4: Attempted measurements of the stability constants of Ni(II) complexes of PAN, L1 and L5 using UV-Visible spectroscopy.

Introduction.

For metal-ligand complexes measurements of stability constants are of fundamental importance. In the development of metallised dyes for use in printer inks, higher stability metal-dye complexes are more favoured than those with lower stability because if a dye-metal complex has a low stability it will be more likely to fade or discolour, and this is obviously undesirable.

Stability constants can be measured in numerous ways such as potentiometric titrations, kinetically using ligand and/or metal exchange reactions, by polarography and by various forms of spectroscopy.[155-162]

In this chapter UV-Visible spectrophotometry was utilised in an attempt to measure the stabilities of Ni(II) complexes formed by the dyes PAN, L1 and L5. In all cases, the data were analysed using SPECFIT/32.

4.1 Results.

Figure 33: UV-Visible spectra for a 50% dioxane-water solution of PAN (2×10^{-5} mol dm^{-3}) reacted with Ni^{2+} using Ni(II):PAN concentration ratios in the range 1:10 to 10:1.

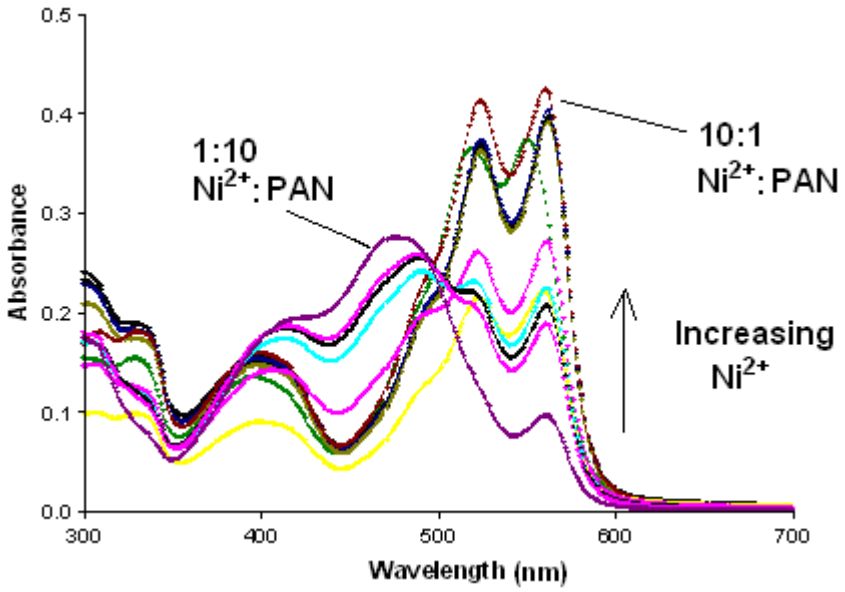

The complete spectra shown in Figure 33 were analysed using the global analysis routine of SPECFIT/32, assuming a model based on the presence of free PAN, $[Ni(PAN)]^+$ and $[Ni(PAN)_2]$. In these calculations the spectra of PAN and $[Ni(PAN)_2]$ were fixed by recording them separately at the same pH. The latter was that found in the presence of excess PAN.

After convergence the spectra shown in Figure 34 were calculated. However, the stability constants for the two complexes could not be determined reliably by this method as discussed later.

Figure 34: Calculated spectrum of $[Ni(PAN)]^+$ at pH 6 and 25 ^oC.

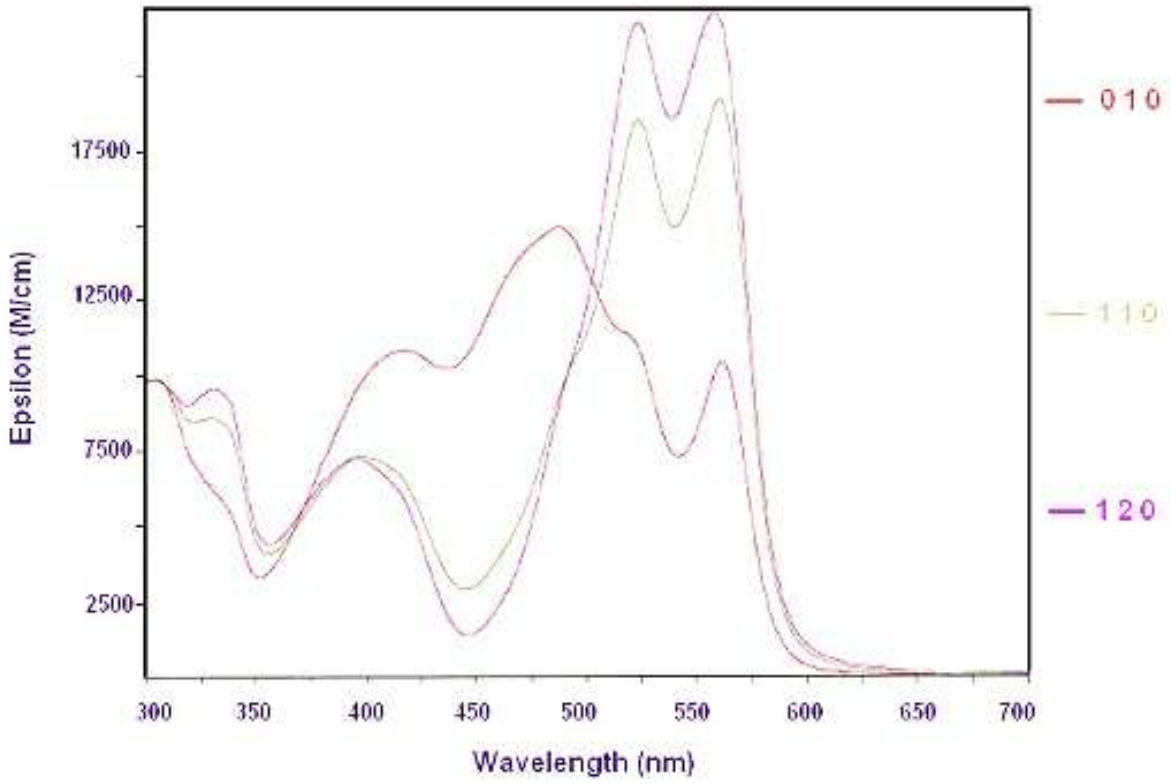

Key: **010 = Free PAN (fixed spectrum)**

110 = $[Ni(PAN)]^+$

120 = $[Ni(PAN)_2]$ (fixed spectrum)

Figure 35: UV-Visible spectra of aqueous solutions of L1 (2×10^{-5} mol dm^{-3}) reacted with Ni^{2+} at pH 6 and 25 °C, with concentration ratios varying from 1:10 to 10:1.

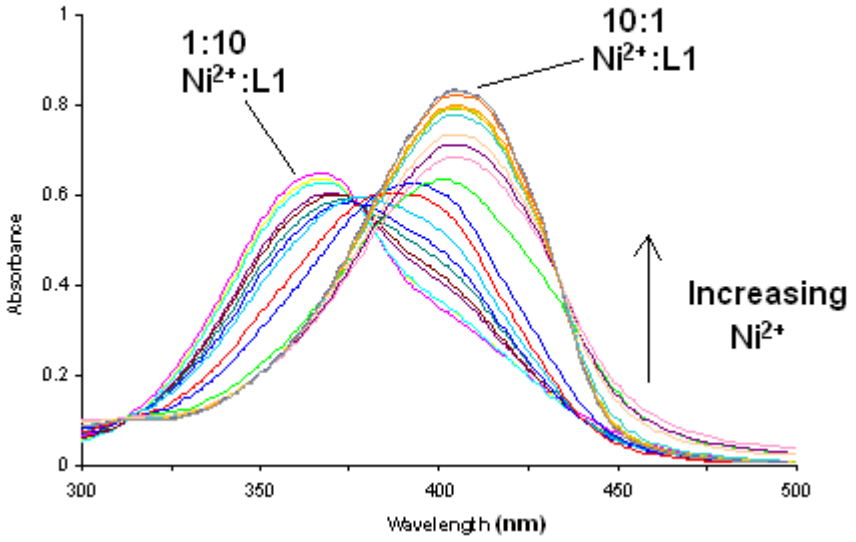

To fit the data in Figure 35, a model involving free dye, the mono- and bis-(L1)Ni(II) complexes and a bi Ni(II)(L1) complex was required to obtain a fit. The stability constants are collected in Table 8.

Figure 36: Calculated spectra for the species involved in the reaction of L1 with Ni^{2+} at pH 6 and 25 ^{o}C.

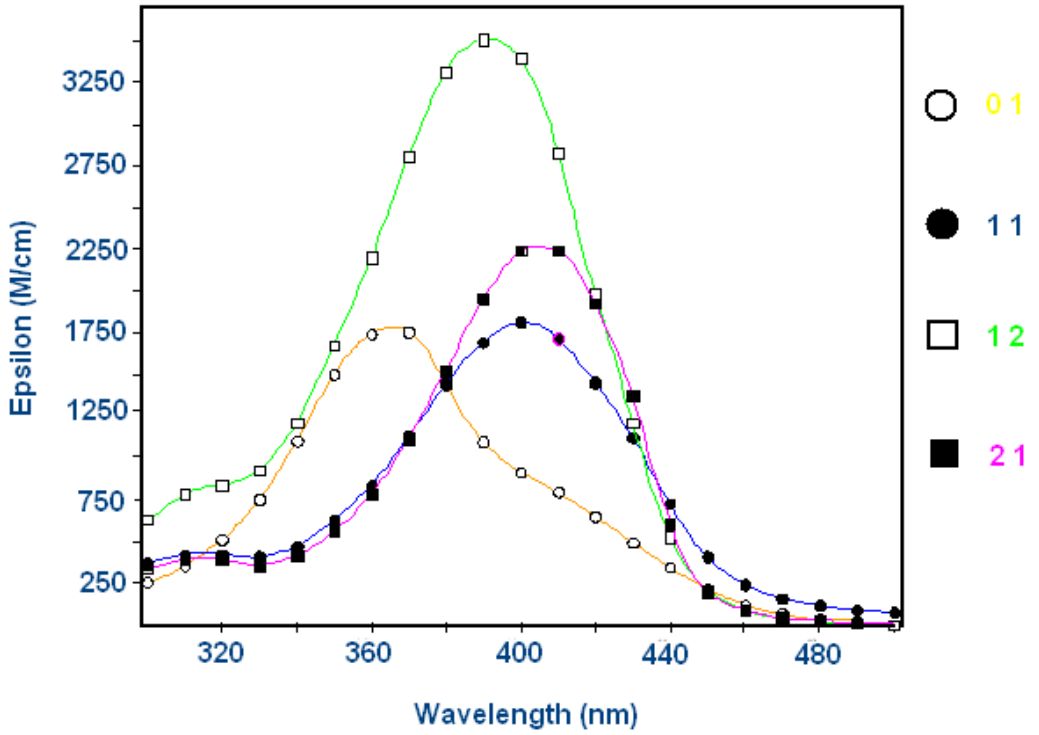

Key **01 = $[HL1]^{3-}$**

12 = $[Ni(L1)_2]^{4-}$

21 = $[Ni_2(L1)]^{+}$

11 = $[Ni(L1)]^{-}$

Figure 37: Spectra of L5 (2×10^{-5} mol dm^{-3}) reacted with Ni^{2+} in aqueous solution at 25 °C in the ratios from 1:10 to 10:1.

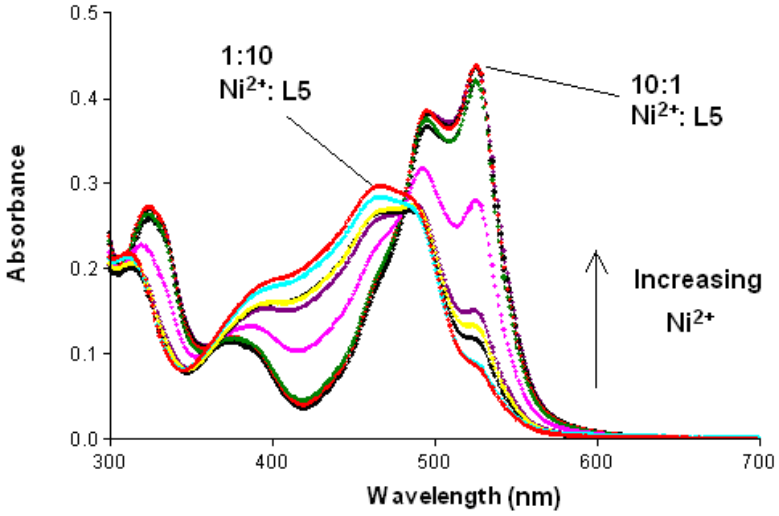

Figure 38: Calculated spectra for the species involved in the reaction of L5 with Ni^{2+} 1:10 to 10:1 at pH 6 and 25 °C.

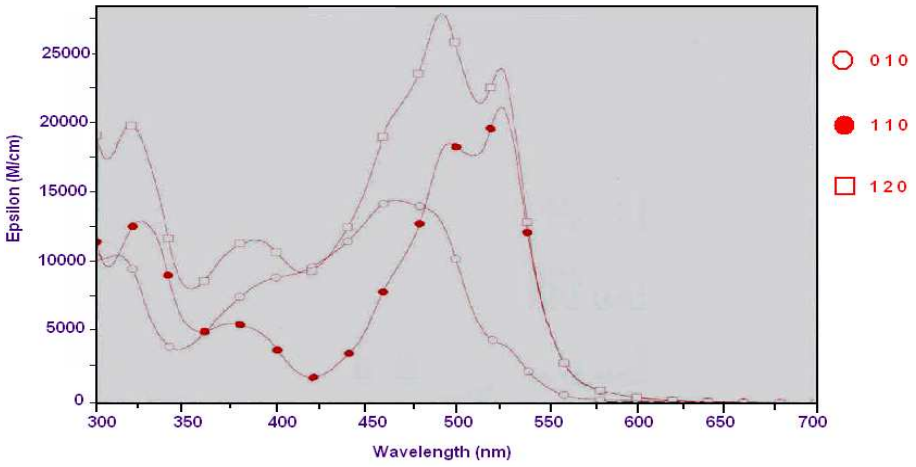

Key: **0 1 0 = $(HL5)^{3-}$** **1 1 0 = $[Ni(L5)]^{3-}$**

1 2 0 = $[Ni(L5)_2]^{8-}$

Table 8: Calculated stability constants for the Ni(II) complexes of PAN, L1 and L5 from SPECFIT/32.

Ligand (solvent)	Log K_1	Log K_2	Log $K(Ni_2L)$
PAN (50% dioxane-water)	*a*	*a*	n/a
L1 (Aqueous)	27.40 ± 0.25	20.65 ± 0.06	26.40 ± 0.25
L5 (Aqueous)	9.04 ± 0.77	5.56 ± 0.19	N/A

a Too large to measure reliably by this method

4.2 Discussion.

4.21 Attempted measurements of the stability constants of PAN with Ni^{2+}.

In this experiment it was necessary to define the spectra of free PAN and $[Ni(PAN)_2]$ in order to obtain a fit. It appears that the stability constants of this system are too large to measure reliably by the spectrophotometric method. In a previous study of the reactions between Ni^{2+} and PAN using potentiometry,[155] stability constants were reported to be $\log(K_1) = 12.7$ and $\log(K_2) = 12.6$. In the current spectral study in the same solvent, convergence was achieved but with $\log(K_1) = 41.5 \pm 0.3$ and $\log(K_2) = 36.8 \pm 0.3$.

The values found by spectrophotometry are impossibly large and clearly fictitious. For other terdentate ligands values are reported to be $\log(K_1) = 10.7$

(2,2':6',2''-Terpyridine)[184] and log(K_1)= 7.86 (Iminodiacetic acid)[185], and for PAN values in the range 12-13 as found potentiometrically are more realistic.

4.22 Attempted measurements of the stability constants of L1 with Ni^{2+}.

The experiment gave a good calculated spectral fit as can be seen in Figure 36. A model involving the species $[Ni(L1)_2]^{4-}$, $[Ni_{2(}L1)]^{+}$ and $[Ni(L1)]^{-}$ was used in order to obtain convergence. Most interestingly in the presence of excess Ni^{2+} the dye L1 can bind two Ni(II) ions.

Postulated structures for $[Ni_{2(}L1)]^{+}$ and $[Ni(L1)]^{-}$ are shown here.

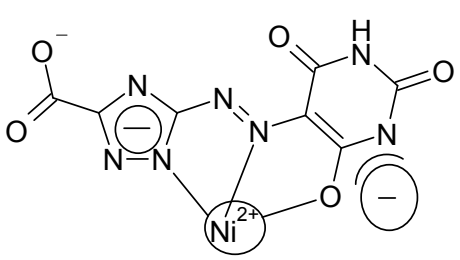

$[Ni(L1)]^{-}$

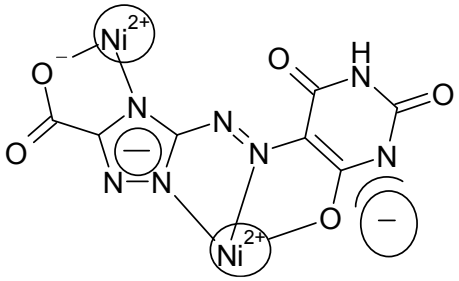

$[Ni_2(L1)]^{+}$

The stability constants were found to be log K_1 = 27.40 ± 0.25, log K_2 = 20.65 ± 0.06 and log $K(M_2L)$ = 26.40 ± 0.25 . These values appear to be rather large when compared to the values found for other terdentate ligands reacted with Ni^{2+} such as PAN[155] and PAR.[157] Other methods are required to confirm these preliminary values.

4.23 Attempted stability constant measurement of L5 with Ni^{2+}.

The experiment gave a good calculated spectral fit as can be seen in Figure 38. The spectrum of free L5 was fixed to help obtain a fit. The stability constant values obtained were log K_1 = 9.04 $\pm$ 0.77 and log K_2= 5.56 $\pm$ 0.19.

These values are in good agreement with the previous studies of 2,2':6',2''-Terpyridine[184] $\log(K_1) = 10.7$ and Iminodiacetic acid[185] $\log(K_1) = 7.86$

4.3 Experimental.

4.31 Stability constant measurements using the UV-Visible method for reactions of PAN, L1 and L5 with Ni(II).

A spectrophotometric study of the reaction of PAN (2×10^{-5} mol dm^{-3}) in 50% dioxane-water with Ni(II) in varying ratios from 10:1 to 1:10 ligand: Ni^{2+} was carried out on a thermostatted Perkin Elmer UV-Visible spectrometer at 25 ^{o}C. A pH of 5.99 $\pm$ 0.01 was held constant using 2,6-Lutidine (0.02 mol dm^{-3}) Spectra were recorded over the wavelength range of 300-700 nm.

Solutions were prepared by adding 2.5 cm^3 of stock dye (2×10^{-4} mol dm^{-3}) along with 5 cm^3 of 2,6-Lutidine(0.1 mol dm^{-3}) to a 25 cm^3 volumetric flask. Stock Ni^{2+} (0.01 mol dm^{-3}) was added by repette to the flask in a ratio that gave 10 parts dye to 1 part Ni^{2+}. The flask was then filled to the mark with 50% dioxane-water. The same procedure was applied for each solution changing the $[Ni^{2+}]$ to cover the range 1-10 to 10 parts Ni^{2+} to 1 part dye.

The data obtained were analysed using the program SPECFIT/32. The program gave an unsatisfactory fit until the spectra of free PAN and $[Ni(PAN)_2]$ were fixed. The fixed spectrum of PAN was obtained by recording its spectrum at the same concentration and same pH, and this was then inserted into the program. The fixed spectrum of $[Ni(PAN)_2]$ was estimated by taking the 10:1 ligand:metal

spectrum and making the assumption that the bis(PAN)Ni(II) complex had completely formed. This left 8 parts of unreacted PAN, so an Excel spreadsheet was used to subtract this from the 10:1 spectrum to give the fixed spectrum of $[Ni(PAN)_2]$ which was inserted into SPECFIT/32.

A spectrophotometric study of the reaction of either L1 or L5 (2×10^{-5} mol dm^{-3}) with Ni(II) was carried out in water using the same conditions used for the study with PAN. Spectra were recorded over the wavelength range of 500-300 nm (L1) and 300-700 nm (L5).

SPECFIT/32 was used to estimate log K_1 and log K_2 but it was necessary to fix the spectra of L1 and L5 to obtain a fit. The results are in Table 8.

Chapter 5: Single wavelength stopped-flow kinetic studies of the reactions of Ni(II) with PAN, PADA, SUDAN I, L3765 and L7.

Introduction.

As discussed in Chapter 1, the stability of metal complexes can be investigated through measurements of the rate constants for formation (k_f) and dissociation (k_d) ($K = k_f / k_d$). In this chapter the mono Ni(II) complexes of the ligands shown in Figure 39 were examined using the stopped-flow method.

5.1 Results.

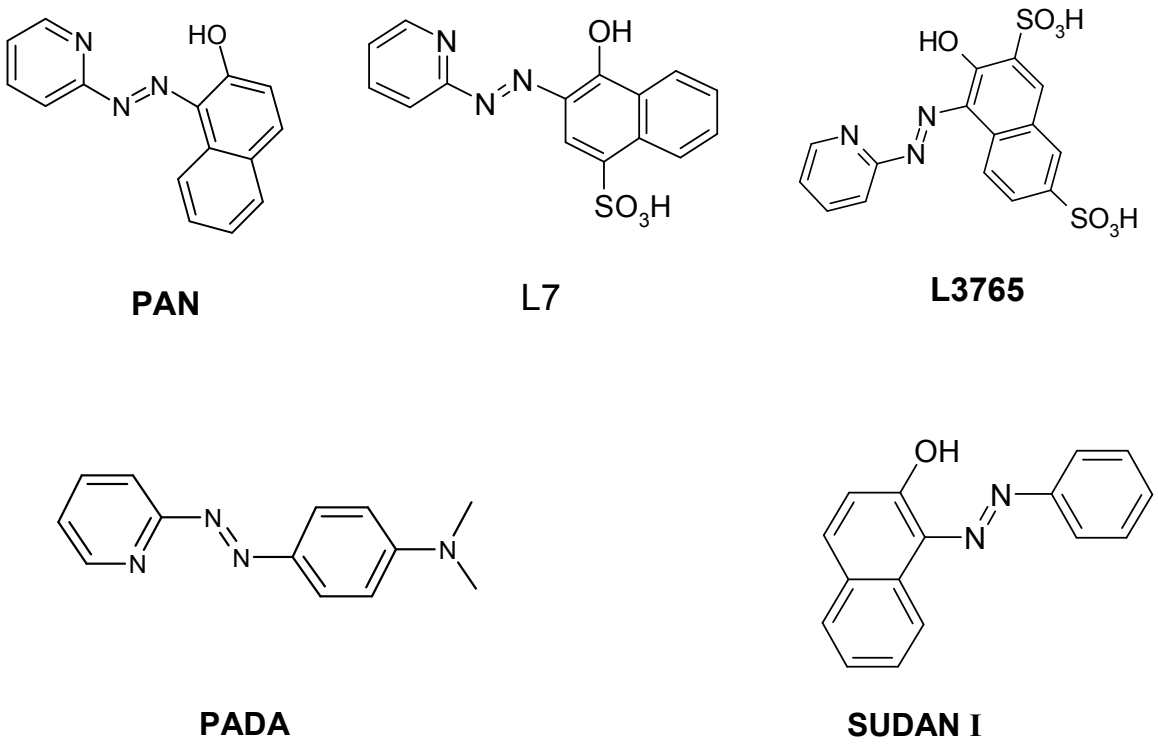

Figure 39: Ligands studied and compared.

The reaction of PAN with excess Ni^{2+} revealed a two step kinetic process as shown in Figures 40-42.

Figure 40: Stopped-flow trace of the reaction of PAN (10^{-5} mol dm^{-3}) with Ni^{2+} (0.0122 mol dm^{-3}) at 460 nm using a split time base of 0.2/5 seconds.

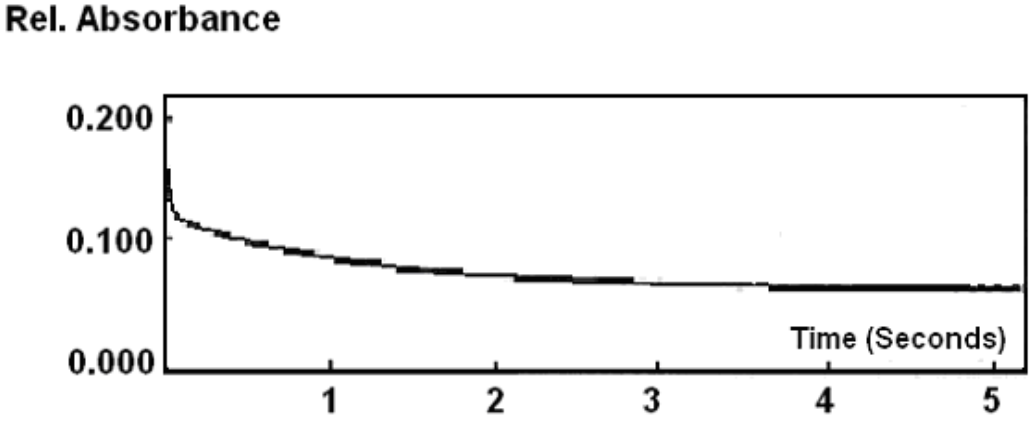

Figure 41: Stopped-flow trace of the reaction of PAN (10^{-5} mol dm^{-3}) with Ni^{2+} (0.0122 mol dm^{-3}) at 460 nm using a split time base of 0.2/5 seconds (the first 0.2 s).

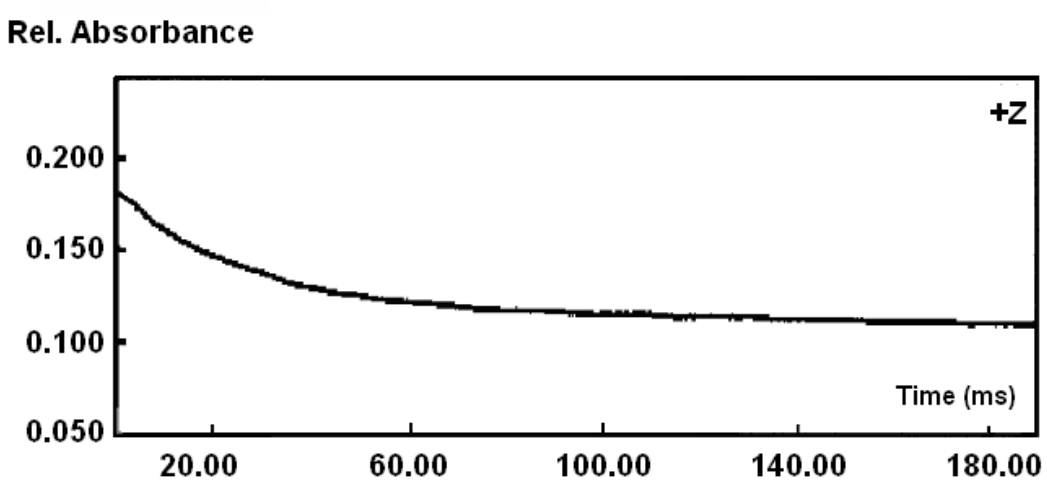

Figure 42: Stopped-flow trace of the reaction of PAN (10^{-5} mol dm^{-3}) with Ni^{2+} (0.0122 mol dm^{-3}) at 460 nm using a split time base of 0.2/5 seconds (the last 5 s).

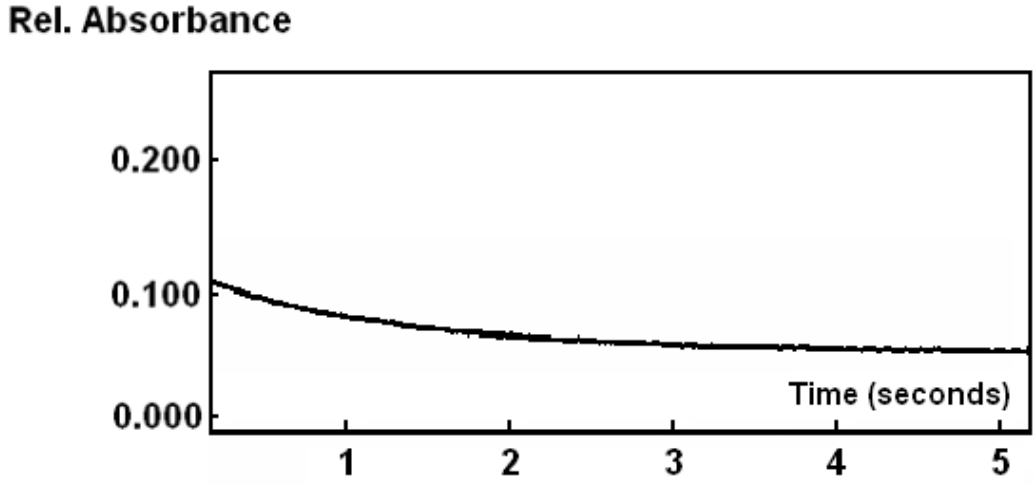

A mechanism that accounts for this two step reaction involves rapid metal chelate formation involving the pyridine *N*-atom and an azo-*N* atom, followed by slower final chelate ring closure by the phenolic *O*-atom. H-bonding is postulated to account for the slower final chelate ring closure as shown in the following schemes:

Proposed mechanism: stage I

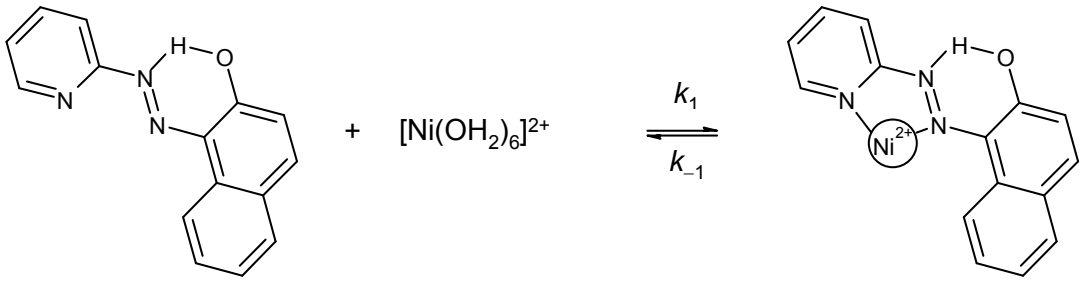

PAN **I**

Proposed mechanism: stage II

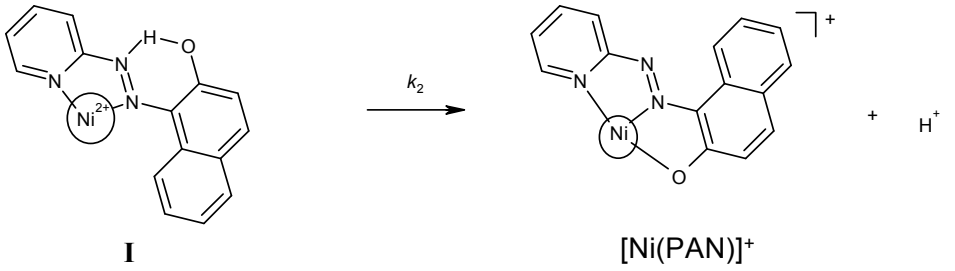

I [Ni(PAN)]+

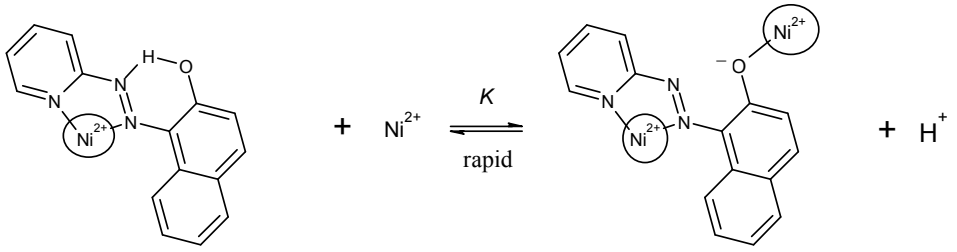

I **II**

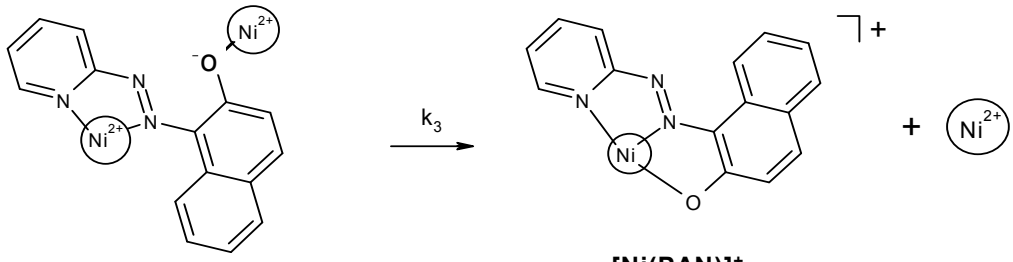

II **[Ni(PAN)]+**

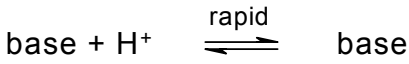

Derivation of the rate-laws for Stages I and II

Stage I

Using excess $[Ni(OH_2)_6]^{2+}$,

$$\frac{d[\mathrm{I}]}{dt} = k_1[\mathrm{Ni}^{2+}][\mathrm{PAN}] + k_{-1}$$

where, $$k_{1\mathrm{obs}} = k_1[\mathrm{Ni}^{2+}] + k_{-1} \qquad (1)$$

and,

$$\frac{d[\mathrm{Ni(PAN)}^{+}]}{dt} = k_2[\mathrm{I}] + k_3[\mathrm{II}]$$

$$= -\frac{d([\mathrm{I}] + [\mathrm{II}])}{dt}$$

Stage II

Defining

$$K = \frac{[\mathrm{II}]}{[\mathrm{I}][\mathrm{Ni}^{2+}]}$$

$$[\mathrm{II}] = K[\mathrm{I}][\mathrm{Ni}^{2+}]$$

Hence

$$-\frac{d[\mathrm{I}](1 + K[\mathrm{Ni}^{2+}])}{dt} = (k_2 + k_3K[\mathrm{Ni}^{2+}])[\mathrm{I}]$$

And

$$-\frac{d[\mathrm{I}]}{dt} = \left(\frac{k_2 + k_3K[\mathrm{Ni}]}{1 + K[\mathrm{Ni}]}\right)[\mathrm{I}] = k_{2\mathrm{obs}}[\mathrm{I}]$$

Where

$$k_{2\mathrm{obs}} = \frac{k_2 + k_3K[\mathrm{Ni}^{2+}]}{1 + K[\mathrm{Ni}^{2+}]} \qquad (2)$$

A plot of k_{1obs} versus [Ni^{2+}] [equation (1)] is shown in Figure 43, and a weighted linear squares analysis gives $10^{-3}k_1 = 3.14 \pm 0.26$ dm^3 mol^{-1} s^{-1} and $k_{-1} = 3.09 \pm 1.68$ s^{-1}.

Figure 43: First stage reaction of Ni^{2+} with PAN at 25°C.

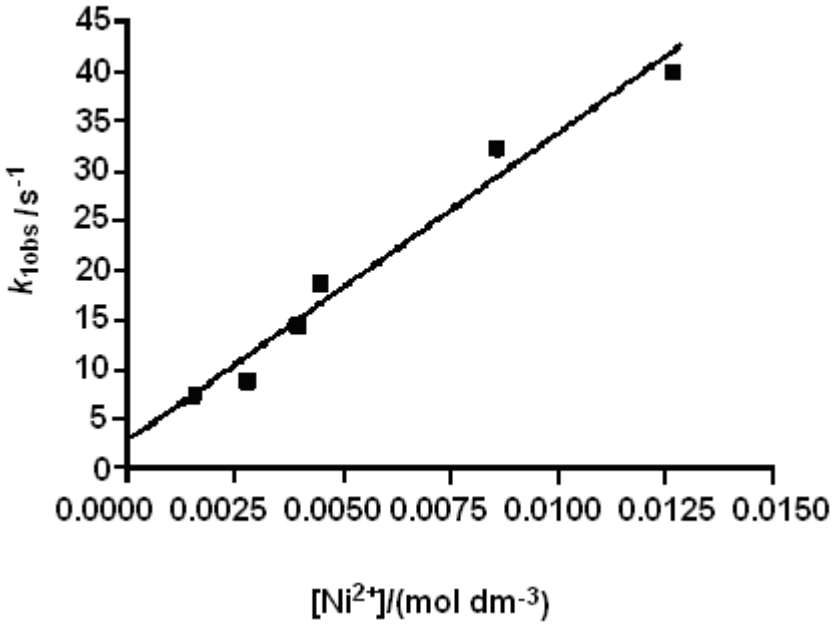

The calculated stability constant for the formation of **I** is therefore:

$$K = (3.14/3.09) \times 10^3 = (1.02 \pm 0.56) \times 10^3 \text{ dm}^3 \text{ mol}^{-1}$$

Figure 44: Second-stage reaction of PAN with Ni^{2+} [Equation (2), p.92].

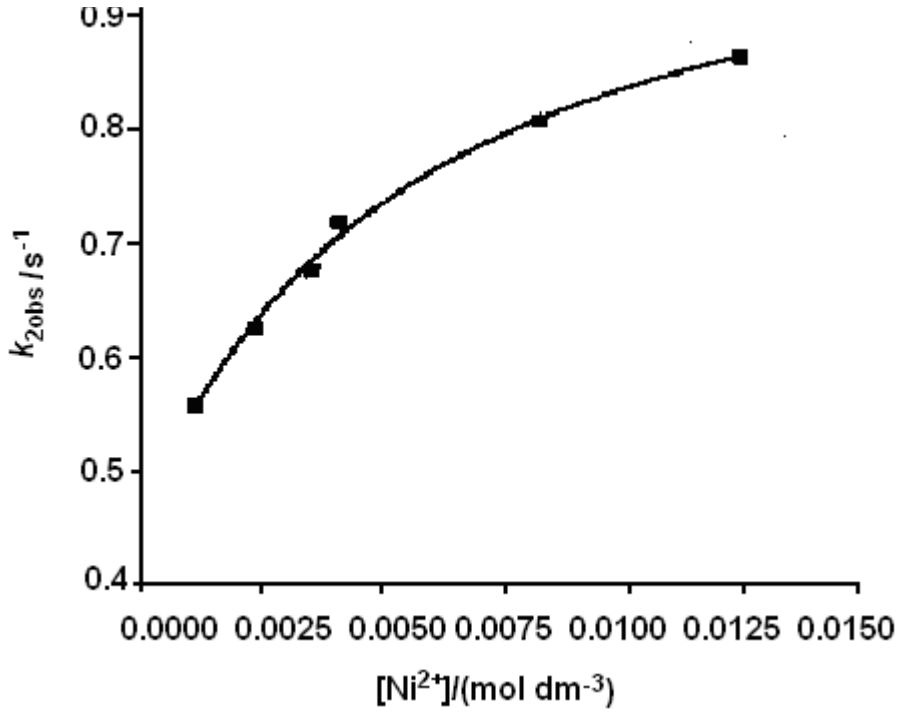

A weighted non-linear least-squares analysis gives

$k_2 = 0.451 \pm 0.026\ s^{-1}$

$k_3 = 1.054 \pm 0.044\ s^{-1}$ and $K = 181.8 \pm 44.4$

Similar results to those found for PAN were also observed for L7, L3765, PADA and SUDAN I, and the values of the rate and equilibrium constants are compared in Table 9.

Table 9: Comparison of rate and equilibrium constants for the reaction of Ni^{2+} with PAN, L7, L3765 and PADA and SUDAN I.

Ligand	$10^{-3}k_1$/ (dm^3 mol^{-1} s^{-1})	k_{-1}/s^{-1}	$10^{-3}K_1 = k_1/k_{-1}$ / (dm^3 mol^{-1})	k_2/s^{-1}	k_3/s^{-1}	[a]K
PAN	3.14 ±0.26	3.09 ±1.68	1.02 ±0.56	0.45 ±0.026	1.05 ±0.04	181.8 ± 44.4
L7	2.18 ±0.18	3.75 ±1.18	0.58 ±0.33	0.32 ±0.17	2.30 ±0.30	173.0 ± 88.3
L3765	2.60 ±0.17	4.79 ±1.08	0.54 ±0.13	0.51 ±0.02	1.09 ±0.06	132.0 ± 34.2
PADA	1.28 ±0.053	0.56 ±0.31	2.31 ±0.71	n/a	n/a	n/a
SUDAN I	0.44 ± 0.020	0.15 ±0.05	2.95 ±0.99	n/a	n/a	n/a

[a]K = equilibrium constant for Ni^{2+}-catalysed pathway.

5.2 Discussion.

5.21 Two stage mechanism of the reaction between Ni^{2+} and PAN.

In a previous stopped-flow kinetic study of the reaction of Ni^{2+} with PAN it was reported[124] that the reaction proceeds in a single step, but the results found in this study give good evidence that the reaction occurs in a two step process.

As discussed earlier the first step involves rapid metal chelate formation involving the pyridine *N*-atom and an azo-*N* atom, followed by slower final chelate ring closure by the phenolic *O*-atom. H-bonding is postulated to account for the slower final chelate ring closure.

In the previous study[124] only one step was reported, and this was the slower final ring closure step; it is concluded that the earlier study missed the more rapid first step.

5.22 Reaction of Ni^{2+} with PADA and SUDAN I to confirm the two stage mechanism found for the reaction of Ni^{2+} with PAN.

To confirm the findings of the two stage mechanism for the reaction of PAN with Ni^{2+}, the experiment was repeated using PADA and SUDAN I. PADA contains only a pyridine and an azo-*N*-donor but no phenol group, hence eliminating the final ring closure step. SUDAN I contains no pyridine but does contain a phenol and an azo-*N*.

The values in Table 9 confirm the findings for PAN. For the reaction of PADA with Ni^{2+}, $k_1 = (1.28 \pm 0.053) \times 10^3$ dm^3 mol^{-1} s^{-1} and this compares favourably with the first step of the reaction of PAN with Ni^{2+}

where $k_1 = (3.14 \pm 0.26) \times 10^3$ dm^3 mol^{-1} s^{-1}. For the reaction of SUDAN I with Ni^{2+}, a single stage reaction is again observed with $k_1 = (0.44 \pm 0.02) \times 10^3$ dm^3 mol^{-1} s^{-1}.

5.23 Stability constant of the bidentate intermediate $[Ni(PAN)]^{2+}$.

The stability constant for the bidentate intermediate **I**, $[Ni(PAN)]^{2+}$, was found to be 1.02×10^3 dm^3 mol^{-1}, and this value compares well with the stability constants of other Ni^{2+} complexes with *bidentate* ligands such as SUDAN I where $K = 2.95 \times 10^3$ dm^3 mol^{-1}, and PADA where $K = 2.31 \times 10^3$ dm^3 mol^{-1}. A much larger stability constant is found for Ni^{2+} complexes with *terdentate* ligands.[156]

From a previous study of PAN the overall stability constant in 50% dioxane-water was found to be log(K) = 12.7.[155] Since this stability refers to the overall reaction, it is given by equation (3). Taking the values found for k_1/k_{-1} and k_2 an estimated value of k_{-2} can be determined.

$$K = \frac{k_1 \, k_2}{k_{-1} \, k_{-2}} \qquad (3)$$

The estimated value for k_{-2} has been found to be 9.12×10^{-11} s^{-1} in line with a very stable terdentate ligand complex.

5.24 Comparison of the results of the reaction of Ni^{2+} with PAN, L7 and L3765.

The results found for PAN and L7 and L3765 are in good agreement. The molecules are almost the same apart from the mono- and di-sulfonate groups in L7 and L3765 respectively. The stability values for the intermediate I of L7 and L3765 are slightly less than found for PAN this is attributed to the influence of the sulphonate groups.

5.3 Experimental.

5.31 Single wavelength stopped-flow kinetics of the reaction of Ni(II) with PAN, L3765 , L7 , PADA and SUDAN I.

The ligands (10^{-5} mol dm^{-3}) were reacted with an excess of Ni(II) [$(0.118 - 1.22) \times 10^{-2}$ mol dm^{-3}] to ensure the formation of the mono(ligand)Ni(II) species. The solutions were buffered at pH 6 with 2,6-Lutidine (0.02 mol dm^{-3}) at a constant ionic strength of 0.12 ($NaNO_3$) and constant temperature of 25.0 ^{o}C.

The reactions were studied with an Applied Photophysics stopped-flow at 460 nm for PAN using a split time base of 0.2 s (200 points) and 5.0 s (200 points). For L7 the reactions were studied at 525 nm, and for PADA at 550 nm using two time bases (0.2 s and 2 s). SUDAN I was studied at 495 nm using a single time base (10 s).

Chapter 6: Multi wavelength stopped-flow kinetics studies of the reactions of Ni(II) with L1, L7, L5 and L5B.

Introduction.

The four ligands shown below were reacted with excess Ni^{2+}; L5 and L5B were also used in excess over Ni^{2+}. The reactions were studied using multi wavelength stopped-flow spectrophotometry. The aims of the experiments were to determine the rate constants for complex formation, k_f, and to find evidence for the species that are produced in the presence of either excess metal ion or excess dye.

Avecia were interested in the species that are formed under different conditions. e.g. when excess metal is used do the ligands form ML or do they also form M_2L (M = metal ion, L = ligand). The molecules L5 and L5B were compared to establish the effect of the carboxyl group in L5 which is absent in L5B. In Figures 45-60 are shown the readouts from the stopped-flow global analysis software.

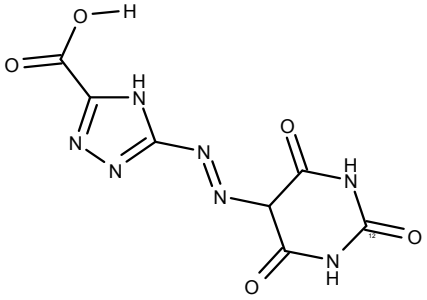

L1

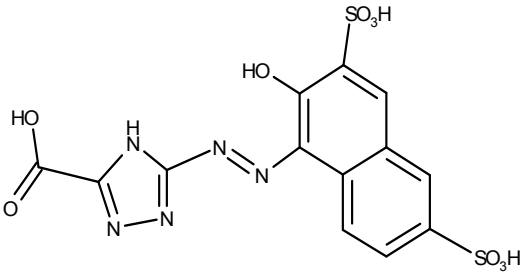

L5

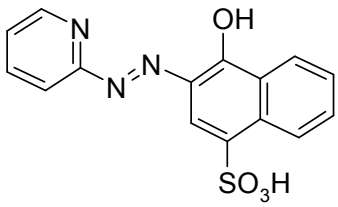

L7

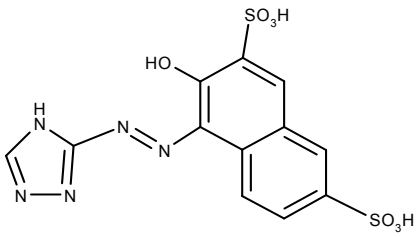

L5B

6.1 Results.

Figure 45: Stopped-flow readouts for the reaction of L1 (10^{-5} mol dm^{-3}) with excess Ni^{2+}(2×10^{-3} mol dm^{-3}) at 25 ^{o}C and at pH 6 using 2,6-Lutidine buffer (0.02mol dm^{-3}).

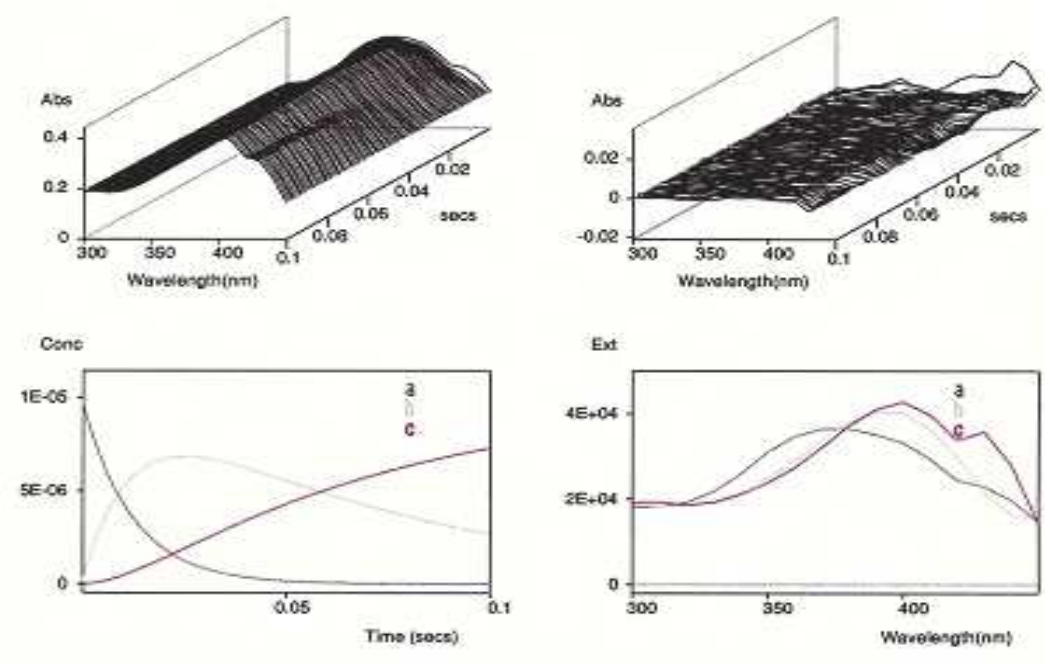

(A) (top left) Absorbance against wavelength against time for the reaction.

(B) (top right) The residuals for the readings.

(C) (bottom left) Variation of the concentrations of (a) $[L1]^{3-}$, (b) $[NiL1]^{-}$ and (c) $[Ni_2L1]^{+}$ with time.

(D) (bottom right) Kinetically determined UV-Visible spectra of the ligand $[L1]^{3-}$, and the metal complexes $[Ni(L1)]^{-}$ and $[Ni_2(L1)]^{+}$

Determination of k_f for the reactions of L1 with Ni^{2+}

The data analysed as a two-step consecutive pseudo-first-order process.

$$Ni^{2+} + L1^{3-} \xrightarrow{k_{f1}} [Ni(L1)]^-$$

$$Ni^{2+} + [Ni(L1)]^- \xrightarrow{k_{f2}} [Ni_2(L1)]^+$$

$k_{1obs} = [Ni^{2+}]k_{f1}$ where, rate = $k_{f1}[Ni^{2+}][L1]$

$k_{2obs} = [Ni^{2+}]k_{f2}$ where, rate = $k_{f2}[Ni(L1)^-][Ni^{2+}]$

From the global software

$k_{1obs} = 82.0 \pm 0.8\ s^{-1}$

$k_{2obs} = 15.1 \pm 0.3\ s^{-1}$

Using excess Ni^{2+} (2×10^{-3} mol dm^{-3})

$k_{f1} = 82/(2 \times 10^{-3})$ and $k_{f2} = 15.1/(2 \times 10^{-3})$ $dm^3\ mol^{-1}\ s^{-1}$

$k_{f1} = (4.10 \pm 0.8) \times 10^4\ dm^3\ mol^{-1}\ s^{-1}$

$k_{f2} = (7.55 \pm 0.4) \times 10^3\ dm^3\ mol^{-1}\ s^{-1}$

Figure 46: Absorbance against wavelength against time for the reaction of L7 (2×10^{-5} mol dm^{-3}) with excess Ni(II) (2×10^{-3} mol dm^{-3}) at 25°C and pH 6 with 2,6-Lutidine (0.02 mol dm^{-3}).

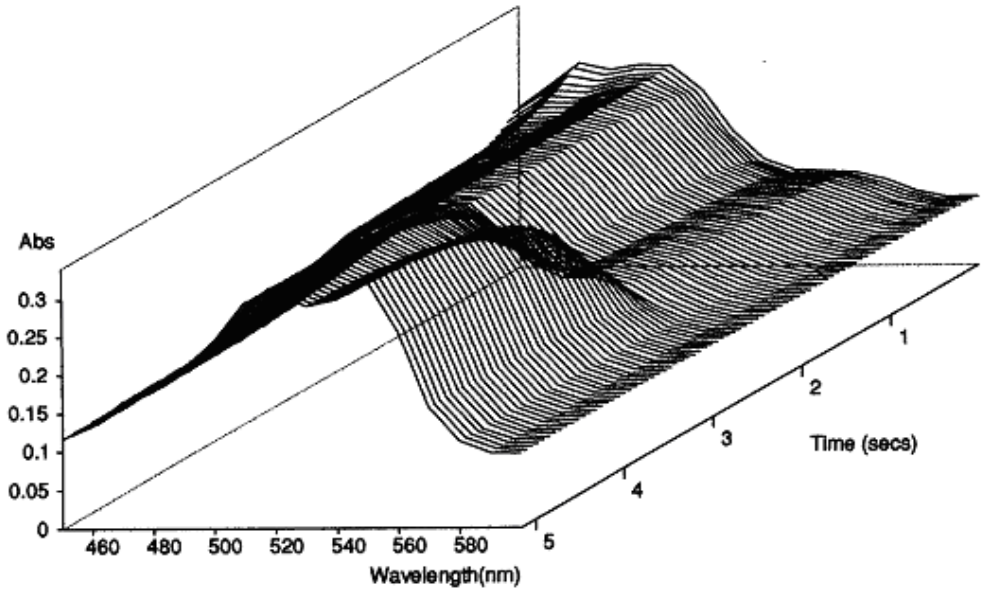

Figure 47: Kinetically determined UV-Visible spectra of the ligand (A) $[L7]^-$, and the metal complex (C) [Ni(L7)].

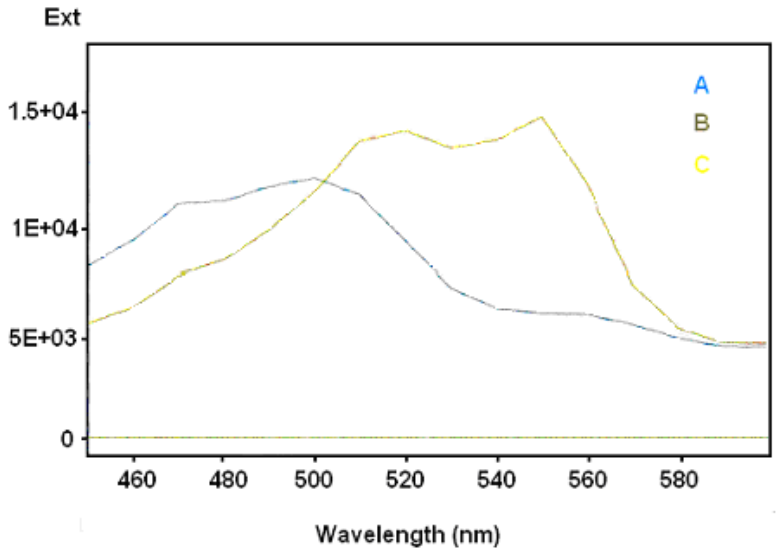

Figure 48: Variation of concentrations of (A) $[L7]^-$ and (B) [Ni(L7)] with time.

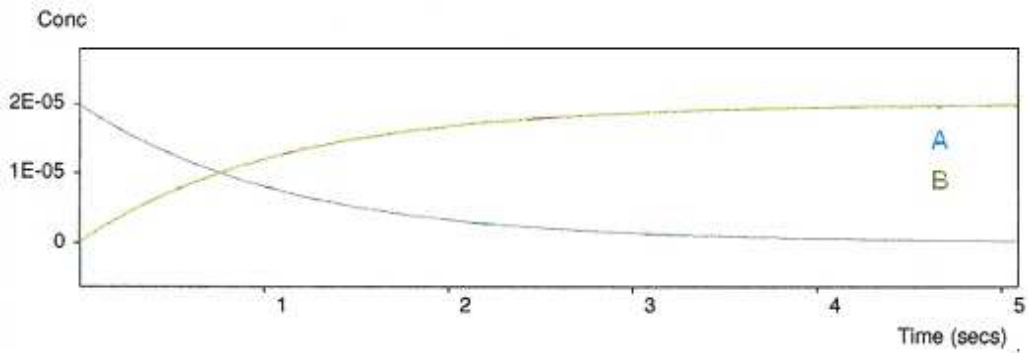

From the global software k_{obs}= 4.46 ± 0.01 s^{-1}

$k_{obs} = [Ni^{2+}]k_f$ where, rate = k_f $[Ni^{2+}][L]$

Using excess Ni^{2+} (2×10^{-3} mol dm^{-3})

$$k_f = 4.46/(2 \times 10^{-3})$$

$$= (2.23 \pm 0.50) \times 10^3 \text{ dm}^3 \text{ mol}^{-1} \text{ s}^{-1}$$

Figure 49: Absorbance against wavelength against time for the reaction of L5 (2×10^{-5} mol dm^{-3}) with excess Ni(II) (8×10^{-5} mol dm^{-3}) at 25°C and pH 6 with 2,6-Lutidine (0.02 mol dm^{-3}).

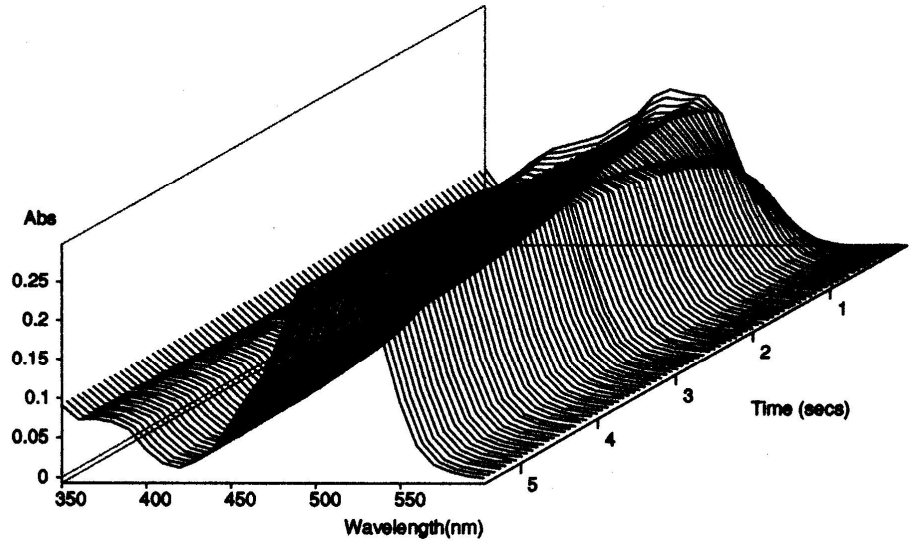

Determining k_f for the reactions of L5 with excess Ni^{2+}

The reactions were studied under second-order conditions, and analysed using the stopped-flow global software to give the following second-order rate constants:

$$k_{f1} = (1.395 \pm 0.0031) \times 10^5 \ \ dm^3\ mol^{-1}\ s^{-1}$$

$$k_{f2} = (2.158 \pm 0.0050) \times 10^4 \ \ dm^3\ mol^{-1}\ s^{-1}$$

Figure 50: Kinetically determined UV-Visible spectra of the ligand (A) $[L5]^{3-}$ and the metal complexes (D) $[Ni(L5)]^{3-}$ and (C) $[Ni_2(L5)]^{-}$.

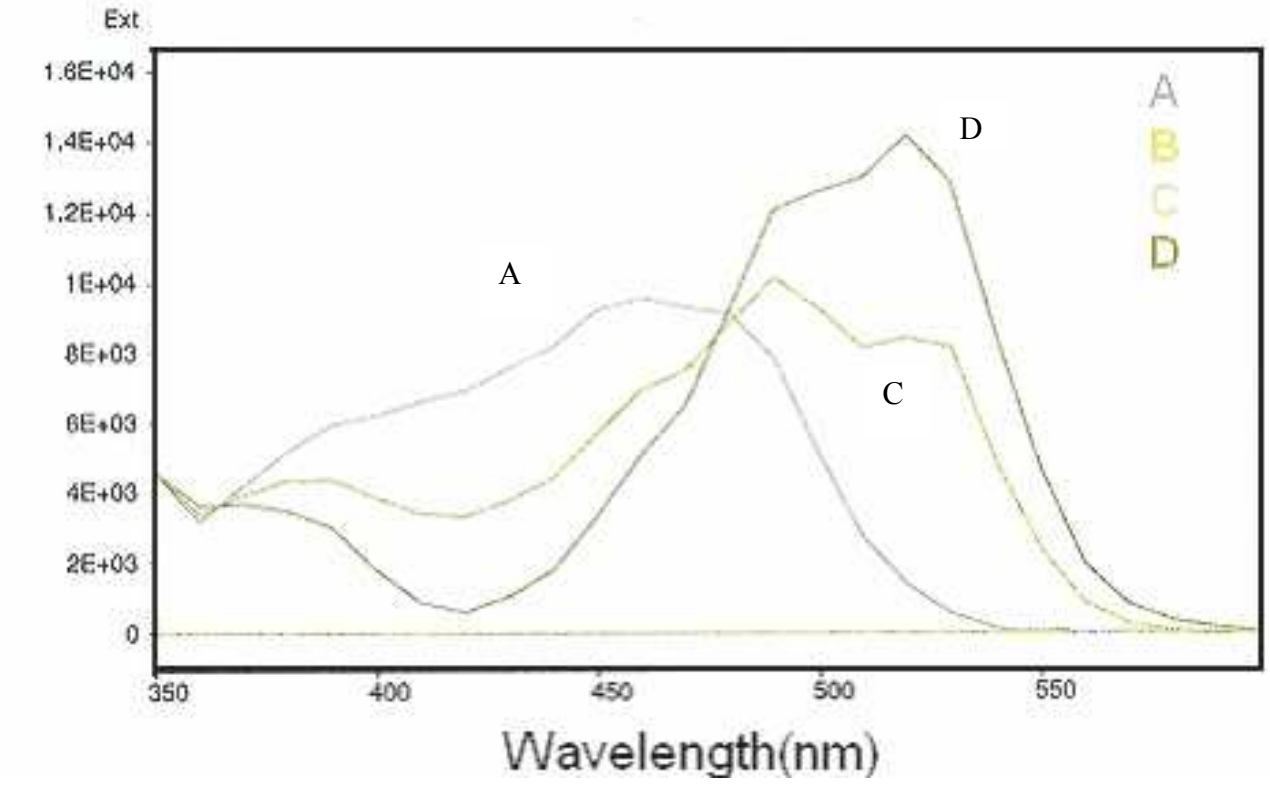

Figure 51: Variation of concentrations of (A) $[L5]^{3-}$, (C) $[Ni_2(L5)]^{-}$ and (D) $[Ni(L5)]^{3-}$ with time.

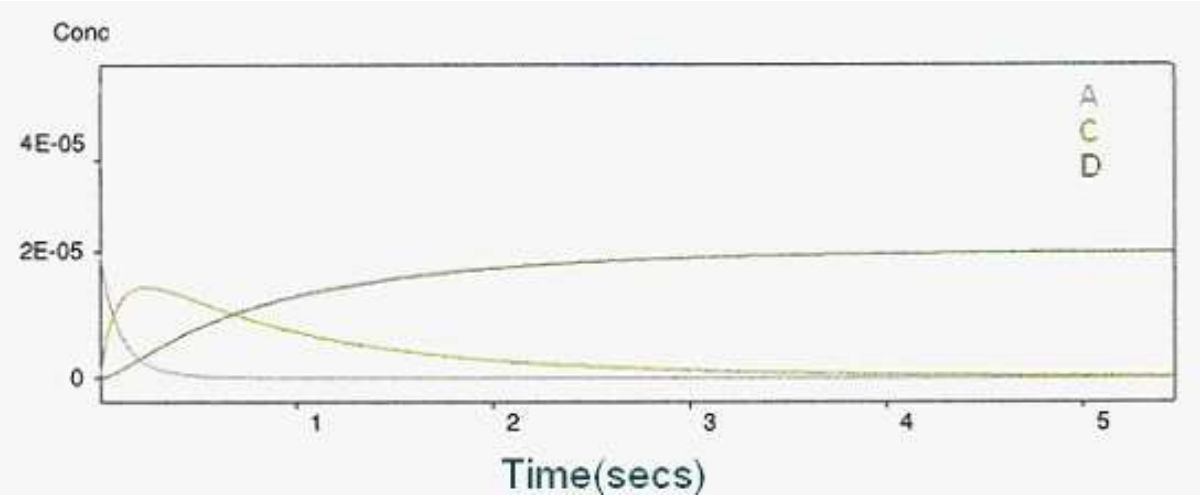

Figure 52: Absorbance against wavelength against time for the reaction of L5B (2×10^{-5} mol dm^{-3}) with excess Ni(II) (8×10^{-5} mol dm^{-3}) at 25 ^{o}C and pH 6 with 2,6-Lutidine (0.02 mol dm^{-3}).

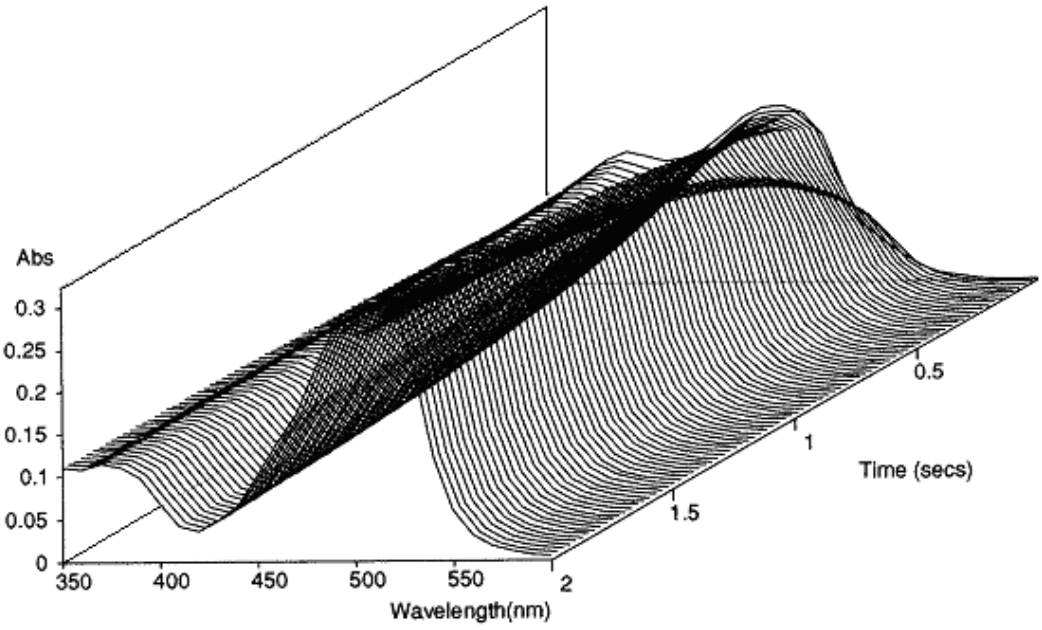

Determining k_f for the reactions of L5B with excess Ni^{2+}

The reactions were studied under second-order conditions, and the data were analysed using the stopped-flow global software to give a second-order rate constant:

$$k_f = (2.131 \pm 0.001) \times 10^4 \text{ dm}^3 \text{ mol}^{-1} \text{ s}^{-1}$$

Figure 53: Kinetically determined UV-Visible spectra of the ligand (A) $[L5B]^{2-}$ and the metal complex (C) $[Ni(L5B)]^{2-}$.

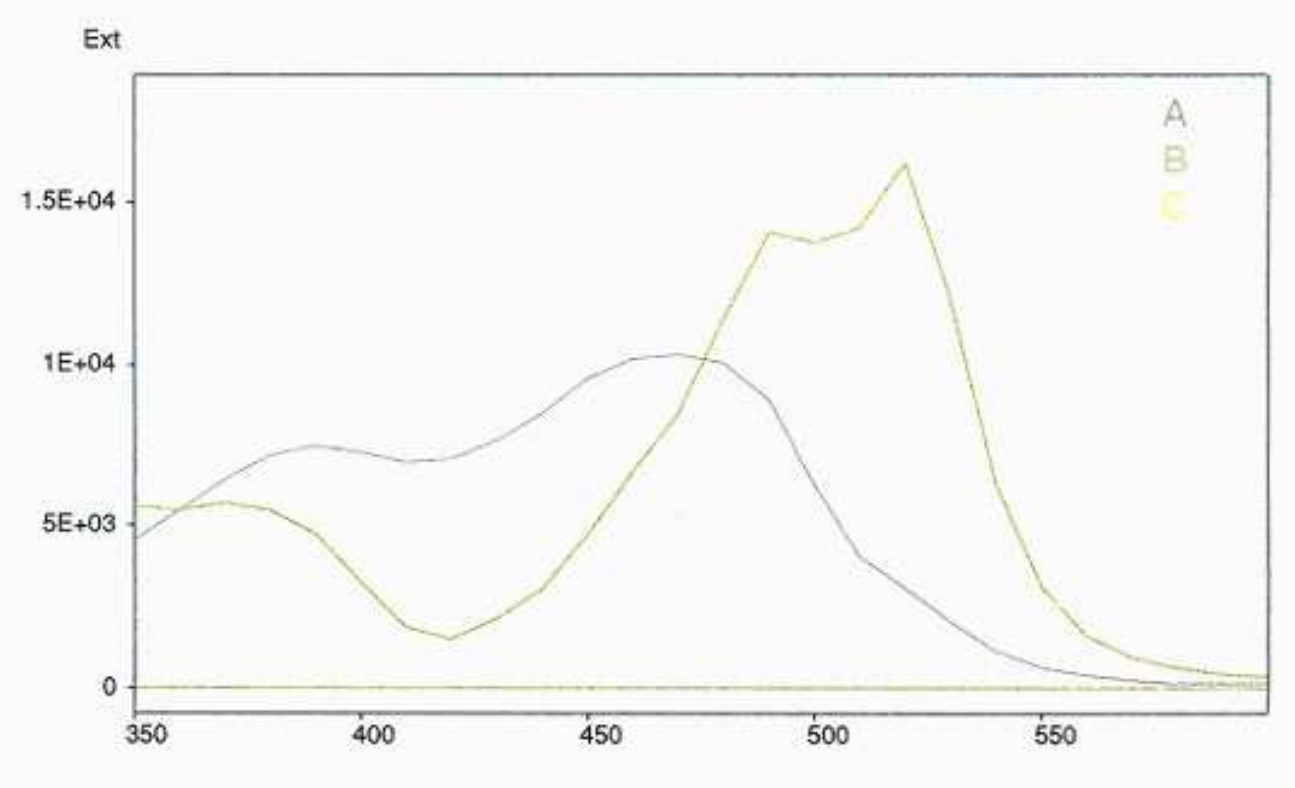

Figure 54: Variation of concentrations of (A) $[L5B]^{2-}$ and (C) $[Ni(L5B)]^{2-}$ with time.

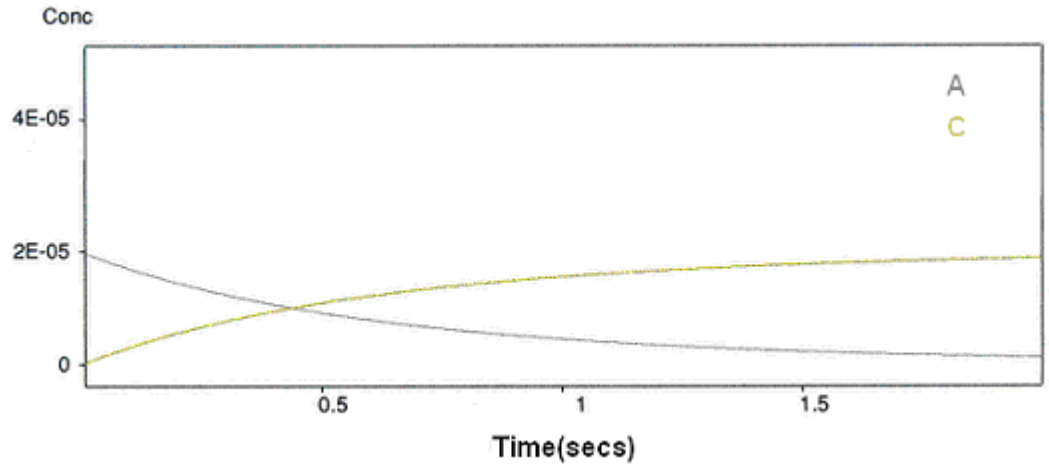

Figure 55: Absorbance against wavelength against time for the reaction of excess L5 (2×10^{-5} mol dm^{-3}) with Ni(II)(5×10^{-6} mol dm^{-3}) at 25°C and pH 6 with 2,6-Lutidine (0.02 mol dm^{-3}).

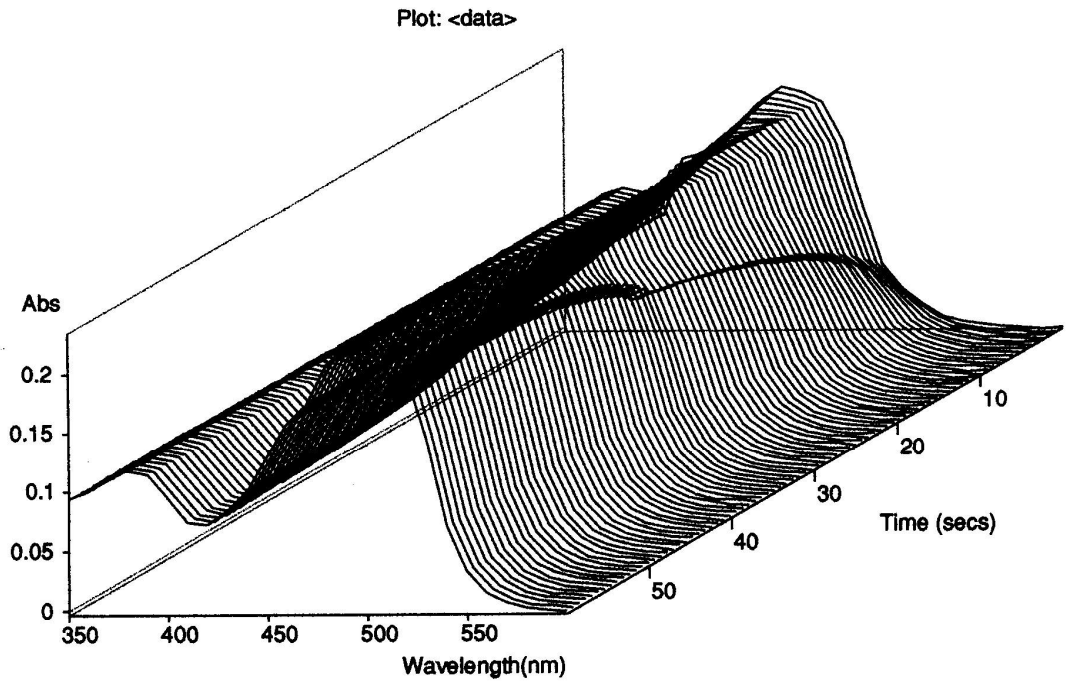

Determination of k_f for the reactions of excess L5 with Ni^{2+}

The reactions were studied under second-order conditions and the data were analysed using the stopped-flow global software to give the following second-order rate constants:

$$k_{f1} = (1.440 \pm 0.025) \times 10^4 \text{ dm}^3 \text{ mol}^{-1} \text{ s}^{-1}$$

$$k_{f2} = (7.200 \pm 0.050) \times 10^3 \text{ dm}^3 \text{ mol}^{-1} \text{ s}^{-1}$$

Figure 56: Kinetically determined UV-Visible spectra of the ligand (A) $[L5]^{3-}$ and the metal complexes (C)$[Ni(L5)]^{3-}$ and (D) $[Ni(L5)_2]^{8-}$.

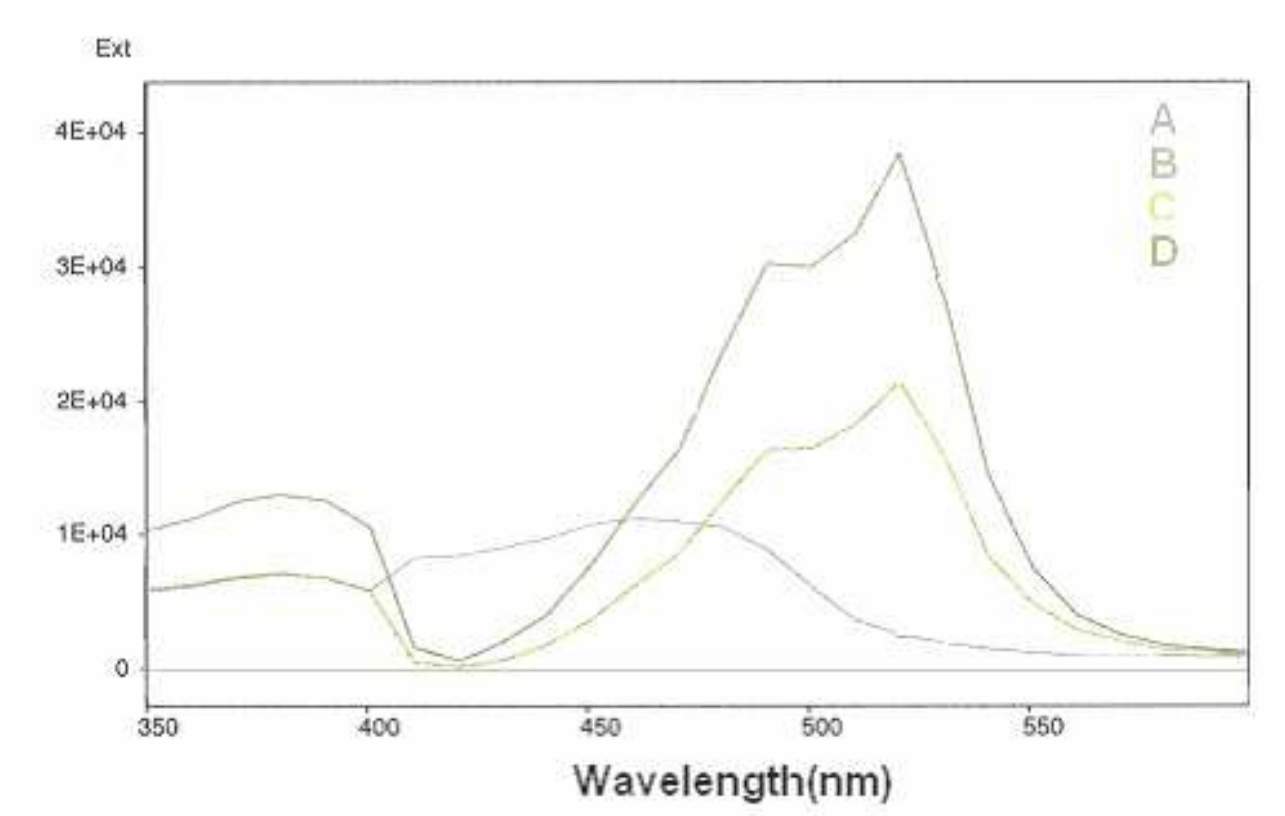

Figure 57: Variation of concentrations of (A) $L5^{3-}$ and (B) $[Ni^{2+}]$ (C) $[Ni(L5)]^{3-}$ and (D) $[Ni(L5)_2]^{8-}$ with time.

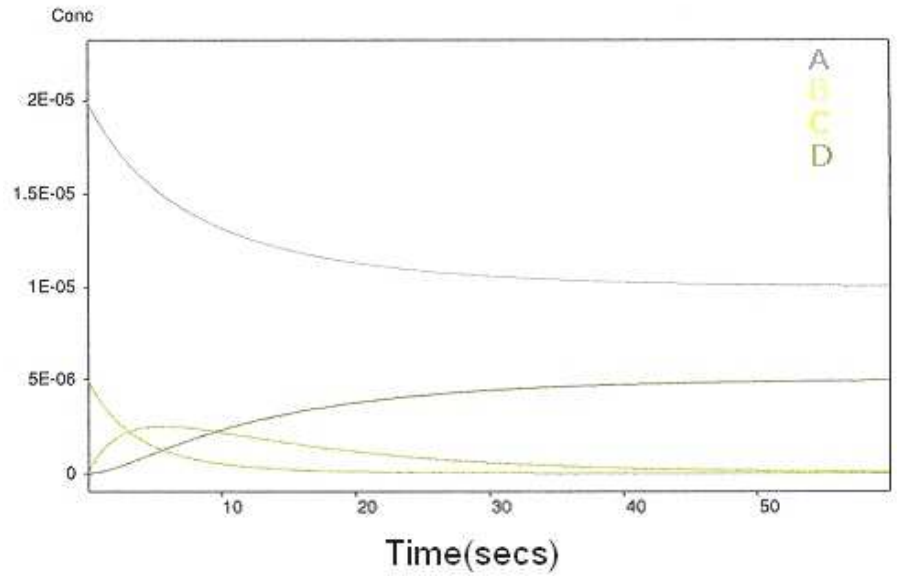

Figure 58: Absorbance against wavelength against time for the reaction of excess L5B (2×10^{-5} mol dm^{-3}) with Ni(II) (5×10^{-6} mol dm^{-3}) at 25°C and pH 6 with 2,6-Lutidine (0.02 mol dm^{-3}).

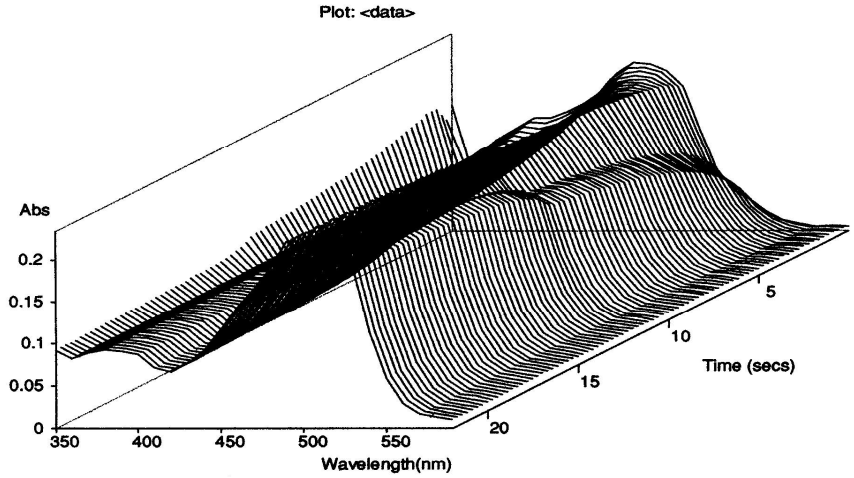

Determining k_f for the reactions of excess L5B with Ni^{2+}

The data were analysed using the global software and second-order rate constants were calculated:

$$k_{f1} = (1.720 \pm 0.012) \times 10^4 \ dm^3 \ mol^{-1} \ s^{-1}$$

$$k_{f2} = (7.730 \pm 0.050) \times 10^3 \ dm^3 \ mol^{-1} \ s^{-1}$$

Figure 59: Kinetically determined UV-Visible spectra of the ligand (A) $L5B^{2-}$ and the metal complexes (C) $[Ni(L5B)]^{2-}$ and (D) $[Ni(L5B)_2]^{6-}$.

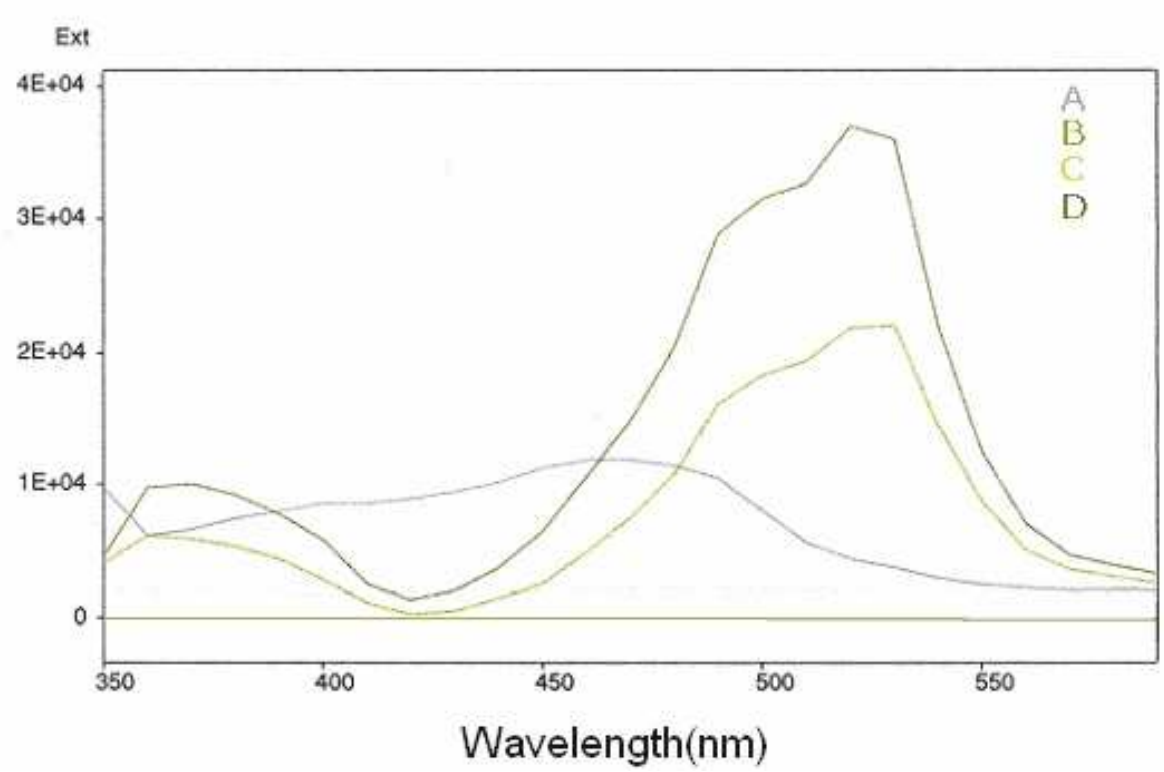

Figure 60: Variation of concentrations of (A)$[L5B]^{2-}$ (B) $[Ni^{2+}]$ (C) $[Ni(L5B)]^{2-}$ and (D) $[Ni(L5B)_2]^{6-}$ with time.

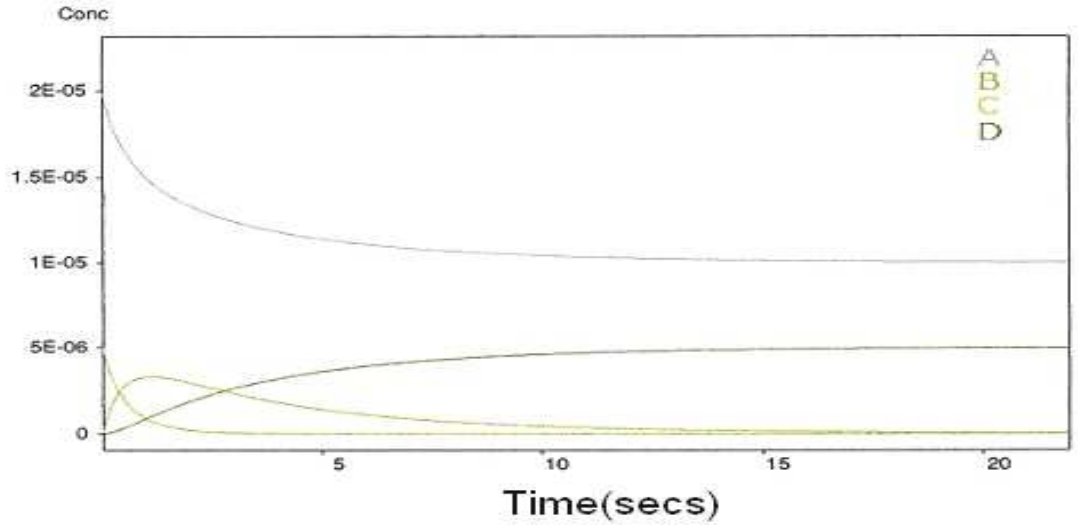

Table 10: Rate constants at 25 ^{o}C for the formation of mono- and bis-(ligand)Ni(II) complexes with L7, L1, L5 and L5B.

Ligand	Conditions	Final species formed[a]	$10^{-4}k_{f1}$/ dm^3 mol^{-1} s^{-1}	$10^{-3}k_{f2}$/ dm^3 mol^{-1} s^{-1}
L7	Excess Ni^{2+}	ML	0.223 ± 0.050	n/a
L1	Excess Ni^{2+}	M_2L	4.10 ± 0.80	7.55 ± 0.40
L5	Excess Ni^{2+}	M_2L	14.00 ± 0.03	21.60 ± 0.50
	Excess L5	ML_2	1.44 ± 0.03	7.20 ± 0.05
L5B	Excess Ni^{2+}	ML	2.13 ± 0.01	n/a
	Excess L5B	ML_2	1.72 ± 0.01	7.73 ± 0.05

a **M = metal ion, L = ligand**

6.2 Discussion.

6.21 Reaction of L1 with excess Ni^{2+}.

From the results it can be seen (Figure 45) that when an excess amount of Ni^{2+} is added to L1 two species are formed. These are postulated to be the mono-Ni(II)ligand species $[Ni(L1)]^-$ and the di-Ni(II)ligand species $[Ni_2(L1)]^+$. Postulated structures for both species are shown below.

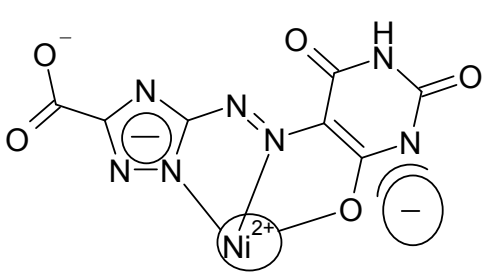

$[Ni(L1)]^-$

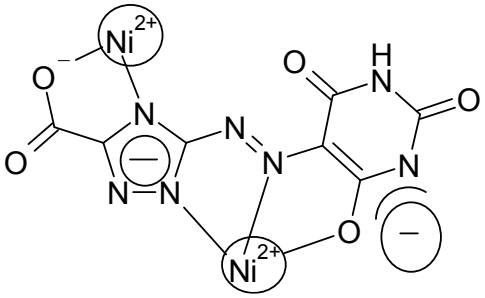

$[Ni_2(L1)]^+$

The slower rate of formation of the di-Ni(II) species is as expected due to charge repulsion between the two Ni^{2+} ions, making addition of the second metal ion more difficult.

6.22 Reaction of L7 with excess Ni^{2+}.

Figures 46-48 show the results of the reaction of L7 with excess Ni^{2+}. It can be seen that this reaction results in only the mono [Ni(L7)] species. This is consistent with the absence of a second strong ligating site in L7. The value of k_1 determined for the reaction (2.23×10^3 dm^3 mol^{-1} s^{-1}) compares well with the value of 2.18×10^3 dm^3 mol^{-1} s^{-1} found previously for the reaction of L7 with excess Ni^{2+} measured at a single wavelength (Chapter 5, Table 9). It also compares quite well to the value

found for PAN measured at a single wavelength of 3.14 $\times 10^3$ dm^3 mol^{-1} s^{-1} and also the value for L3765 (2.60 $\times 10^3$ dm^3 mol^{-1} s^{-1}).

6.23 Reaction of L5 with excess Ni^{2+}.

L5 is analogous to L1 in having two metal ligating sites. The results in Figures 49-51 confirm that both a mono- and a di-Ni(II)ligand species form. Postulated structures for both species are shown below.

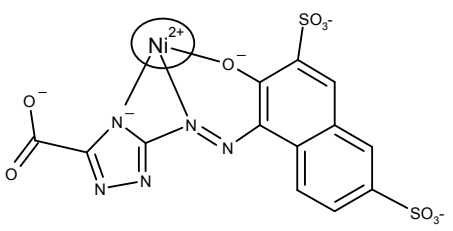

$[Ni(L5)]^{3-}$

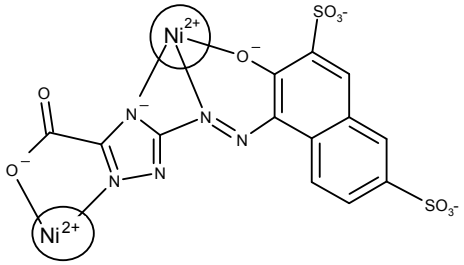

$[Ni_2(L5)]^{-}$

For L5, rate constants for the formation of both the mono- and di-Ni(II) species are approximately three times as large as the values found for the analogous species formed with L1. This is consistent with the larger negative charge of L5 compared with L1. Based on the Eigen-Wilkins mechanism for metal complex formations, the values of $k_f = k_{ex}K_o$ where k_{ex} is the rate constant for total solvent exchange, and K_o is the outer-sphere pre-association constant. Values of K_o are expected to be larger for more negatively charged ligands, which will make values of k_f correspondingly larger.

6.24 Reaction of L5B with excess Ni^{2+}.

The absence of the carboxylate group in L5B compared with L5 results in the observation of a single rate constant for complex formation in the presence of excess

Ni(II), which is good confirmation of the postulated species formed by L5. The rate constant found for L5 is almost seven times as large as the corresponding value found for L5B, again in line with the larger negative charge of L5.

6.25 Reaction of either excess L5 or excess L5B with Ni^{2+}.

Under these conditions reactions with two different rates are observed, consistent with the formation of both mono(ligand)Ni(II) and bis(ligand)Ni(II) complexes. Interestingly the value of k_f for the formation of the mono(ligand)Ni(II) species using excess L5B (1.72×10^4 dm^3 mol^{-1} s^{-1}) is as expected rather similar to that measured when using excess Ni^{2+} (2.13×10^4 dm^3 mol^{-1} s^{-1}). However, for L5 the corresponding rate constants are significantly different; with excess L5 the observed rate constant for mono(ligand)Ni(II) formation (1.44×10^4 dm^3 mol^{-1} s^{-1}) is an order of magnitude smaller than when using excess Ni^{2+} (1.40×10^5 dm^3 mol^{-1} s^{-1}). The value found when using excess L5 is very similar to the values found for L5B.

The enhanced value found for L5 in the presence of excess Ni^{2+} is puzzling, especially as no significant rate enhancement was observed for L5B in the presence of excess metal ion. Perhaps for L5, greater outer-sphere ion-pairing occurs when using a large excess of Ni^{2+} due to the presence of two ligating sites, and extra negative charge, and this would result in the observed rate enhancement. An alternative interpretation that cannot be completely ruled out would involve excess Ni^{2+} attacking first at the bidentate carboxylate and triazole site, followed by attack at the terdentate azo-site. The latter interpretation is postulated to be less likely.

6.3 Experimental.

All stopped–flow studies of the metal complex formations were carried out at 25.0 ^{o}C, and at pH 6 in the presence of 2,6-Lutidine buffer (0.02 mol dm^{-3}) .

6.31 Reaction of L1 with excess Ni(II).

Concentrations after mixing were L1 (1×10^{-5} mol dm^{-3}) and Ni^{2+} (2×10^{-3} mol dm^{-3}). Ni^{2+} was kept in excess to ensure $[mono(L1)Ni(II)]^{2-}$ formation. The wavelength range of the instrument was set from 500 to 300 nm, and the absorbance range was set to 0 to 0.4. Multi wavelength studies were carried out. The instrument was set to take readings every 10 nm and over a time base of 0.1 seconds at each wavelength (400 points per run). The combined data were then analysed with the stopped-flow global analysis software.

6.32 Reaction of L7 with excess Ni(II).

Conditions were kept the same as for L1 apart from the dye concentration (2×10^{-5} mol dm^{-3}); the wavelength range of the instrument was set from 600 to 250 nm, and the absorbance range was set to 0 to 0.4. Multiwavelength studies were carried out. The instrument was set to take readings every 10 nm and over a time base of 5 seconds (400 points per run).

6.33 Reaction of either L5 or L5B with excess Ni(II).

Concentrations after mixing were L5 (2×10^{-5} mol dm^{-3}) and Ni^{2+} (8×10^{-5} mol dm^{-3}). Ni^{2+} was kept in excess to ensure [mono(L5)Ni(II)] formation. The wavelength range of the instrument was set from 600 to 350 nm, and the absorbance range was set to 0 to 0.4. Multi wavelength studies were carried out. The instrument

was set to take readings every 10 nm and over a time base of 5 seconds (400 points per run). For L5B the conditions were kept exactly the same apart from the time base was set to 2 seconds (400 points per run).

6.34 Reaction of Ni(II) with excess L5 and L5B.

Conditions were kept the same as the reaction of L5 (2×10^{-5} mol dm^{-3}) with excess Ni(II) except the concentration of Ni^{2+} used was (5×10^{-6} mol dm^{-3}) and a split time base of 10 seconds (200 points) and 60 seconds (200 points) was used. For L5B conditions were kept the same as for L5, except the split time base used was 5 seconds (200 points) and 20 seconds (200 points).

Chapter 7: Measurement of the rates of dissociation of [Ni(PAN)$_2$] using ligand exchange with an excess of either EDTA or 2,2':6',2''-Terpyridine (Terpy).

Introduction.

The relative stabilities of metal-ligand complexes can be determined by measuring the relative rates of dissociation. Equation 5 shows the relationship between the stability constant *K,* and the rate constants for formation and dissociation (k_f and k_d respectively).

$$K = k_f / k_d \qquad (5)$$

Values of k_d can be determined either by metal exchange (equation 6) or by ligand exchange studies (equation 7):

$$ML + M' \rightleftharpoons M'L + M \qquad (6)$$

$$ML + L' \rightleftharpoons ML' + L \qquad (7)$$

To study reactions of type (6), either an excess of metal ion M', or a metal ion M' that forms a more stable complex with ligand L is used. For reaction (7) to proceed it requires either an excess of ligand L', or the ligand L' to form a more stable complex than ligand L with the metal ion M.

In the following experiments the kinetics of dissociation of [Ni(PAN)$_2$] by either EDTA or 2,2':6',6''-Terpyridine (Terpy) to give free PAN and $[Ni(L')_n]^x$ (L' = EDTA, n = 1, x = 2-; L' = Terpy, n = 2, x = 2+) were studied. Reactions were examined spectroscopically in the visible region, and the effects on the rates of

dissociation by varying the concentrations of either the EDTA or Terpy were investigated. The effect of varying excess PAN concentration was also studied. Terpy was chosen to effect dissociation since it has the same number of coordination sites as PAN, and like PAN Terpy also only coordinates to a metal ion meridonally. It is also a neutral molecule, whereas EDTA is a ligand with a 4– negative charge that is hexadentate. Use of both EDTA and Terpy was investigated to try to decide whether or not the incoming ligand coordinates prior to complete dissociation of the first PAN molecule.

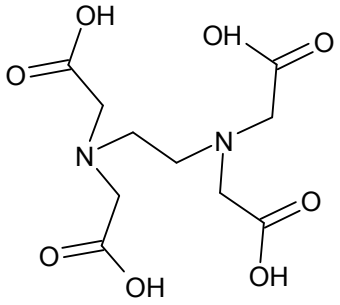

EDTA (ethylenediaminetetraacetic acid)

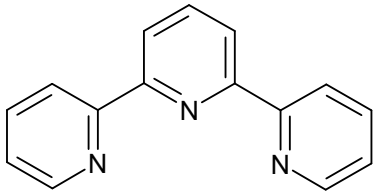

Terpy (2,2':6',2"-Terpyridine)

7.1 Results and Discussion.

Reactions were studied with a Cary 50 rapid scanning spectrophotometer. This instrument allows complete spectra to be accurately recorded every second.

7.11 Dissociation of $[Ni(PAN)_2]$ with excess EDTA.

Figure 61: Spectra of $[Ni(PAN)_2]$ (10^{-5} mol dm^{-3}) reacted at 25.0 ^oC with excess EDTA (2×10^{-4} mol dm^{-3}) studied over 5 min with complete spectra recorded every 10 seconds.

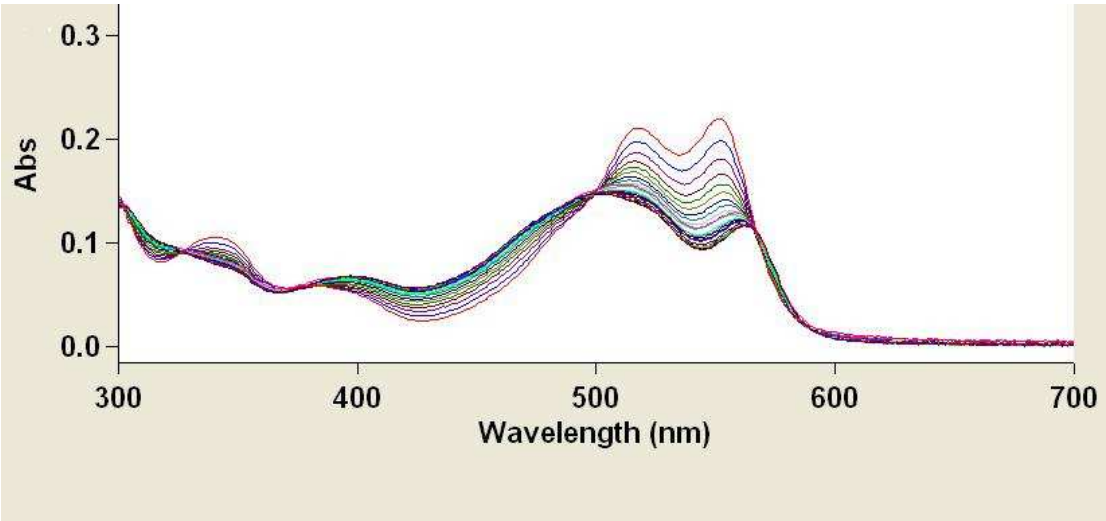

The reaction was initially studied over five minutes, but it was found that it does not go to completion in this time so it was necessary to study the reaction for a longer period of time (Figures 62 and 63).

Figure 62: Spectra of $[Ni(PAN)_2]$ (10^{-5} mol dm^{-3}) reacted with EDTA (2×10^{-4} mol dm^{-3}) studied over 20 minutes with spectra recorded every 30 s.

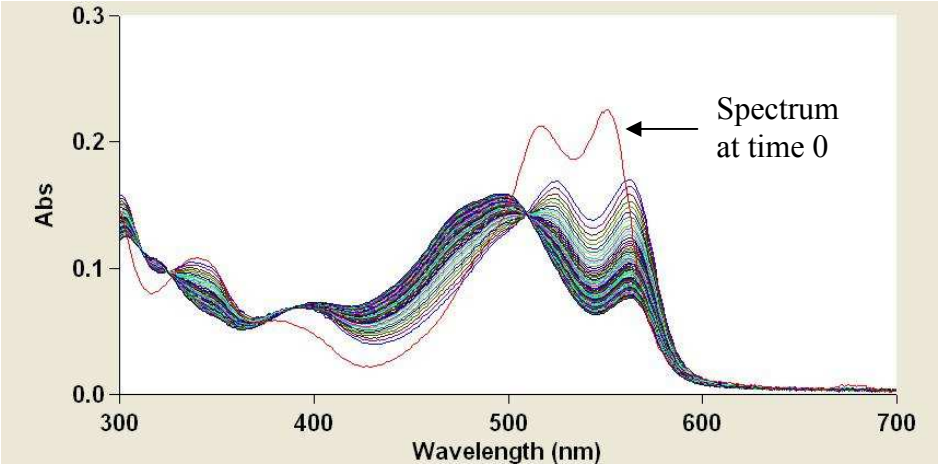

In Figure 62 is shown the reaction over twenty minutes and again the reaction does not go to completion. It should be noted that the spectrum at time zero (soon after mixing) is to the left of the following traces indicating the presence of a multi-stage kinetic process.

Figure 63: Spectra of $[Ni(PAN)_2]$ (2×10^{-5} mol dm^{-3}) reacted with EDTA (4×10^{-4} mol dm^{-3}) studied over 4 hours, with spectra recorded every 20 minutes.

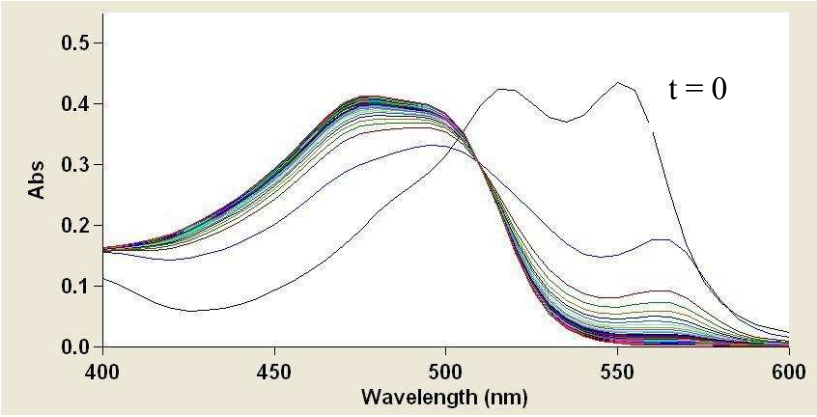

In Figure 63 is shown the reaction studied over four hours with the spectra recorded every twenty minutes. The reaction can be seen to go to completion and again it can be seen that the initial spectrum does not cross through the same isosbestic point as the following spectra, again confirming that the reaction is a multi-step process.

7.12 Effect of varying the EDTA concentration on the rate of dissociation of $[Ni(PAN)_2]$.

In these studies the reaction was studied at a fixed analytical wavelength of 550 nm. The absorbance/time curves analysed as a consecutive first-order process, with two first-order rate constants, k_1 and k_2.

Figure 64: Kinetic trace of $[Ni(PAN)_2]$ (2×10^{-5} mol dm^{-3}) reacted with three times excess EDTA (6×10^{-5} mol dm^{-3}) at a fixed wavelength of 550 nm.

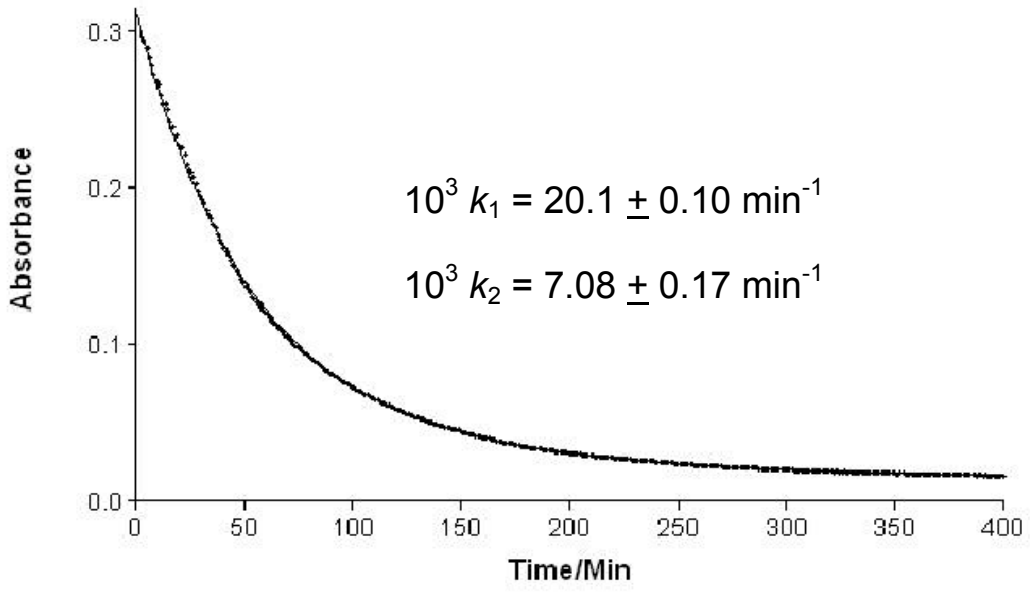

Figure 65: Kinetic trace of $[Ni(PAN)_2]$ (2×10^{-5} mol dm^{-3}) reacted with 25 times excess EDTA (5×10^{-4} mol dm^{-3}) at a fixed wavelength of 550 nm.

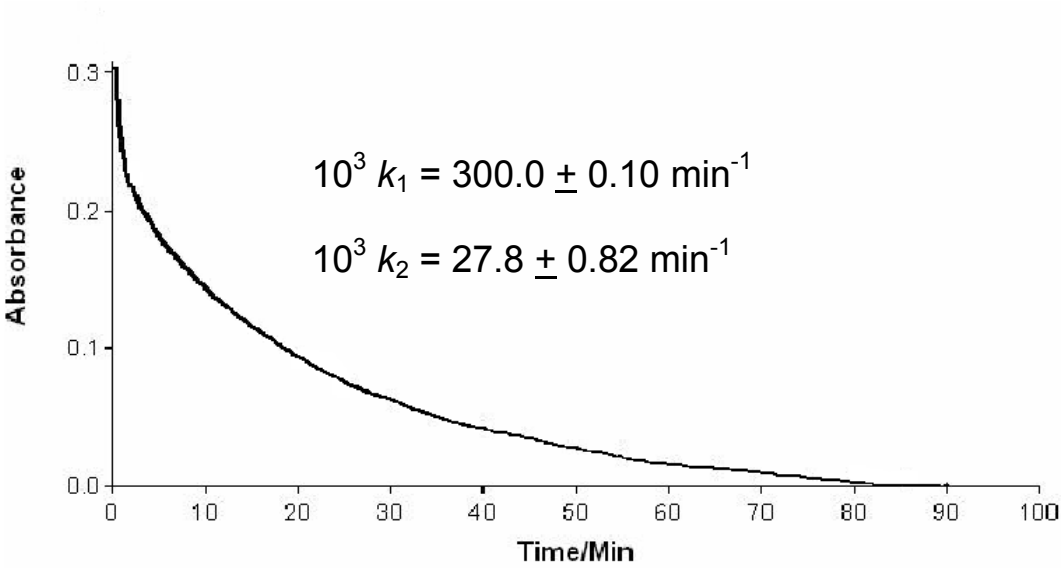

Possible structures for the $[(PAN)Ni(EDTA)]^{3-}$ intermediate are sketched below.

Possible structures for the intermediate $[(PAN)Ni(EDTA)]^{3-}$ (vacant sites on the Ni are occupied by the meridonally coordinated PAN molecule, and the charges are omitted for convenience).

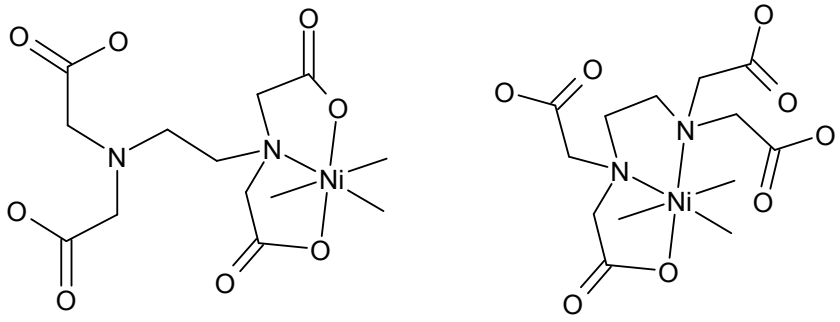

7.13 Effect of varying the PAN concentration on the dissociation of [$NiPAN_2$] by EDTA.

For both stages of the reaction the rate decreases as the PAN concentration increases.

Figure 66: Plot of k_{1obs} against [PAN]

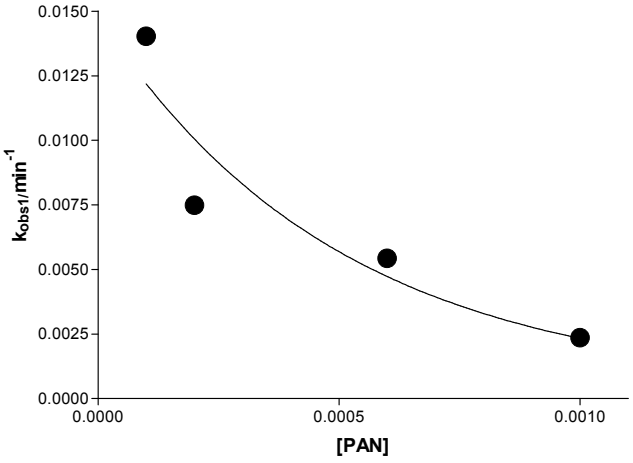

Figure 67: Plot of k_{2obs} against [PAN].

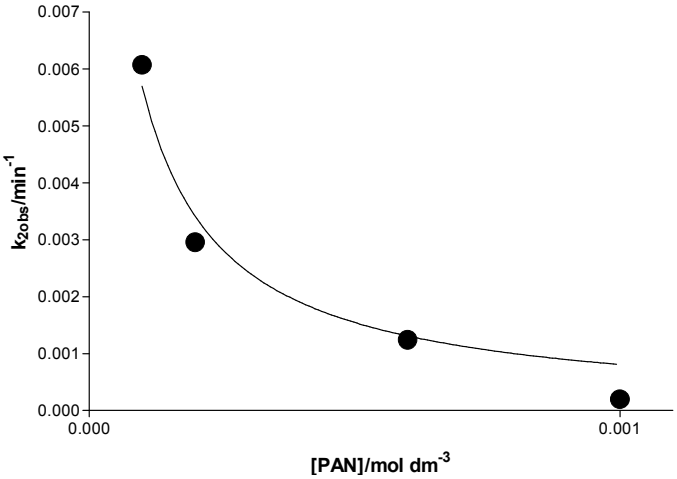

For each stage, the rate decrease can be accounted for with the following postulated mechanisms.

Postulated mechanism for the two-step dissociation of $[Ni(PAN)_2]$ by EDTA

- **Stage 1**
- We shall assume that EDTA does not coordinate prior to complete dissociation of a PAN molecule. Let P represent PAN, L represent EDTA, S represent solvent (water) and omitting charges for convenience:

$$NiP_2 \underset{k_{-1}}{\overset{k_1}{\rightleftharpoons}} S_3NiP + P$$

$$S_3NiP + L \xrightarrow{k_2} LNiP + 3S$$

- Applying the steady-state approximation to S_3NiP, $d[S_3NiP]/dt = 0$, hence:

$$k_1[NiP_2] = k_{-1}[P][S_3NiP] + k_2[S_3NiP][L]$$

$$\text{and } [S_3NiP] = \frac{k_1[NiP_2]}{k_{-1}[P] + k_2[L]}$$

Therefore for stage 1:

$$\frac{d[LNiP]}{dt} = k_2[L][S_3NiP]$$

$$= \frac{k_2 k_1[NiP_2][L]}{k_{-1}[P] + k_2[L]}$$

$$= k_{1obs}[NiP_2]$$

$$where,\ k_{1obs} = \frac{k_2 k_1[L]}{k_{-1}[P] + k_2[L]} = \frac{k_1}{\frac{k_{-1}[P]}{k_2[L]} + 1}$$

- In the presence of excess L, [L] is approximately constant and k_{1obs} will decrease with increasing [P]

- Inverting the equation gives:

$$\frac{1}{k_{1obs}} = \frac{k_{-1}[\mathrm{P}]}{k_1 k_2[\mathrm{L}]} + \frac{1}{k_1}$$

A plot of $k_{1\mathrm{obs}}^{-1}$ versus [P] should be a straight line with slope = $k_{-1}[\mathrm{P}]/k_1k_2[\mathrm{L}]$ and intercept at [P] = 0 of k_1^{-1}.

Stage 2

$$[\mathrm{LNiP}] \underset{k_{-3}}{\overset{k_3}{\rightleftharpoons}} [\mathrm{LNiS_3}] + \mathrm{P}$$

$$[\mathrm{LNiS_3}] \xrightarrow{k_4} [\mathrm{NiL}] + 3\mathrm{S}$$

Applying the steady-state approximation to $[\mathrm{LNiS_3}]$:

$$k_3[\mathrm{LNiP}] = k_{-3}[\mathrm{P}][\mathrm{LNiS_3}] + k_4[\mathrm{LNiS_3}]$$

$$[\mathrm{LNiS_3}] = \frac{k_3[\mathrm{LNiP}]}{k_{-3}[\mathrm{P}] + k_4}$$

$$\text{Hence,} \quad \frac{d[\mathrm{NiL}]}{dt} = \frac{k_4 k_3[\mathrm{LNiP}]}{k_{-3}[\mathrm{P}] + k_4} = k_{2obs}[\mathrm{LNiP}]$$

$$\text{and,} \quad k_{2obs} = \frac{k_4 k_3}{k_{-3}[\mathrm{P}] + k_4}$$

Inverting this equation gives:

$$k_{2\mathrm{obs}}^{-1} = k_{-3}[\mathrm{P}] / k_3k_4 + 1/k_3 \qquad (4)$$

A plot of $k_{2\mathrm{obs}}^{-1}$ *versus* [P] should be a straight line, with slope k_{-3}/k_3k_4 and intercept at [P] = 0 of $1/k_3$.

Figure 68: Plot of $1/k_{1obs}$ against [PAN].

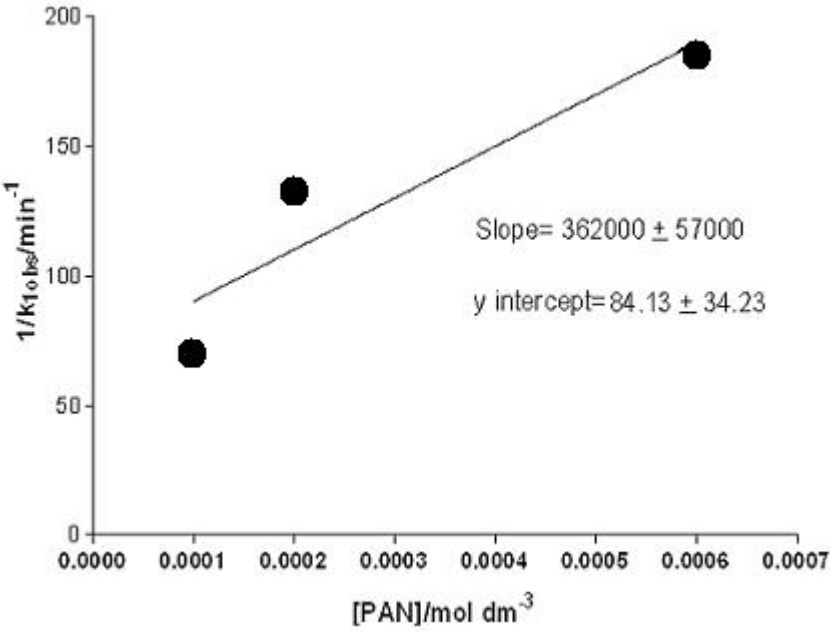

- For stage 1, fitting data to the equation gives slope = $(3.62 \pm 0.57) \times 10^5$
- $= k_{-1}/k_1k_2$[L], and intercept at [P] = 0 of $84 \pm 34 = 1/k_1$.
- Since, slope/intercept = k_{-1} / k_2[L] and [L] = 4×10^{-4} mol dm^{-3} it follows that $k_{-1} / k_2 = 1.72 \pm 0.75$.
- From the intercept, $k_1 = 0.01189 \pm 0.00484$ min^{-1}.

  i.e. $10^2 k_1 = 1.189 \pm 0.484$ min^{-1}.

Figure 69: plot of $1/k_{2obs}$ against [PAN].

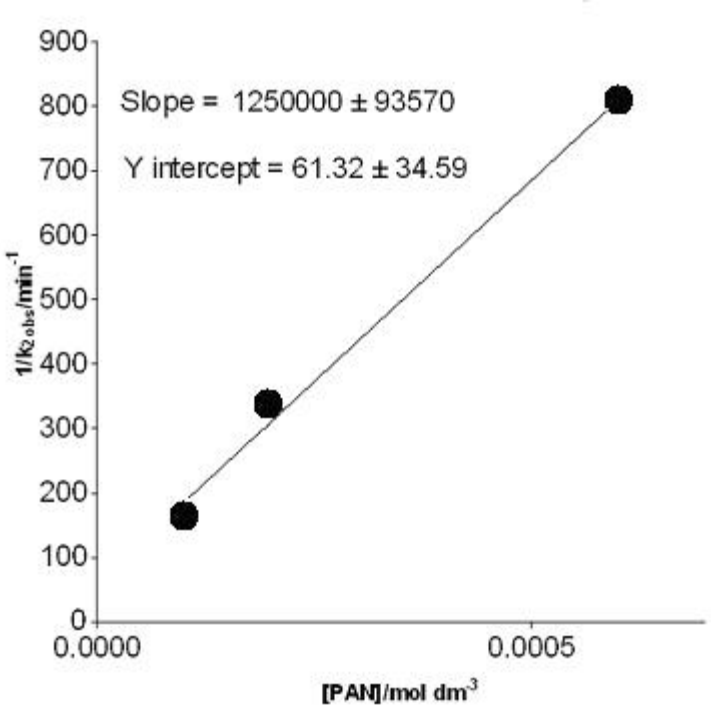

- For stage 2, fitting data to equation (4) gives slope = 1.25×10^6 = k_{-3} / k_3k_4 and intercept at [P] = 0 of $61 \pm 35 = 1/k_3$.

  Since, slope/intercept = $k_{-3}/k_4 = (2.04 \pm 1.15) \times 10^4$ dm^3 mol^{-1} and $k_3 = 0.0163 \pm 0.009199$ min^{-1}.

  i.e. $10^{-4}(k_{-3}/k_4)$ 2.04 ± 1.15 dm^3 mol^{-1}, and $10^2k_3 = 1.63 \pm 0.92$ min^{-1}.

7.2 Dissociation of $[Ni(PAN)_2]$ with excess Terpy.

As found for the reaction with EDTA, a two-stage kinetic process was observed (Figures 70 and 71).

Figure 70: Spectra of $[Ni(PAN)_2]$ (2×10^{-5} mol dm^{-3}) reacted with excess Terpy (4×10^{-4} mol dm^{-3}) studied over 1 hour with spectra recorded every 30 s.

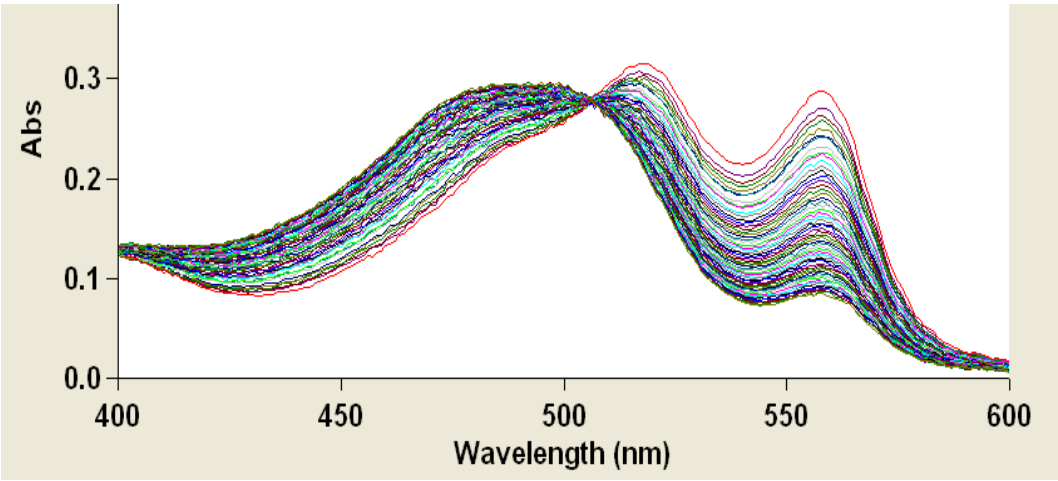

Figure 71: Spectra of $[Ni(PAN)_2]$ (2×10^{-5} mol dm^{-3}) reacted with excess Terpy (4×10^{-4} mol dm^{-3}) studied over 24 hours, spectra recorded every 30 mins.

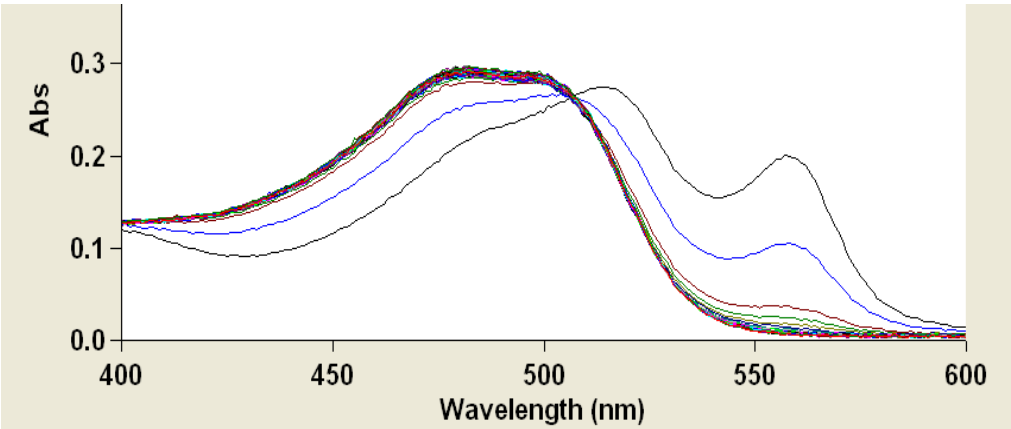

In Figure 71 is shown the dissociation going to completion studied over twenty-four hours. It is apparent that all the spectra go through the same isosbestic point, and this would appear to illustrate only one stage of dissociation, but from studying the kinetic data in the same way as the EDTA dissociation studies, it was found that the dissociation does in fact have two consecutive first-order stages.

The effect of varying the PAN concentration on the rates of each stage was then investigated:

7.22 Effects of varying the PAN concentration on the dissociation of $[Ni(PAN)_2]$ (2×10^{-5} mol dm^{-3}) by Terpy (4×10^{-4} mol dm^{-3}).

Figure 72: Plot of k_{1obs} against [PAN].

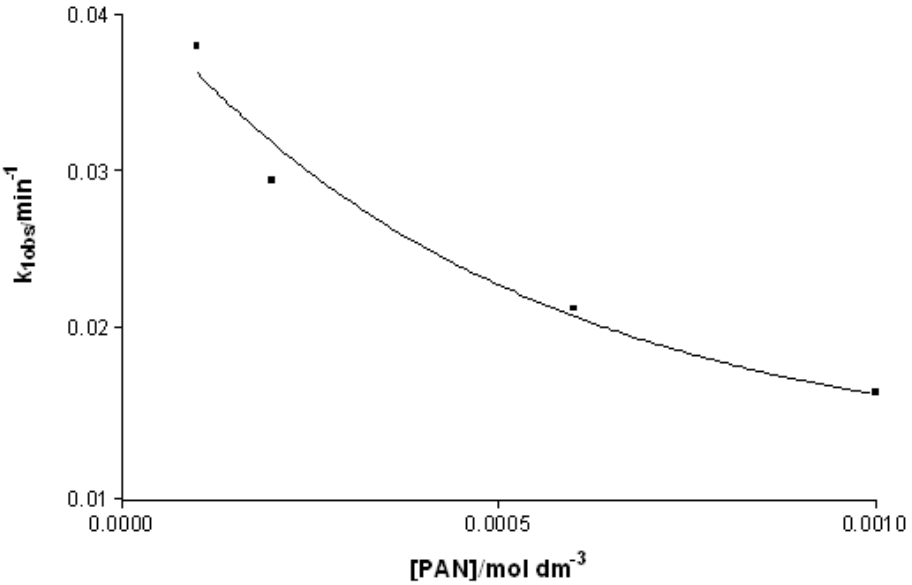

Figure 73: Plot of k_{2obs} against [PAN].

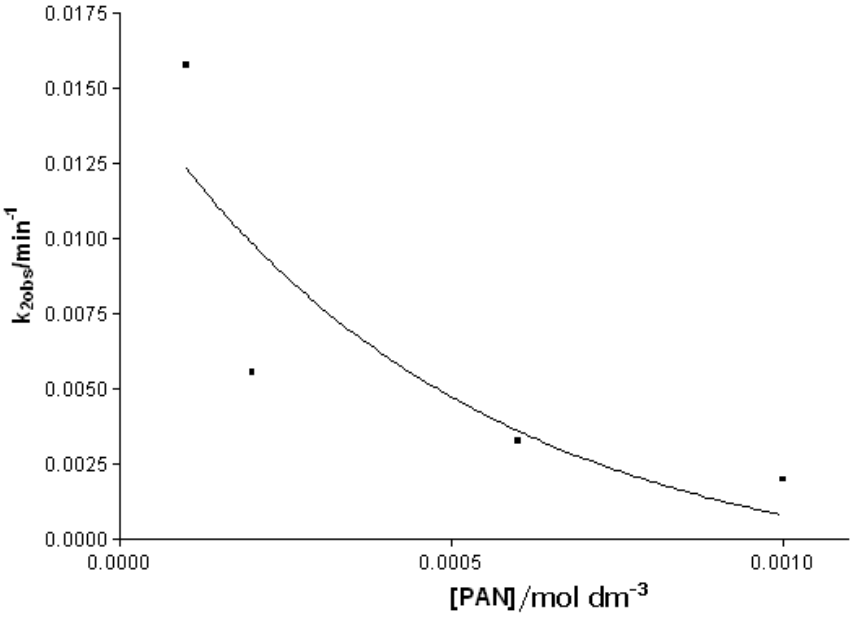

Postulated mechanism for the two-step dissociation of $[Ni(PAN)_2]$ by Terpy.

- Stage 1 follows the same mechanism as for dissociation with EDTA as illustrated earlier (P = PAN, L = Terpy, S = H_2O)

$$[NiP_2] \underset{k_{-1}}{\overset{k_1}{\rightleftharpoons}} [S_3NiP]^+ + P$$

$$[S_3NiP]^+ + L \xrightarrow{k_2} [LNiP]^+ + 3S$$

Following the same derivation as used for EDTA gives the equation

$$\frac{1}{k_{1obs}} = \frac{k_{-1}[P]}{k_1 k_2 [L]} + \frac{1}{k_1}$$

Hence a plot of k_{1obs1}^{-1} *versus* [P] will be a straight line with a slope of $k_{-1}/k_1k_2[L]$ and an intercept at [P] = 0 of $1/k_1$.

Stage 2

$$[LNiP]^{+} \underset{k_{-3}}{\overset{k_3}{\rightleftharpoons}} [LNiS_3]^{2+} + P$$

$$[LNiS_3]^{2+} + L \xrightarrow{k_4} [NiL_2]^{2+} + 3S$$

Applying the steady-state approximation to $[LNiS_3]^{2+}$:

$$k_3[LNiP^+] = k_{-3}[P][LNiS_3{}^{2+}] + k_4[L][LNiS_3{}^{2+}]$$

$$[LNiS_3{}^{2+}] = \frac{k_3[LNiP^+]}{k_{-3}[P] + k_4[L]}$$

$$\text{Hence, } \frac{d[NiL_2]}{dt} = \frac{k_4 k_3[LNiP^+][L]}{k_{-3}[P] + k_4[L]}$$

$$= k_{2obs}[LNiP^+]$$

$$\text{and, } \quad k_{2obs} = \frac{k_3 k_4[L]}{k_{-3}[P] + k_4[L]} = \frac{k_3 k_4'}{k_{-3}[P] + k_4'}$$

where $k_4' = k_4[L]$

Inverting this equation gives:

$$1/k_{2obs} = k_{-3}[P] / k_3 k_4' + 1/k_3$$

A plot of k_{2obs}^{-1} *versus* [P] should be a straight line with slope $k_{-3} / k_3 k_4'$ and intercept at [P] = 0 of $1/k_3$.

Figure 74: Plot of k_{1obs}^{-1} against [PAN].

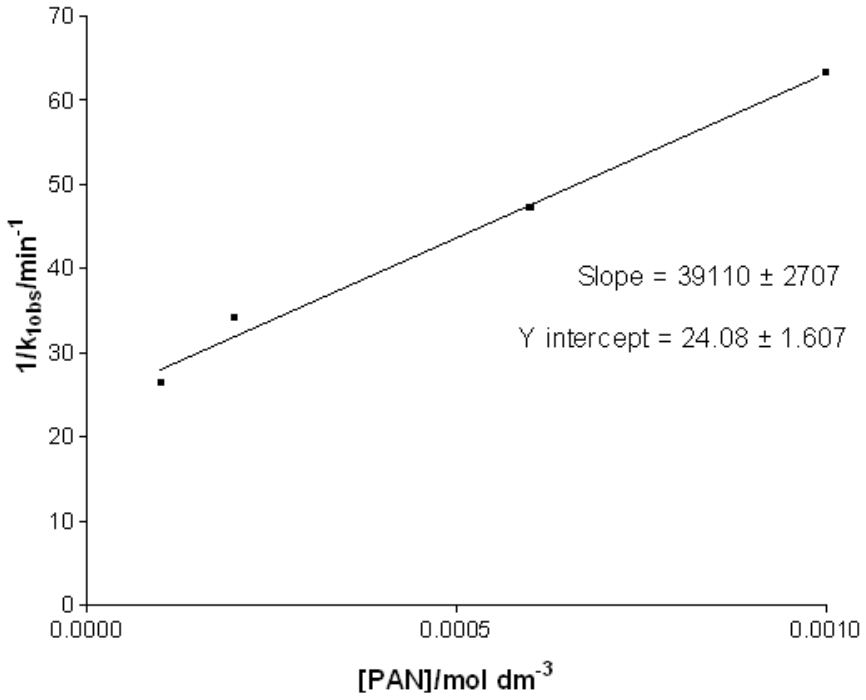

- For stage 1, fitting the data gives slope = $(3.92 \pm 0.27) \times 10^4 = k_{-1}/k_1k_2$[L], and the intercept at [P] = 0 of $24.08 \pm 1.61 = 1/k_1$.

  Since, slope/intercept = k_{-1} / k_2[L] and [L] = 4×10^{-4} mol dm^{-3} it follows that

  $k_{-1} / k_2 = 0.650 \pm 0.062$

  and, $k_1 = (4.15 \pm 0.28) \times 10^{-2}$ min^{-1}

Figure 75: Plot of $1/k_{2obs}$ against [PAN].

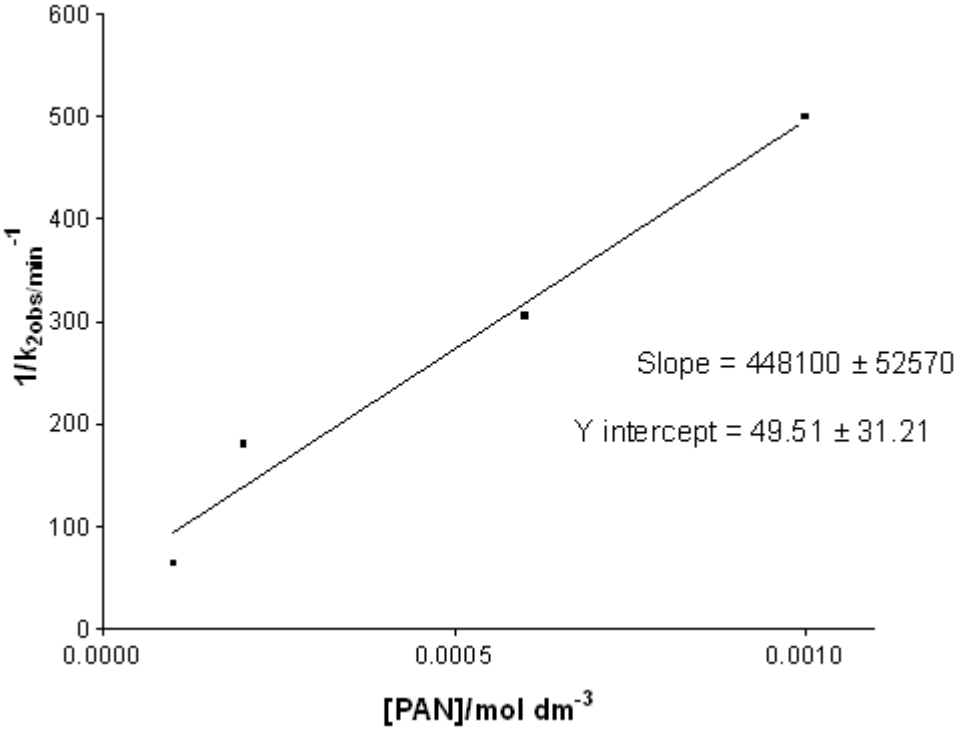

- For stage 2, fitting data to a straight line gives slope = $(4.48 \pm 0.53) \times 10^5$ = k_{-3} / k_3k_4' and intercept at [P] = 0 of $49.51 \pm 31.21 = 1/k_3$.

  slope/intercept = k_{-3}/k_4' = $(9.05 \pm 5.80) \times 10^3$ dm^3 mol^{-1}

  and $k_3 = 0.0202 \pm 0.0127$ min^{-1}.

  Since k_4' = k_4[L] and [L] = 4×10^{-4} mol dm^{-3},

  $k_{-3}/k_4 = 3.6 \pm 2.3$

7.31 Effect of varying the EDTA concentration on the dissociation of [Ni(PAN)$_2$].

As can be seen from Figures 62-63 the dissociation takes place in two stages, the first stage involves one of the PAN molecules being displaced by EDTA giving a [(PAN)Ni(EDTA)]$^{3-}$ intermediate; the coordinated EDTA then displaces the second PAN and gives the final products of free PAN and [Ni(EDTA)]$^{2-}$. At 25 ^{o}C, the rate constants obtained when using three times excess EDTA are 10^3k_1 = 20.1 $\pm$ 0.10 min^{-1} and 10^3k_2 = 7.08 $\pm$ 0.17 min^{-1}, whilst for 25 times excess EDTA, 10^3k_1 = 300.0 $\pm$ 0.10 min^{-1} and 10^3k_2 = 27.8 $\pm$ 0.82 min^{-1}. It can be seen in both cases that the dissociation of the first PAN molecule is faster than the second in line with the normal stability constant trend, $K_1 > K_2$. The smaller stability constant for the bis(PAN)Ni(II) complex results in a faster rate of dissociation of the first PAN molecule.

As the concentration of EDTA increases, each stage of the reaction goes faster. As each PAN dissociates, competition of the EDTA with the released PAN for the vacant sites on the Ni(II) accounts for the rate acceleration with increasing [EDTA]. In agreement with this conclusion, increasing the [PAN] retards the coordination of the EDTA (section 7.32).

7.32 Effect of varying [PAN] on the rate of dissociation of [Ni(PAN)$_2$].

As discussed in 7.31 the dissociation of [Ni(PAN)$_2$] by EDTA takes place in two stages. The effect of varying the PAN concentration on the rate of dissociation can be seen in Figures 66 and 67. As the PAN concentration increases the rate of each stage in the dissociation decreases.

As the $[Ni(PAN)_2]$ dissociates, and the EDTA binds to the Ni(II), the PAN molecules compete with EDTA. An increase in the concentration of PAN hinders the EDTA molecules from binding.

7.33 Rate of dissociation of $[Ni(PAN)_2]$ with Terpy.

As can be seen from Figures 70-71 Terpy dissociates $[Ni(PAN)_2]$ to give $[Ni(Terpy)_2]^{2+}$ and free PAN. Studying the reaction kinetically, and using non-linear regression analysis, showed that the reaction takes place in two stages and gave two rate constants, one for each step. The first stage involves a Terpy molecule replacing the first coordinated PAN giving $[(PAN)Ni(Terpy)]^{+}$ and the second stage involves a second Terpy molecule displacing the second coordinated PAN molecule.

7.34 Effect of varying PAN concentration on the dissociation of $[Ni(PAN)_2]$ with Terpy.

Figures 72-75 show the effects of varying the PAN concentration on the dissociation of $[Ni(PAN)_2]$ with Terpy. It can be clearly seen as the PAN concentration increases the rate of dissociation decreases. For stage one the dissociation is faster than for stage two, in line with the normal stability sequence order, $K_1 > K_2$.

7.35 Comparison of the relative rates of dissociation using EDTA and Terpy.

Using a twenty fold excess of replacing ligand (i.e. EDTA and Terpy) over $[Ni(PAN)_2]$ and looking at the dissociation of the $[(Terpy)Ni(PAN)]^{+}$ and $[(EDTA)Ni(PAN)]^{3-}$ complexes, the values found were $0.031 \pm 2.3 \times 10^{-4}$ min^{-1} and $0.0012 \pm 1.7 \times 10^{-5}$ min^{-1} respectively. This shows that the coordinated Terpy increases the rate of loss of the second PAN by a factor of *ca.* 25 compared with the

effect of coordinated EDTA. Pi-stacking between coordinated and free Terpy might account for the greater rate enhancement by Terpy compared with EDTA.

7.36 Combination of formation and dissociation rate constants k_f and k_d to estimate the relative stability constants Ni(II)L3765$^-$, Ni(II)PAN$^+$ and Ni(II)L7.

Values of k_f for the formation of Ni(II)PAN, Ni(II)L7 and Ni(II)L3765 have been determined by the stopped-flow method using the values found in (Chapter 5, Table 9). Dissociation values have also been determined by dissociating the same complexes with Terpy using the method shown in this Chapter and (Chapter 8, Table 12).

Combining these two values as previously discussed will give an estimate of the relative stability.

$$[LNiP]^+ \underset{k_{-3}}{\overset{k_3}{\rightleftharpoons}} [LNiS_3]^{2+} + P$$

$$[LNiS_3]^{2+} + L \xrightarrow{k_4} [NiL_2]^{2+} + 3S$$

If its assumed that k_3 for $LNiP^+$ is not very different from that for S_3NiP^+ then we can estimate the stability constant for NiP^+ as follows.

$$K_1 = \frac{399.2 \pm 193.3}{(3.366 \pm 2.116)x10^{-4}}$$

$$= 1.188 \times 10^6 \text{ dm}^3\text{mol}^{-1}$$

$$\log_{10}K_1 = 6.073 \pm 0.79$$

Table 11: Comparison of the estimated relative stabilities of Ni(II)PAN$^+$, Ni(II)L7 and Ni(II)L3765$^-$.

Complex	k_f / dm^3 mol^{-1} s^{-1} [c]	$10^4 k_d$/s^{-1} [a]	log K_1 [b]
[Ni(II)PAN]$^+$	399.2 ± 193.3	[e]3.37± 2.12	6.07± 0.79
[Ni(II)L7]	171.4 ± 94.7	[e1]4.50± 0.04	5.58 ± 0.55
[Ni(II)L3765]$^-$	250.2 ± 57.5	[e1]4.50± 0.01	5.75 ± 0.23

[a] assumes dissociation rate for $[(H_2O)_3NiL]$ is the same as that for [(Terpy)NiL]

[b] $K_1 = k_f / k_d$; these values are in aqueous solution.

[c] $k_f = k_1k_2/(k_{-1} + k_2)$ (Derivation and calculations can be seen in the Appendix)

[e] Value from p.133 [e1]Values from Table 12(Chapter 8)

For PAN, it can be seen that the kinetically determined stability constant in water is significantly smaller than the value reported from potentiometric studies in 50% dioxane-water (log K_1 = 12.7). Stability constants in solvents of lower dielectric constant are often larger than those in aqueous solution, but the difference found here is somewhat larger than might have been expected.

The stability constant for the bidentate intermediate $[Ni(II)(PAN)]^{2+}$, was found to be 1.02×10^3 dm^3 mol^{-1}, and this value compares well with the stability constants of other Ni^{2+} complexes with *bidentate* ligands such as SUDAN I where $K = 2.95 \times 10^3$ dm^3 mol^{-1}, and PADA where $K = 2.31 \times 10^3$ dm^3 mol^{-1}. The estimated stabilities of the corresponding bidentate intermediates formed by L7 and L3765 are in good agreement with the stability found for $[Ni(II)(PAN)]^{2+}$. The values are slightly less than $[Ni(II)(PAN)]^{2+}$ and this is attributed to the influence of the sulphonate groups.

The stability constant for the formation of $[Ni(PAN)_2]$ from $[Ni(PAN)]^+$ may also be estimated by assuming the value of k_f for $[Ni(PAN)_2]$ is the same as that found for $[Ni(PAN)]^+$. Here the loss of the first PAN by Terpy is not affected by prior Terpy coordination (as is the problem for $LNiP^+$), although pi-stacking by PAN is complicating the case. Assuming little pi-stacking:

For $[Ni(PAN)_2]$ the value of k_d is $(6.92 \pm 0.47) \times 10^{-4}$ s^{-1}, hence $K_2 = (399.9 \pm 193.3) / (6.92 \pm 0.47) \times 10^{-4} = (5.78 \pm 2.82) \times 10^5$ dm^3 mol^{-1}. Therefore, in water we may estimate $\log K_2 = 5.76 \pm 0.49$. This is as expected, and compares favourably with the value of $\log K_1$ of 6.07 ± 0.79. In water the difference $\log K_1 - \log K_2 = 0.31$ compared with a difference of *ca* 0.1 in 50% dioxane-water.

7.4 Experimental.

7.41 UV-Visible study of the reaction of $[Ni(PAN)_2]$ with EDTA.

$[Ni(PAN)_2]$ was formed using a four fold excess of PAN (10^{-5} mol dm^{-3}) to Ni(II) (2.5×10^{-6} mol dm^{-3}) to ensure complete formation of the bis(PAN)Ni(II) species. The complex was then reacted with a twenty fold excess of EDTA(2×10^{-4} mol dm^{-3}), a powerful hexadentate ligand, to remove the Ni(II) and give $[Ni(EDTA)]^{2-}$ and free PAN dye.

The reaction was buffered at pH 6 using 2,6-Lutidine (0.02 mol dm^{-3}), and monitored with a Carey 50 UV-Visible spectrometer between 300-700 nm and thermostatted at 25 ^oC. $[Ni(EDTA)]^{2-}$ is colourless at the concentration and in the

wavelength range used, so the spectral changes show the $[Ni(PAN)_2]$ dissociating to give free PAN ligand.

Firstly the reaction was studied over five minutes with readings taken every 10 s. The reaction was then studied over twenty minutes with readings taken every 30 s. The concentrations were then changed as follows: PAN (2×10^{-5} mol dm^{-3}), Ni(II) (5×10^{-6} mol dm^{-3}) and EDTA (4×10^{-4} mol dm^{-3}) and the reaction was studied for four hours taking readings every twenty minutes.

7.42 Effect of varying the EDTA concentration on the kinetics of the reaction with $[Ni(PAN)_2]$.

Dissociation to free PAN was studied at a 550 nm using EDTA concentrations of 25 (5×10^{-4} mol dm^{-3}) and 3 (6×10^{-5} mol dm^{-3}) times that of the $[Ni(PAN)_2]$ complex (2×10^{-5} mol dm^{-3}). The reaction was buffered at pH 6 using 2,6-Lutidine (0.02 mol dm^{-3}) and studied at 25 ^{o}C by UV-Visible spectrophotometry.

7.43 Effect of varying the PAN concentration on the kinetics of the reaction with $[Ni(PAN)_2]$ and EDTA.

The effect of varying the PAN concentration on the rate at which $[Ni(PAN)_2]$ (2×10^{-5} mol dm^{-3}) dissociates to free PAN was studied at a fixed wavelength of 550 nm using PAN concentrations between five and fifty times that of $[Ni(PAN)_2]$. Usual buffer conditions and thermostatting were applied.

7.44 UV-Visible study of the reaction of $[Ni(PAN)_2]$ with excess Terpy.

$[Ni(PAN)_2]$ was formed using a fourfold excess of PAN (2×10^{-5} mol dm^{-3}) to Ni(II) (5×10^{-6} mol dm^{-3}) to ensure complete formation of the bis(PAN)Ni(II)

species. The complex was then reacted with a twenty fold excess of Terpy (4×10^{-4} mol dm^{-3}), to remove the PAN and give $[Ni(Terpy)_2]^{2+}$ and free PAN. The reaction was buffered at pH 6 using 2,6-Lutidine (0.02 mol dm^{-3}), and monitored by UV-Visible spectrophotometry at 25°C over the wavelength range 400-600 nm. $[Ni(Terpy)_2]^{2+}$ is colourless at the concentration and in the wavelength range used, so the spectral changes show the $[Ni(PAN)_2]^{2+}$ dissociating to give free PAN ligand. Firstly the reaction was studied over one hour with readings taken every 30 s. The reaction was then studied over 24 hours with readings taken every 30 minutes.

7.45 Effect of varying the [PAN] concentration on the kinetics of the reaction of Terpy with $[Ni(PAN)_2]$.

The effect of varying [PAN] on the rate at which $[Ni(PAN)_2]$ (2×10^{-5} mol dm^{-3}) dissociates to free PAN was studied at a fixed wavelength of 550 nm using PAN concentrations between 5 and 50 times that of $[Ni(PAN)_2]$. Usual buffer conditions and thermostatting were applied.

Chapter 8: Dissociation of Ni(II) complexes of L1, L5, L5B, L6, PAN, L7 and L3765 using excess Terpy.

Introduction.

In the following experiments the kinetics of dissociation of the mono(ligand)Ni(II) complexes of L1, L5, L5B, L6 , PAN, L7 and L3765 have been determined using Terpy as the exchanging ligand. As discussed in Chapter 7 the kinetics of dissociation can give an indication of the relative stabilities of metal complexes.

The purpose of this study was to show a comparison of the relative stabilities of a variety of azo dye ligands which are of commercial interest to Avecia. Results can be seen in Figures 76-85. In Table 12 the rates of dissociation of the various mono(ligand)Ni(II) complexes are compared.

8.1 Results

Figure 76: Spectra of $[Ni_2L1]$ (2×10^{-5} mol dm^{-3}) reacted with excess Terpy (4.6×10^{-4} mol dm^{-3}) studied over 30 minutes taking readings every minute.

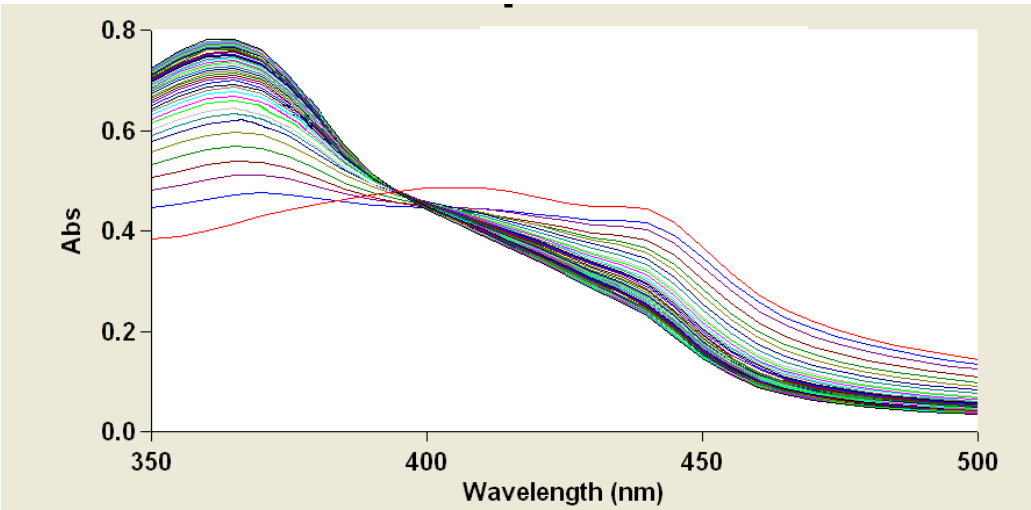

Figure 77: Absorbance against time for the reaction of $[Ni_2L1]$ (2×10^{-5} mol dm^{-3}) with excess Terpy (4.6×10^{-4} mol dm^{-3}) at 450 nm and 25.0 ^{o}C.

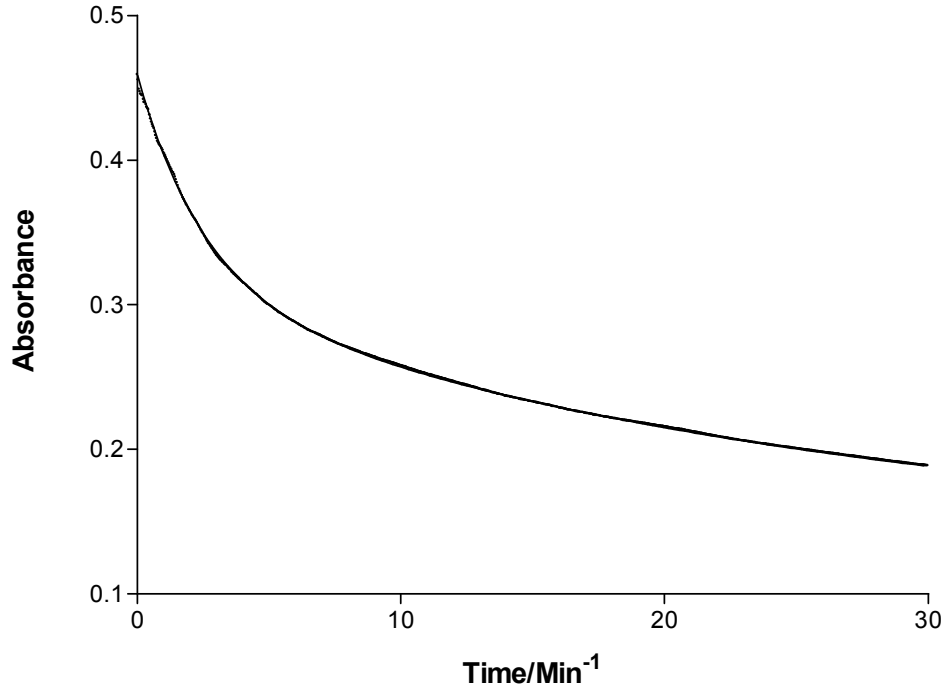

Figure 78: Spectra of $[NiL5]^{2-}$ (2×10^{-5} mol dm^{-3}) reacted with excess Terpy (4.6×10^{-4} mol dm^{-3}) studied over 30 seconds taking readings every second.

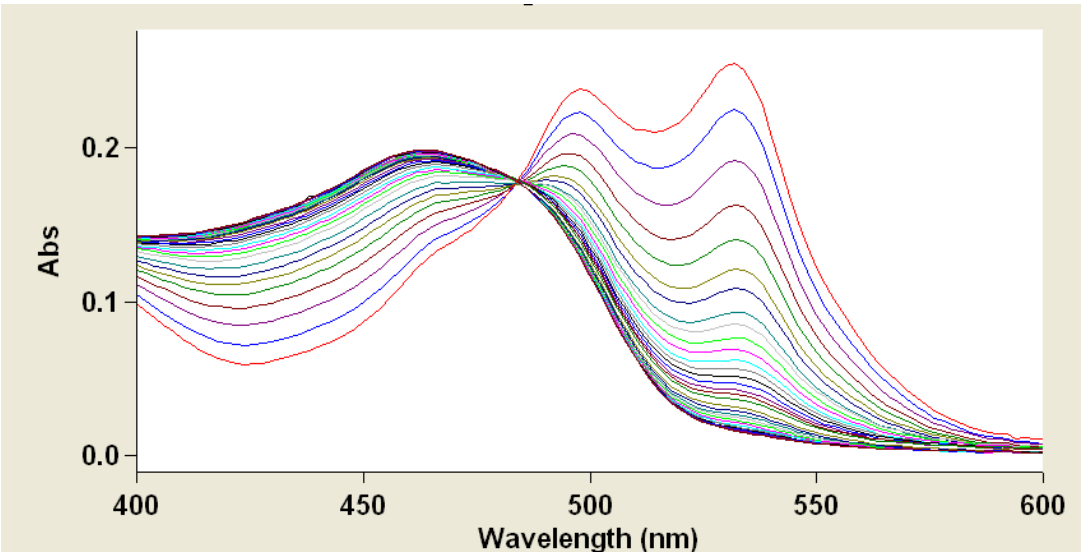

Figure 79: Absorbance against time for the reaction of $[NiL5]^{-2}$ (2×10^{-5} mol dm^{-3}) with excess Terpy (4.6×10^{-4} mol dm^{-3}) at 540 nm and 25.0 ^{o}C.

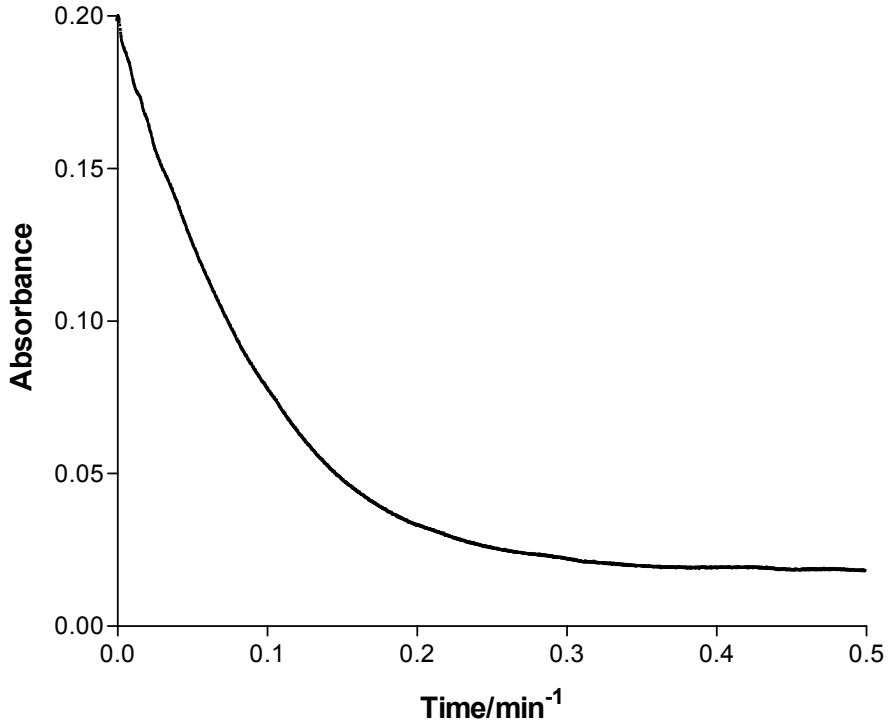

Figure 80: Spectra of $[NiL5B]^{-}$ (2×10^{-5} mol dm^{-3}) reacted with excess Terpy (4.6×10^{-4} mol dm^{-3}) studied over 30 seconds taking readings every 2 seconds.

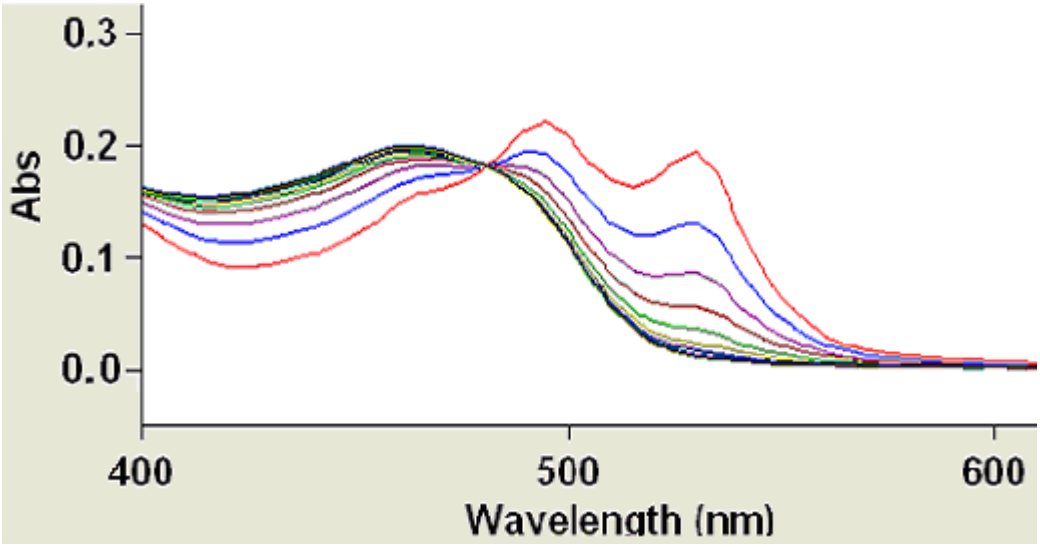

Figure 81: Absorbance against time for the reaction of $[NiL5B]^-$ (2×10^{-5} mol dm^{-3}) with a 20 fold excess Terpy (4.6×10^{-4} mol dm^{-3}) at 540 nm and 25.0 ^oC.

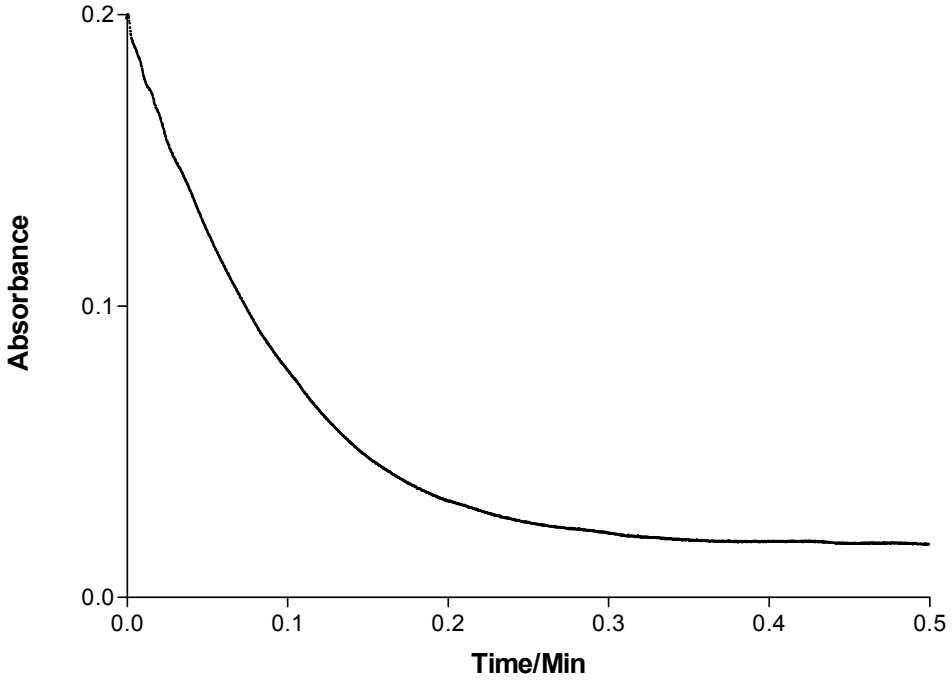

Figure 82: Spectra of $[NiL6]^{2-}$ (2×10^{-5} mol dm^{-3}) reacted with excess Terpy (4.6×10^{-4} mol dm^{-3}) studied over 5 minutes taking readings every 10 seconds.

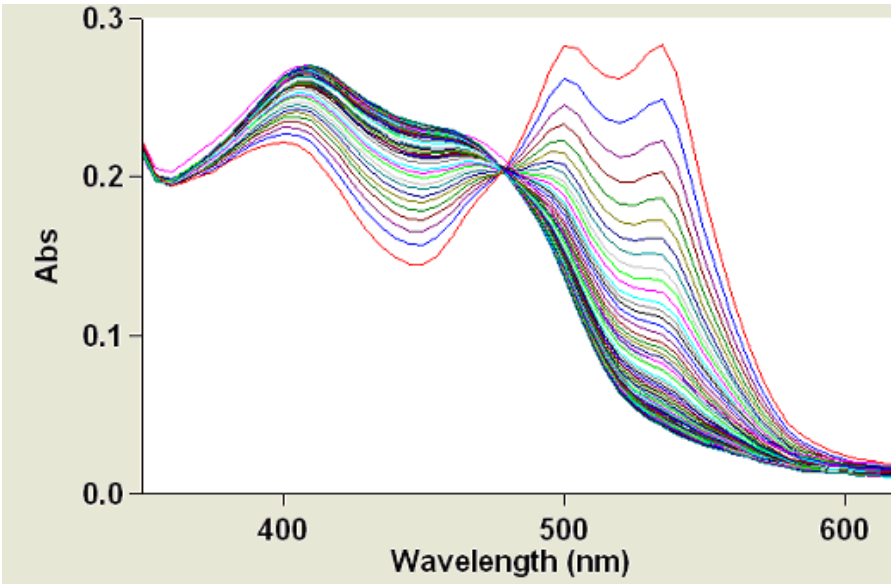

Figure 83: Absorbance against time for $[NiL6]^{2-}$ (2×10^{-5} mol dm^{-3}) reacted with excess Terpy (4.6×10^{-4} mol dm^{-3}) at 545 nm and 25.0 ^{o}C.

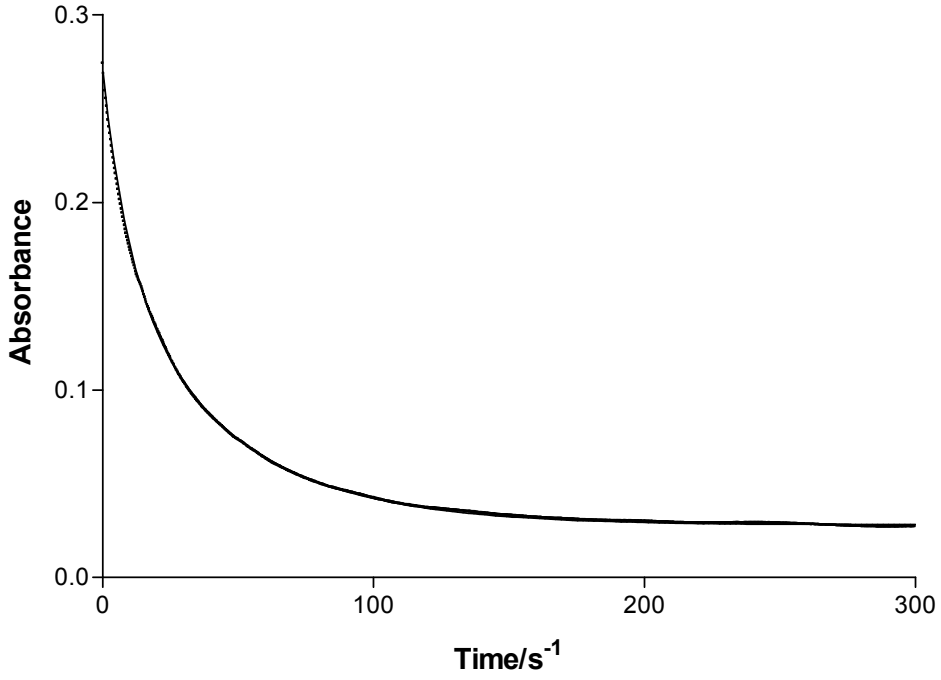

Figure 84: Spectra of $[NiPAN]^{+}$ (2×10^{-5} mol dm^{-3}) reacted with excess Terpy (4.6×10^{-4} mol dm^{-3}) studied over 24 hours taking readings every 30 minutes.

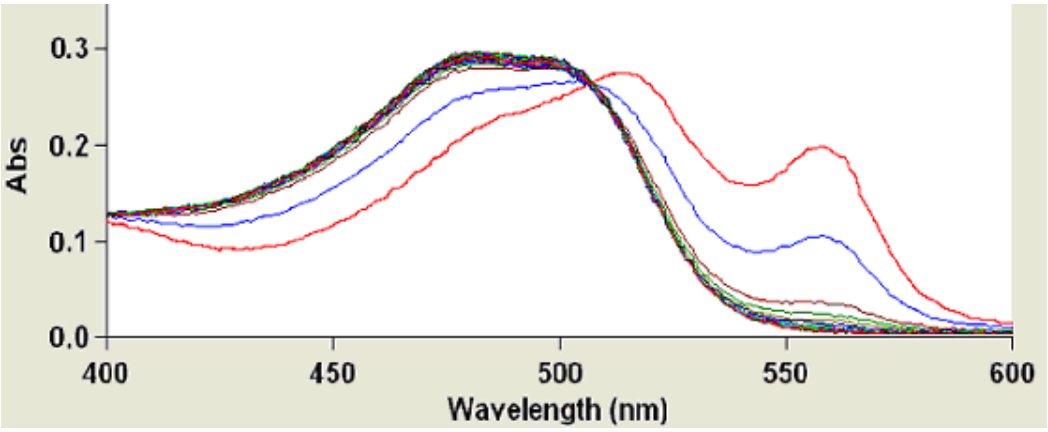

Figure 85: Absorbance against time for $[NiPAN]^+$ (2×10^{-5} mol dm^{-3}) reacted with excess Terpy (4.6×10^{-4} mol dm^{-3}) at 550 nm and 25.0 ^oC.

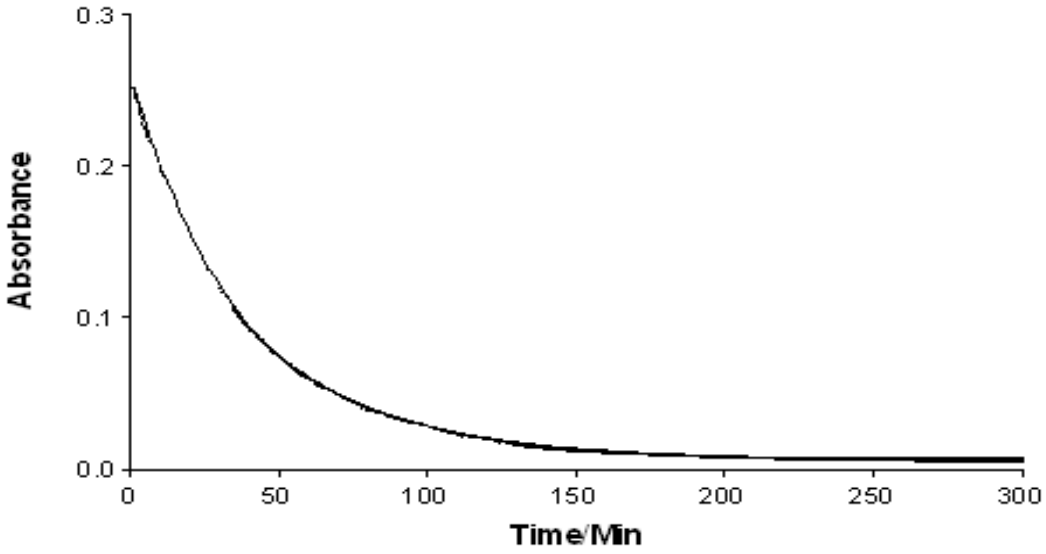

Table 12: Comparison of the rate constants for the dissociation of mono(ligand)Ni(II) species (2×10^{-5} mol dm^{-3}) with excess Terpy (4.6×10^{-4} mol dm^{-3}) at 25 ^oC and pH 6.

Species dissociated	$10^4 k_{obs}/s^{-1}$
$[(Terpy)Ni(L1)]^-$	13.20± 0.08
$[(Terpy)Ni(L5)]^{3-}$	41.70 ± 2.20
$[(Terpy)Ni(L5B)]^{2-}$	31.70 ± 0.35
$[(Terpy)Ni(L6)]^{2-}$	20.00 ± 1.50
[(Terpy)Ni(L7)]	4.50± 0.04
$[(Terpy)Ni(PAN)]^+$	5.17± 0.01
$[(Terpy)Ni(L3765)]^-$	4.50± 0.01

8.2 Discussion.

From the results it can be seen that the relative stabilities of the mono(ligand)(Terpy)Ni(II) complexes vary with the ligand in the order:

L7 and L3765 < PAN < L1 < L6 < L5B < L5

L7, L3765 and PAN all have a similar relative stability and are the most stable of all the complexes studied. This could be attributed to the fact these three complexes contain a pyridine ring whereas for the other ligands all contain carboxy triazole and hence the electronic effects of the pyridine ring could be possibly more stabilising to the complex than the carboxy triazole.

Another reason for the relative stability order could be related to charge. The charges on the complexes are L7(Neutral), $L3765^{-}$, PAN^{+}, $L1^{-}$, $L6^{2-}$, $L5^{3-}$ and $L5B^{2-}$. The trend of increasing charge follows the trend of decreasing relative stability. The complexes of L7, L3765, PAN all have similar relative stabilities although one L7 is neutral, L3765 has a 1^{-} charge and PAN has a 1^{+} charge. This illustrates that charge does not play as an important role for these three complexes as it does for the other ligands. L1 has a charge of 1−, L6 and L5B have a 2−charge and L5 a 3−charge.

As an illustration the L5 complex dissociates over nine times faster than the L7 complex. L5 and L5B are essentially the same molecule apart from the fact that L5B has an absent carboxylic acid group and hence reduces the negative charge on the ligand and hence the complex. In turn this makes L5B slightly more stable than L5.

8.3 Experimental.

8.31 UV-Visible study of the reaction of [Ni_2L1] with excess Terpy.

[Ni_2L1] was formed by reacting a four-fold excess of Ni(II) (8×10^{-5} mol dm^{-3}) with L1 (2×10^{-5} mol dm^{-3}). This was then reacted with a 20 fold excess of Terpy plus an extra amount of Terpy to compensate for the excess Ni(II) (4.6×10^{-4} mol dm^{-3}). The reaction was monitored using UV-Visible spectrophotometry in the wavelength range 350-500 nm under the usual buffer conditions and temperature.

8.32 Kinetic study of the reaction of [Ni_2L1] with excess Terpy.

[Ni_2L1] (2×10^{-5} mol dm^{-3}) was reacted with Terpy (4.6×10^{-4} mol dm^{-3}) and the dissociation was studied kinetically at 25^{o}C with a UV-Visible spectrophotometer at a fixed wavelength of 450 nm over 30 minutes.

8.33 UV-Visible study of the reaction of $[NiL5]^{2-}$ with excess Terpy.

$[NiL5]^{2-}$ was formed in the same way as for [Ni_2L1] and all concentrations were kept the same. The UV-Visible wavelength range used was 400-600 nm.

8.34 Kinetic study of the reaction of $[NiL5]^{2-}$ with excess Terpy.

The conditions were the same as for [Ni_2L1] except the fixed wavelength used was 540 nm.

8.35 UV-Visible study of the reaction of $[Ni(L5B)]^{-}$ with excess Terpy.

$[Ni(L5B)]^{-}$ was formed in the same way as for [Ni_2L1] and all concentrations were kept the same. The UV-Visible wavelength range used was 400-600 nm.

8.36 Kinetic study of the reaction of $[Ni(L5B)]^-$ with excess Terpy.

Reaction conditions and concentrations were the same as for $[Ni_2L1]$ except the fixed wavelength used was 540 nm.

8.37 UV-Visible study of the reaction $[Ni(L6)]^{2-}$ with excess Terpy.

$[Ni(L6)]^{2-}$ was formed in the same way as for $[Ni_2L1]$ and all concentrations were kept the same. The UV-Visible wavelength range used was 400-600 nm.

8.38 Kinetic study of the reaction of $[Ni(L6)]^{2-}$ with excess Terpy.

Reaction conditions and concentrations were the same as for $[Ni_2L1]$ except the fixed wavelength used was 545 nm.

8.39 UV-Visible study of the reaction of $[NiPAN]^+$, [NiL7] and $[NiL3765]^-$ with excess Terpy.

$[NiPAN]^+$, [NiL7] and $[NiL3765]^-$ were formed in the same way as for $[Ni_2L1]$ and all concentrations were kept the same. The UV-Visible wavelength range used was 400-600 nm.

8.310 Kinetic study of the reaction of $[NiPAN]^+$, [NiL7] and $[NiL3765]^-$ with excess Terpy.

Reaction conditions and amounts were the same as for $[Ni_2L1]$ except the fixed wavelength used was 550 nm.

9.1 Conclusions.

After analysis using atomic absorption spectroscopy (AAS) it was discovered that most of the dyes contained sodium which arises from the method of synthesis. It is believed that the sodium is associated with the sulfonate groups of the dyes. After consultation with Avecia it was also found that it is common for the dyes to contain water of crystallisation which is also present.

pK_a values determined for PAN, L7, L3765 were in good agreement with those of a previous study.[150] pK_a values determined for L1 were compared to a theoretical study and it was shown that the dye L1 appeared to be in the hydrazo form as opposed to the azo tautomeric form. pK_a values were determined for L5 and L5B and the values were very similar as was expected. However the missing pK_a around 3 for L5B confirmed the absence of any carboxylic group in L5B.

Attempts to measure stability constants by multiwavelength UV-Visible spectroscopy for the reaction of Ni^{2+} with PAN returned values that were too high [$\log(K_1) = 41.5 \pm 0.3$ and $\log(K_2) = 36.8 \pm 0.3$)] and it was established that the stability constants of this system are too large to measure reliably by this method. Stability constants were also estimated spectroscopically for reactions of Ni^{2+} with L1 and L5. The values for L1 appeared to be quite large compared with those reported for other terdentate ligands. However, it was observed that in the presence of excess Ni^{2+}, L1 can bind two Ni(II) ions. The values for L5 gave a very good

calculated spectral fit, and values which are more realistic than those found for the other ligands studied (log K_1 = 9.04 $\pm$ 0.77 and log K_2 = 5.56 $\pm$ 0.19).

Stopped-flow kinetic studies of the reaction of Ni^{2+} with PAN, L7 and L3765 showed two kinetic steps. This did not agree with a previous kinetic study of the reaction between Nickel(II) and PAN which only showed one step.[124] The results found in this study suggest that the first step involves rapid metal chelate formation involving the pyridine N-atom and an azo-N atom which is then followed by the breaking of a hydrogen bond giving a slower final chelate ring closure by the phenolic *O*-atom.

Stopped-flow kinetic studies of the reaction of L1 with excess Ni^{2+} led to the formation of the mono-Ni(II)(ligand) species $[Ni(L1)]^-$ and the di-Ni(II)ligand species $[Ni_{2(}L1)]^+$. As expected L7 forms only the mono metal species due to the absence of a second strong ligating site. The reaction of L5 with excess Ni^{2+} gave both the mono- and di-Ni(II) ligand species. In contrast L5B forms only the mono metal species as expected due to the lack of the carboxylic acid group.

Reaction of excess L5 and L5B with Ni^{2+} leads to mono(ligand)Ni(II) and bis(ligand)Ni(II) formation. Using excess ligand, the formation rate of the mono(ligand)Ni(II) species for L5B compares well with the value found when this ligand is reacted with excess Ni(II). However, the rate observed when Ni(II) is reacted with excess L5 is significantly less by an order of magnitude than when reacted with excess Ni(II).

The enhanced value found for L5 in the presence of excess Ni^{2+} is puzzling, especially as no significant rate enhancement was observed for L5B in the presence of excess metal ion. Perhaps for L5, greater outer-sphere ion-pairing occurs when using a large excess of Ni^{2+} due to the presence of two ligating sites, and extra negative charge, and this would result in the observed rate enhancement.

An alternative interpretation that cannot be completely ruled out would involve excess Ni^{2+} attacking first at the bidentate carboxylate and triazole site, followed by attack at the terdentate azo-site. The latter interpretation is postulated to be less likely.

The dissociation of $[Ni(PAN)_2]$ by EDTA takes place in two stages. The first stage involves substitution of a PAN molecule by EDTA giving a $[(PAN)Ni(EDTA)]^{3-}$ intermediate; the coordinated EDTA then displaces the second PAN to give $[Ni(EDTA)]^{2-}$ with release of the second PAN molecule. As the concentration of EDTA increases, each stage of the reaction goes faster. If the concentration of PAN is increased this leads to the retardation of the rate of EDTA coordination.

The dissociation of $[Ni(PAN)_2]$ by Terpy also occurs in two stages. The first stage involves Terpy replacing the first coordinated PAN giving $[(PAN)Ni(Terpy)]^{+}$ and the second stage involves a second Terpy molecule displacing the second coordinated PAN molecule. Again if the free PAN concentration is increased there is a decrease in the rate of coordinated PAN dissociation.

The measured formation and dissociation rate constants were used to estimate relative stabilities for $[Ni(II)(L3765)]^{-}$, $[Ni(II)(PAN)]^{+}$ and [Ni(II)(L7)]. These

values found in water are around log K of 6, significantly less that that reported for $[Ni(II)(PAN)]^+$ from a potentiometric study in 50% dioxane-water where log K_1 is reported to be 12.7. This difference in the magnitudes of the stability constants can be partially understood because values in solvents of lower dielectric constant are often larger than those in aqueous solution. Also the values determined kinetically are significantly less accurate than those from the potentiometric study, so the difference may not be so large.

The stability constant found kinetically for the bidentate intermediate formed during the formation of $[Ni(II)(PAN)]^{2+}$ (1.02×10^3 dm^3 mol^{-1}) compares well with values reported for similar bidentate ligands such as SUDAN I (2.95×10^3 dm^3 mol^{-1}) and PADA (2.31×10^3 dm^3 mol^{-1}). The values found for the bidentate intermediates formed by L7 and L3765 are slightly less, and this is attributed to the influence of the sulphonate groups.

The stability constant determined kinetically for the formation of $[Ni(PAN)_2]$ from $[Ni(PAN)]^+$ was estimated to be log K_2 = 5.76 $\pm$ 0.49 which compares well with log K_1 of 6.07 $\pm$ 0.79. In water the difference log K_1 - log K_2 = 0.31 compared with a difference of *ca* 0.1 in 50% dioxane-water.

The relative stabilities of the mono(ligand)(Terpy)Ni(II) complexes vary with the ligand in the order: L7 and L3765 < PAN < L1 < L6 < L5B < L5

9.2 Possible future work.

If more time was available it would have been interesting to investigate the following:

- The effects of temperature and pH on complex formation and dissociation
- Crystal growth of azo dyes and their metal complexes to obtain crystal structures
- Investigations using different first-row transition metal ions
- To study the effects of stacking interactions on the rates of formation and dissociation of the azo/metal complexes
- To study azo dye tautomerism under a variety of conditions
- To perform metal exchange studies
- To perform azo dye ligand exchange studies

References.

1 P. Gregory, *Prog Coloration. Rev*., 1994, **24,** 1-16

2 P. Gregory, *Journal of the Royal Microscopical Society*., 2001, 16-22

3 J. Heinzl and C.H Hertz, *Advances in Electronics and Electron Physics*, 1985, 65

4 I. Endo, Y. Sato, S. Saito. T. Nagakiri and S. Ohno, 1979., *GB Patent* 2007162

5 M.B Lyne, *J. Imaging Technol*., 1986, **12**, 80

6 J.L Vaught, F.L Cloutier, D.K Donald, J.D Meyer, C.A Tacklind and H.H Taub, 1984., *US Patent* 4490728

7 D.L Hammond, *Hewlett-Packard J*., March 1984, 44

8 Exxon, *European Patent*., 1984, 181, 198A

9 Howtek, *European Patent*., 1984, 187, 352A

10 Tektronix, *European Patent*., 1985, 206, 286

11 A.B. Jaffe and R.N Mills, *Proceedings of the SID*., 1983, **24(**3), 219

12 P. Gregory, *High-technology Applications of Organic Colorants*., 1991, 177-180

13 R.W Kenyon, *Chemistry and Technology of Printing and Imaging Systems*., **5**, 113

14 K. Suzuki, *SPSE Third International Congress on Advances in Non-impact Printing Technologies*., San Francisco 1986, 148

15 N. Ohata, *J. Appl. Photogr. Engr*, 1976, **2**, 75

16 P. F. Gordon and P. Gregory, '*Organic chemistry in colour*,' Springer-Verlag., 1987

17 C.H Giles, C.D Shah, D.P Johani and R.S Sinclair, *J. Soc. Dyers Colorists*., 1972, 88.59

18 Y. Suga, T. Eida, S. Koike and T. Ohta, *SPSE Fourth International Congress on Advances in Non Impact Printing Technologies* (*Advance Printing of Paper Summaries*), New Orleans., March 20-25, 1988. 123

19 P. Gregory, *Dyes and Pigments*, 1986, **7**, 45

20 A.B Jaffe, E.W Luttman, and W. Crooks, *ACS Symposium on Reprography*., September 1981.

21 T. Kitao, *Dyestuffs and Chemicals*., 1982, 17(12)

22 R.E. Littleford, M.P.Hughes, G. Dent, D. Tackley, W.E.Smith, *Appl. Spectrosc*., 2003, **57**(8), 977-983

23 A.R. Kennedy, M.P. Hughes, M.L. Monaghan and W.E. Smith, *J. Chem Soc., Dalton Trans.*, 2001, 2199-2205

24 C. Rodger, C. Dent, J. Watkins and W. E. Smith, *Appl. Spectrosc*., 2000, 1567-1576.

25 K. Muraki, T. Aruga and M. Shimada, *SPSE Fourth International Congress on Advances in Non-Impact printing Technologies (Advance printing of paper summaries)*., New Orleans, March 20-25, 1988, 131

26 E. Mitscherlich, *Ann*., 1884, **12**, 311

27 N. Zinin, *J. Prakt.Chem*., 1841, **36**, 93

28 A. Kekule, *Lehrbuch der organischen chemie*., Erlangen, 1866, **Vol II,** 716

29 H. Zollinger. *Azo and diazo chemistry, Aliphatic and aromatic compounds*., Interscience, 1961. 7-9

30 P. Griess, *Ann*., 1858, **106**, 123

31 T. Curtius, *Ber*., 1883, **16**, 2230

32 H. Staudinger and J. Siegwart, *Ber*., 1916. **49,** 1918

33 M. Khamis, B. Bolus, F. Jumean, A, Manassra, and M. Dakiky, *Dyes and Pigments*., 2005, **66**, 179-183

34 S. Alaa E. Abd-El-Aziz and Tarek H. Afifi, *Dyes and Pigments*., 2006, **70**, 8-17

35 P. F. Gordon and P. Gregory, *Organic chemistry in colour*., Springer-Verlag 1987.

36 R. Aranyosi, M.Czilik, E. Remi, G. Parlagh, A. Vig and I. Rusznak, *Dyes and Pigments*., 1999, **43**(3) 12-20

37 C. Galindo and A.Kalt, *Dyes and Pigments*., 1999, **42**(3) 20-31

38 K.J Sirbladze, A. Vig, V.M. Anyisimov, O.M Anyisimova, G.E Krichevskiy and I. Rusznak , *Dyes and Pigments*., 1990, **14**(1), 23-34

39 E. Lewandowsky, R.Mayer, J. Marx, H. Böttcher, *Dyes and Pigments*., 1990, **14(**1**),** 15-22

40 E. Lewandowsky and R.Mayer, *Angewandte Makromolekulare Chemie*., 1992, **197**(1), 175-184

41 C. Galindo and A. Kalt, *Dyes and Pigments*., 1999, **40(**19), 27-33

42 G. Hallas and J.H Choi, *Dyes and Pigments*., 1999, **42**(3), 249-260

43 S. Stoyanov and L. Antonov., *Dyes and Pigments*., 1988, **10**(1), 33-45

44 A. MacKay and J.J. Pignatello., *Helv. Chim. Acta*., 2001, **49**(3), 2589

45 G. M. Kinhikar and K. N. Munshi., *Microchemical Journal*., 1979, **24**(4), 444-453

46 R. Price, '*The chemistry of metal complex dyestuffs*.'in '*The chemistry of synthetic dyes*,' Academic Press, New York, London., 1970 **3**, 303-383.

47 E. N. Abrahart, '*Dyes and their intermediates'*, 2nd ed., London, Edward Arnold 1977, 108.

48 A. Sanaa, Y. Amin, Y. El-Emeri and Z. Kamel., *Journal für Praktische Chemie*, 1972, **314**, 857.

49 M. S Hadjistoreriou and R. A. James, Avecia Limited(UK), Brit, UK 2002, Patent number: GB 2372750

50 K. M. Tawarah and H. M. Abu-Shamleh, *Dyes and Pigments*., 1991, **16**(3), 241-251

51 T. Hihara, Y. Okada and Z. Morita, *Dyes and Pigments*., 2004, **61**(3), 199-255

52 T. Hihara, Y. Okada and Z. Morita, *Dyes and Pigments*., 2003, **59**(3), 201-222

53 S. Stoyanov and L. Antonov, *Dyes and Pigments*., 1989, **10**(1), 33.

54 P. Ball and C. H. Nicholls, *Dyes and Pigments*., 1982, **3**(1), 5.

55 P. Jacques, H. Strub, J. See and J.P Fleury, *Tetrahedron*., 1979, **35**(17) 2071

56 C.H. Munro, W.E. Smith, D.R. Armstrong and P.C. White, *J. Phys. Chem*., 1995, **99** (3), 879

57 P. Imnek and V. Bertolasi, *J. Mol. Struct*., 2002, **642**, 41

58 A. Burawoy , A. Salem, A.G Thompson, *J. Chem. Soc*., 1952, 4793

59 P. Ball and C. H. Nicholls, *Dyes and Pigments*., 1985, **6**(1), 13-25

60 B. R. Hsieh, D. Désilets and P. M. Kazmaier, *Dyes and Pigments*., 1990, **14**(3), 165-189

61 L. Antonov and S. Stoyanov, *Dyes and Pigments*., 1995, **28**(1), 31-35

62 J. Kelemens, S. Moss and S. Glitsch, *Dyes and Pigments*., 1984, **5**(2), 83-108

63 M. Piotr, *Spectrochimica Acta Part A: Molecular Spectroscopy*., 1985, **41**(9), 1035-1039

64 J. Kelemen, S. Moss, H. Sauter and T. Winkler, *Dyes and Pigments*., 1982,**3**(1), 27-47

65 Q. Peng, M. Li, K. Gao and L. Cheng, *Dyes and Pigments*., 1990, **14**(2), 89-99

66 T. Hatta, S. Mataka and M. Tashiro, *Dyes and Pigments*., 1990, **13**(2), 107-116

67 A. Lycka, Z. Vrba and M. Vrba, *Dyes and Pigments*., 2000, **47**(1-2), 45-51

68 A. Lycka, *Dyes and Pigments*., 1999, **43**(1), 27-32

69 A. Lycka and V. Machacek, *Dyes and Pigments*, 1986, **7**(3), 171-185

70 K. Yamamoto, K. Nakai and T. Kawaguchi., *Dyes and Pigments*, 1989, **11**(3), 173-177.

71 A. Lycka, *Dyes and Pigments*, **12**, 1990, 179-185

72 J. Kelemen, G. Kormány and G. Rihs, *Dyes and Pigments*, 1982, **3**(4), 249-271

73 A.C Olivieri, R.B Wilson, I.C Paul and D.Y Curtin, *J. Am. Chem. Soc*., 1989, **111**, 5525-5532

74 J. Kelemen, *Dyes and Pigments*., 1981, **2**(2), 73-91

75 Q. Peng, M. Li, K. Gao and L. Cheng, *Dyes and Pigments*, 1991, **15**(4), 263-274

76 L. Antonov, S. Kawauchi, M. Satoh and J. Komiyama, *Dyes and Pigments.,* 1995, **40** (2-3), 164-168

77 L. Antonov, S. Kawauchi, M. Satoh and J. Komiyama, *Dyes and Pigments*., 1999, **40**(2-3), 163-170

78 Q. Peng, M. Li, K. Gao and L. Cheng, *Dyes and Pigments*, 1992, **18**(4), 271-286

79 A. Lyčka, J. Jirman, B. Scneider and J. Straka, *Dyes and Pigments*, 1989, **26**, 507

80 V. Bekarek, K. Rotschein, P. Vetsnik, and P. Vecera, *Tetrahedron Lett*., 1968, 3711

81 A. Berrie, H. Hampson, P. Longworth and S.W Mathias, *J. Chem. Soc. B*, 1968 , 1308

82 V. Bekarek, J. Dobas, J. Socha, J. Vestesnik and P. Vecera, *Coll. Czeck. Chem. Commun*., 1970, **35**, 1406

83 A. Lycka, D. Snobl, D. Machacek and V. Vecera, *Org. Magn., Reson*., 1981, **15**, 390

84 A. Burawoy, A.G Salem and A.R Thompson, *J. Chem. Soc*., 1952, 4793

85 M. Miyahara and M. Eisei, Shikensho Hokuku., 1982, 100, 135; *Chem. Abstr*., 1984, 100, 5716

86 K. Morgan, *J. Chem. Soc*. 1961, 2151

87 D. Kobelt, E. Paulus and F. Kunstman, *Acta Crystallogr*., 1972, B28, 1319

88 D. Kobelt, E. Paulus and F. Kunstman, *Acta Crystallogr*., 1974, **139**, 15

89 A. Whitaker, *Z. Kristallogr*., 1977, **145**, 271

90 A. Whitaker, *Z. Kristallogr*., 1977, **146**, 173

91 A. Whitaker, *Z. Kristallogr*., 1978, **147**, 99

92 A. Whitaker, *Z. Kristallogr*., 1980, **152**, 227

93 C. Grainger and T. McConnell, *Acta Crystallogr*., 1979, **B25**, 1962

94 A. Lycka, D. Snobl, V. Machacek and V. Vecera, *Org. Magn. Reson*., 1981, **16**,17

95 M. Miyahara, M. Eisei and S. Hokoku, *Chem. Abstr*. 1984, 100

96 L. Antonov, S. Kawauchi, M. Satoh and J. Komiyama, *Dyes and Pigments*., 1998, **38**(1-3), 157-164

97 C. Öğretir, T.A. Demir and M. Özkaya, *Journal of Molecular Structure*: THEOCHEM., 2005, **732**(1-3), 183-199

98 D. Nedeltcheva, B. Damyanova and Simeon Popov, *J. Molecular Structure*., 2005, **749**(1-3), 36-44

99 F. Lio and L.F.C De Oliverira, International Journal of Quantum Chemistry., 2000, **80**(4-5), 1076-1086

100 R. L. Reeves, M. S. Maggio, and S. A. Harkaway, *J. Phys. Chem.*, 1979, **83**, 2359

101 P. Skrabal, F. Bangerter, K. Hamada and T. Iijima, *Dyes and Pigments.,* 1987, **8**(5), 371-374

102 M. Dakiky, K. Kanan and M. Khamis, *Dyes and Pigments*., 1999, **41**(3), 199-209

103 P. Simunek, V. Bertolasi and V. Machacek, *J. Molecular Structure*., 2002, **642**(1-3), 41-51

104 Navarro and F. Sanz, *Dyes and Pigments*., 1999, **40**(2-3), 131-139

105 K. Hamada, H. Nonogaki, Y. Fukushima, B. Munkhbat and M. Mitsuishi, *Dyes and Pigments*., 1991, **16**(2), 111-118

106 M. Dakiky and I. Nemcova, *Dyes and Pigments*., 1999, **40**(2-3), 141-150

107 M. H. Habibi, A. Hassanzadeh and A. Zeini-Isfahani, *Dyes and Pigments*., 2006, **69**(3), 111-117

108 A. P. Mazurek, L. Skulski and J. Cz. Dobrowolski, *J. Molecular Structure*., 1997, **410-411**, 421-424

109 M. S. Masoud, *Inorg. Chim. Acta*., 1980, **40**, 160-161

110 B. Millicevic and G. Eigenmann, *Helv. Chim. Acta*., 1964, **47**, 1039.

111 E. Coates and B. Rigg, *Trans. Faraday Soc*., 1961, **57,** 1637

112 A. R. Monahan and D. F. Blossey, *J. Phys. Chem.,* 1970, **74**, 4014

113 K. Bredereck and C. Schumacher, *Dyes and Pigments*., 1993, **21**(1), 23-43

114 N. Kawashima, N. Fujimoto and K. Meguro, *J. Colloid and Interface Science*., 1985, **103**(2), 459-465

115 S. Millefiori, F. Zuccarello, A. Millefiori and F. Guerrera, *Tetrahedron.*, 1974, **30**(6), 735-738

116 C. Daescund and M. Calcaterra, *Dyes and Pigments*, 1998, **38**(1-3), 173-180

117 R. L. Reeves and R. S. Kaiser, *J. Org. Chem*., 1970, **35**, 3670

118 R. L. Reeves, R. S. Kaiser and K. T. Finlay, *J. Chromatogr.,* 1970, **47**, 217

119 D. Simov, T. Deligeorgiev, N. Gadjev, A. Penchev, *Dyes and Pigments*., 1990, **15,** 83

120 S. Yanlong, E. M. Eyring and R. van Eldik, *J. Chem. Soc, Dalton Trans*., 1998, 3565–3576

121 M. Tanaka, S. Funahashi and K. Shirai, *Anal. Chim. Acta*, 1967, **39**, 437

122 B. Perlmutter–Hayman and R. Shinar, *Inorg. Chem.,* 1976, **15**, 2932

123 R. L Reeves, *Inorg Chem*., 1986, **25**, 1473

124 R. H. Hoyler, C. D. Hubbard, S. F.A Kettle, and R.G Wilkins, *Inorg. Chem*., 1966, **5**, 622

125 R. L. Reeves, G. S. Calabrese and S. A. Harkaway, *Inorg. Chem*., 1983, **22**, 3076

126 E. Mentasti and P. Baiocchi, *J. Chem. Soc, Dalton Trans*., 1985, 2615

127 H. L. Fritz and J. H. Swinehart, *Inorg Chem.*, 1975, **14**, 1935

128 G. Meyers, F. M. Michaels, R. L. Reeves and P. P. Trotter, *Inorg. Chem*., 1985, **24,** 731

129 M. Cusumano, *Inorg. Chim. Acta*, 1977, **25**, 207

130 S. Funahashi and M.Tanaka, *Inorg Chem*, 1969, **8**, 2159

131 C. D. Hubbard and A. D. Pacheco, *J. Inorg. Nucl. Chem.*, 1977, **39**, 1373

132 C. F. Shaw, J. E. Laib, M. M. Savas and D. H. Petering, *Inorg Chem*., 1990, **29**, 403

133 V. Velich and V. DlaskK, *Dyes and Pigments*., 1985, **6**(6), 445-461

134 R. L. Reeves, M. S. Maggio, and S. A. Harkaway *J. Phys. Chem.*, 1979, **83**, 2359

135 M. A. Cobb and D. N. Hague, *J. Chem. Soc., Faraday Trans*., 1972, **68**, 932.

136 H. P. Bennetto and Z. S. Imani, *J. Chem. Soc., Faraday Trans*., 1975*,* **71***,* 1143

137 A. D. James and B. H. Robinson, *J. Chem. Soc., Faraday Trans*., 1978, **74,** 10

138 B. H. Robinson and N. C. White, *J. Chem. Soc., Faraday Trans.,* 1978, **74**, 2625

139 M.A. Rauf, Z. Akhter and S. Kanwal, *Dyes and Pigments*., 2004, **63**(2) 213-215

140 S. Mamdouh, D. Masoud, A. Ekram, A Khalil M. Ahmed, *Dyes and Pigment*s., 2004, **12,** 2807-2817

141 H. P. Bennetto and E. F. Caldin, *J. Chem. Soc. D*., 1969, 599

142 K. Chattopadhyay and J.F Coetzee, *Inorg. Chem*., 1973, **12**, 113

143 P. Moore, and D. M. W. Buck, *J. Chem.Soc. Dalton Trans*., 1973, 1602.

144 P. K. Chattopadhyay and J. F. Coetzee, *Anal. Chem*., 1974, **46**, 2014

145 D. M. W Buck and P. Moore, *J. Chem. Soc. Dalton Trans.,* 1974, 2082

146 P.K Chattopadhyay and J.F Coetzee, *Inorg. Chem*., 1976, **15**, 400

147 J. F. Coetzee, and D. M. Gilles, *Inorg. Chem*., 1976, **15**, 405

148 H. L. Fritz and J. H. Swineheart, *Inorg Chem*., 1973, **12**, 1259

149 G. A. Meyers, F. M. Michaels, R. L. Reeves and P. J. Trotter, *Inorg. Chem*., 1984, **24,** 731

150 M. Kortuglu, N. Birbicer , U, Kyimyonsen, and S. Serin, *Dyes and Pigments*., 1998, **41,** 143

151 B. F. Pease and M. B. Williams, *Anal. Chem*., 1959, **31**, 1044

152 G. J. Mohr, T. Werner, and O.Wolfsbein, *Dyes and Pigments*., 1993, **21**(1), 23-43

153 K. Bredereck, B. Gulec and B. Helfrich, *Dyes and Pigments*, 1987, **8**(4), 265-279

154 M. Kurtoglu, N. Birbicer, U. Kimyon and S. Serin, *Dyes and Pigments*, 1999, **41**(1-2), 143-147

155 B. F. Pease and M.B Williams *Analytical Chem*., 1959, **31**, 1044

156 R. H. Holyer, C. D. Hubbard, S.F.A Kettle and R.G Wilkins, *Inorg. Chem*., 1965, **4**, 7

157 W. J. Geary, G. Nickless and F. H. Pollard, *Anal. Chim. Acta*., 1962, **27,** 71-79

158 G. Nickless, F. H. Pollard and T.J. Samuelson, *Anal. Chim. Acta*., 1967, **39,** 37-46

159 A. Rauf, Z. Akhter and S. Kanwal, *Dyes and Pigments*., 2004, **63**(2), 213- 215

160 W. G. Hanna, *Talanta*., 1999, **50**(4) 809-818

161 S. Zar and J Melke., *Pharmaceutica Acta Helvetiae*., 2000, **74**(4), 361- 364

162 R. Bing, R. K Crandall and B. A Weinstein,.*Dyes and Pigments*., 1991,**17**(2), 141-151

163 H. S. Freeman, J. C. Posey, Jr. and P. Singh, *Dyes and Pigments*., 1992, **20**(4), 279-289

164 M. M. Omar and G. G. Mohamed, *Spectrochimica Acta Part A: Molecular and Biomolecular Spectroscopy*., 2005, **61**(5), 929-936

165 E. Kucharska, J. Hanuza, A. Waśkowska and Z. Talik, *Chem.Physics*., 2004, 306(1-3), 71-92

166 S. Soylu, H. Kocaokutgen, M. Gür and P. Lönnecke, *Acta Cryst*., 2004, **60**, 498-500.

167 W. Yang, X. L.You, Y. Zhang and D. C. Zhang, *Acta Cryst*., 2006, **68**(1), 1-77

168 S. Ooi, D. Carter, Q. Fernando, *Chem Commun*., 1967, 1301

169 S. Kurosaki, S. Kashino and M. Haisa, *Acta Cryst.*, 1976, **32**, 3160-3163

170 C. C. Ersanli, Ç. Albayrak, M. Odabasoglu, C. Kazak and A. Erdönmez, *Acta Cryst*., 2004, **60**, 455-457

171 S. Isik, M. Aygün, S. Sasmaz, E. Kendi, O. Büyükgüngör and A. Erdönmez, *Acta Cryst*., 1997, 53, 593-594

172 X. L. You, Y. Zhang, Y. Zhang and D. C. Zhang, *Acta Cryst*., 2005, 61, 2656-2658

173 X. G. Liu, Y. Q. Feng, Z. P. Liang and W. Wang, *Acta Cryst*., 2005, 61, 3857-3858

174 J. Ma, S. P. Zhang, L. Q. Sheng, M. Fan, Y. L. Yang and S. C. Shao, *Acta Cryst*., 2005, 61, 1747-1748

175 S. Shan, X. J. Wang, W. X. Hu, *Acta Cryst*., 2004, 60, 1345-1347

176 R. Salmen, K. E. Malterud and B. F. Pedersen, *Acta Chem. Scand*., 1988, **42**, 493-499

177 H. Wang, H.-M. Liu and W.-Q. Zhang, *Acta Cryst*., 2005, **61**, 3808-3809

178 A. X. Li and L. L. Liu, *Acta Cryst*., 2005. **61**, 277- 279

179 S. C. Shao, Z. L. You, S. H. Fan, L. L. Tang, Z. D. Xiong and H. L. Zhu, *Acta Cryst*., 2004, **60**, 2183-2184

180 S. C. Shao, Z. L. You, L. L. Tang, Y. S. Lin and H. L. Zhu, *Acta Cryst*., 2004**, 60**, 2185-2186

181 G. Sadik, D. Necmi, Y. Ibrahim, Ç. Alaaddin and M. Dinçer, *Acta Cryst*., 2004, **60**, 889-891

182 J. A. J. Jarvis, *Acta Cryst*., 1961, **14**, 961

183 A. Lycka, D. Lustinec, J. Holecek, M. Nadvornik, M. Holcapek, *Dyes and Pigments*., 2001, **50**, 203-209

184 R. H. Holyer, C. D. Hubbard, S. F. A. Kettle and R. G. Wilkins, *Inorg Chem*., 1965, **5**(4), 622-62

185 F. Oakley, N. M Horn and A. L Thomas, *J.Physiol*., 2004, **561**(2),525-534

186 B. Busing, H. Elias, I Eslick and K.J Wannowius, *Inorganica Chemica Acta.,* 1988, **150**, 223-226

187 B. Pullman, Ed., "Molecular Associations in Biology", Academic Press, New York, N.Y., 1968

188 D. G. Duff and C. H. Giles in "Water, a Comprehensive Treatlise", Vol 4, F. Franks, Ed., Plenum Press, New York, N.Y., 1975

189 T. G. Dewey, P. S. Wilson and D. H. Turner, *J. Am. Chem. Soc.*, 1978, **14**, 100

190 G. A. Breault, C. A. Hunter and P. C. Mayers, *J. Am. Chem. Soc*., 1998, **120**, 3402-3410

191 G. R. Cayley and D. W. Margerum, *J.C.S Chem. Comm.,* 1974, 1002-1004

Appendix

Derivation of $k_f = \frac{k_1 k_2}{k_{-1} + k_2}$

$$\frac{d[\text{Terdentate}]}{dt} = k_2[\text{Bidentate}]$$

$$\frac{d[\text{Bidentate}]}{dt} = 0 \quad \text{Therefore } k_1[\text{P}][\text{Ni}] = (k_{-1} + k_2)[\text{Bidentate}]$$

Hence $[\text{Bidentate}] = \frac{k_1[\text{P}][\text{Ni}]}{k_{-1} + k_2}$

$$\frac{d[\text{Terdentate}]}{dt} = \frac{k_1 k_2 [P][Ni]}{k_{-1} + k_2} = k_f[\text{P}][\text{Ni}]$$

Therefore $k_f = \frac{k_1 k_2}{k_{-1} + k_2}$

Calculation of k_f using values found in Table 9 for $[\text{Ni(II)PAN}]^+$, [Ni(II)L7] and $[\text{Ni(II)L3765}]^-$

Using the above derived equation and the values in table 9

$[\text{Ni(II)PAN}]^+$

$$k_f = \frac{3.14x10^3 x0.45}{3.09 + 0.45} = 399.2 \text{ dm}^3 \text{ mol}^{-1} \text{ s}^{-1}$$

[Ni(II)L7]

$$k_f = \frac{2.18x10^3 x0.32}{3.75 + 0.32} = 171.4 \text{ dm}^3 \text{ mol}^{-1} \text{ s}^{-1}$$

$[\text{Ni(II)L3765}]^-$

$$k_f = \frac{2.60x10^3 x0.51}{4.79 + 0.51} = 250.2 \text{ dm}^3 \text{ mol}^{-1} \text{ s}^{-1}$$

Synthetic, equilibrium, kinetic and mechanistic studies of the reactions between azo dye ligands and Ni^{2+}

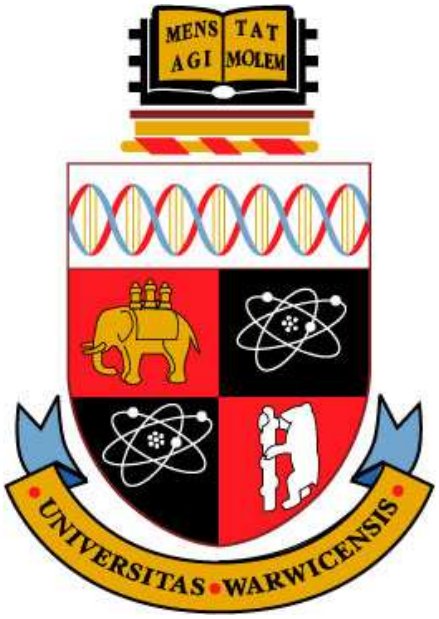

The University Of Warwick

By

Jay A. Blount

A thesis submitted as part requirement for the degree of Doctor of Philosophy

Department of Chemistry

University of Warwick

August 2008

Chapter 1

Introduction

Chapter 2

Azo dye ligand syntheses and characterisation

Chapter 3

Determination of the pK_a values of PAN, L7 and L3765, L1, L5, and L5B by visible spectroscopy using the program SPECFIT/32

Chapter 4

Attempted measurements of the stability constants of Nickel(II) complexes of PAN, L1 and L5 using UV-Visible spectroscopy

Chapter 5

Single wavelength stopped-flow kinetics studies of the reactions of Ni(II) with PAN, PADA, SUDAN I, L3765 and L7

Chapter 6

Multi wavelength stopped-flow kinetics studies of the reactions of Ni(II) with L1, L7, L5 and L5B

Chapter 7

Measurement of the rates of dissociation of $[Ni(PAN)_2]$ using ligand exchange with an excess of either EDTA or 2,2':6',2''-Terpyridine (Terpy)

Chapter 8

Dissociation of Ni(II) complexes of L1, L5, L5B, L6, PAN, L7 and L3765 using excess Terpy

Chapter 9

Conclusions

and future work

References

Appendix